

GRADUATE SCHOOL OF NATURAL AND APPLIED SCIENCES

THESIS

July 2014

**REPUBLIC OF TURKEY
YILDIZ TECHNICAL UNIVERSITY
GRADUATE SCHOOL OF NATURAL AND APPLIED SCIENCES**

ANALYSIS AND SYNTHESIS OF REFLECTARRAY ANTENNA

SELAHATTİN NESİL

**PhD. THESIS
DEPARTMENT OF ELECTRONICS & COMMUNICATION
ENGINEERING
PROGRAM IN TELECOMMUNICATIONS**

**ADVISER
PROF. DR. FİLİZ GÜNEŞ**

İSTANBUL, 2014

REPUBLIC OF TURKEY
YILDIZ TECHNICAL UNIVERSITY
GRADUATE SCHOOL OF NATURAL AND APPLIED SCIENCES

ANALYSIS AND SYNTHESIS OF REFLECTARRAY ANTENNA

A thesis submitted by Selahattin NESİL in partial fulfillment of the requirements for the degree of **PhD (DOCTOR OF PHILOSOPHY)** is approved by the committee on 21.07.2014 in Department of Electronics and Communication Engineering Communication Engineering Program.

Thesis Adviser

Prof. Dr. Filiz GÜNEŞ
Yıldız Technical University

Co-Adviser

Prof. Dr. Bahattin TÜRETKEN
Karabük University

Approved By the Examining Committee

Prof. Dr. Filiz GÜNEŞ
Yıldız Technical University

Prof. Dr. Bahattin TÜRETKEN, Member
Karabük University

Prof. Dr. Ahmet Serdar TÜRK, Member
Yıldız Technical University

Prof. Dr. Hasan DİNÇER, Member
Istanbul Kültür University

Assoc. Prof. Dr. Erdal KORKMAZ, Member
Fatih University

Assist. Prof. Dr. Ş. Taha İMECİ, Member
Istanbul Commerce University

Assist. Prof. Dr. Salih DEMİREL, Member
Yıldız Technical University

This study was supported by the Scientific Research Projects Coordinatorship of Yıldız Technical University (TURKEY) Project No: 2012-04-03-DOP02.

ACKNOWLEDGEMENTS

I wish to express my sincere appreciation to my advisor, Prof. Dr. Filiz GÜNEŞ, for constant support, precious scientific discussions, providing me an excellent working environment and helping me to have better perspective in my scientific thinking throughout my doctorate. She will always be in my memories as a very kind and splendid personality.

I also wish to express my sincere thanks to Prof. Dr. A. Serdar TÜRK and Prof. Dr. Sedef KENT for serving on my thesis committee. I highly appreciate their interest in my study as well as their precious comments and questions.

I would like to offer my special thanks to my co-advisor, Prof. Dr. Bahattin TÜRETKEN for his valuable and constructive suggestions during the planning and development at the outset of this thesis.

I would like to express my deep gratitude to Assist. Prof. Dr. Salih DEMİREL for his guidance, encouragement during my thesis. I deeply thank him for helping me in understanding the theoretical concepts of optimization techniques as well as the computer applications. And also he always helped me whenever I was in need. I am very grateful to him.

I am equally indebted to Assoc. Prof. Dr. Erdal KORKMAZ for providing all needed equipment, material and software and for ensuring the harmony within his group. I offer my special thanks to him for his all support and help.

I am very grateful to my wife, Atike NESİL for her endless emotional support and understanding during my doctoral dissertation.

None of this would have been possible without the prayers, support and encouragement of my parents. I owe them everything. Their continuous prayers had always given me a hidden support and confidence.

July, 2014

Selahattin NESİL

TABLE OF CONTENTS

	Page
LIST OF SYMBOLS	vii
LIST OF ABBREVIATIONS.....	viii
LIST OF FIGURES	ix
LIST OF TABLES	xii
ABSTRACT.....	xiii
ÖZET	xv
CHAPTER 1	
INTRODUCTION	1
1.1 Literature Review.....	1
1.2 Objective the Thesis.....	4
1.3 Hypothesis.....	5
CHAPTER 2	
FUNDAMENTALS OF REFLECTARRAY ANTENNAS.....	6
2.1 Reflectarray Antenna Concept	6
2.2 Microstrip Reflectarray Antennas (MRA)	7
2.2.1 Advantages of MRA.....	9
2.2.2 Disadvantages of MRA	10
2.3 MRA Design and Analysis Techniques	10
2.3.1 H-wall waveguide simulator technique.....	11
2.3.2 Infinite Array Approach	12
2.3.3 Path Length and Phase Shift.....	13
2.4 Radiation Pattern Analysis of Reflectarray Antennas.....	15
CHAPTER 3	
DESIGN AND ANALYSIS OF MINKOWSKI RA USING PARTICLE SWARM OPTIMIZATION BASED ON MLP NN.....	17

3.1 Introduction.....	17
3.2 Reflectarray Element Design Analysis	18
3.2.1 Generation of the Training and Validation Data.....	18
3.2.2 Black-Box Model	21
3.2.3 Performance of the MLP Black Box Model.....	24
3.3 The Optimization of the Minkowski Element with Particle Swarm Algorithm	32
3.4 Design of Minkowski RA with Substantially-Optimized Parameters	35
3.5 Results and Discussion for the Optimum Minkowski Reflectarray Antenna	37
 CHAPTER 4	
A NOVEL DESIGN APPROACH USING HYBRID GA-NM OPTIMIZATION BASED ON COMPLETE MLP ANN MODEL	
	43
4.1 Introduction.....	43
4.2 Reflection Phase Characterization of Minkowski Unit Element	44
4.3 MLPNN Black-box modeling in the analysis	45
4.4 The Optimization of Minkowski Element using the Memetic Algorithm	49
4.4.1 Objective Function	49
4.4.2 The Memetic Algorithm.....	50
4.4.3 Tolerance analysis of the optimization.....	54
4.5 Design and Analysis of Minkowski RA with Fully-Optimized Parameters .	56
4.6 Circular Polarization Characteristics of Fully-Optimized Minkowski RA...	62
 CHAPTER 5	
CONCLUSION.....	65
REFERENCES	67
CURRICULUM VITAE.....	71

LIST OF SYMBOLS

c	Speed of light in free space
e	Electron charge
f	Frequency
D	Vertical edge size of array surface
F	Focal distance of feed antenna
f_r	Resonance frequency
h	Substrate thickness
k	Propagation constant in the medium
m	Length of the patch
M	Number of divisions in x-direction
N	Number of division in y-direction
n	Cavity ratio of minkowski patch
ε	Dielectric permittivity
ε_e	Effective dielectric permittivity
ε_r	Relative dielectric constant of the substrate
η_s	Spillover efficiency
η_t	Taper efficiency
γ_g	Propagation constant in waveguide
λ_0	Free space wavelength
λ_r	Wavelength in the substrate
μ	Dielectric permeability
δ	Loss angle

LIST OF ABBREVIATIONS

ANN	Artificial Neural Networks
CST	Computer Simulation Technology
GA	Genetic Algorithm
MLP	Multi Layered Perceptron
MRA	Microstrip Reflectarray Antenna
MWS	Microwave Studio
NASA	National Oceanic and Atmospheric Administration
NM	Nelder-Mead
NN	Neural Networks
PBC	Periodic Boundary Condition
PSO	Particle Swarm Optimization
RA	Reflectarray Antenna
SLL	Side Lobe Level

LIST OF FIGURES

		Page
Figure 1.1	Waveguide reflectarray antenna with staggered rows [5]	2
Figure 1.2	Reflectarray using a 4-arm spiral as element with switching diodes at center to achieve a 2-bit phase-shift system for circular polarization [4] ...	3
Figure 2.1	Reflectarray radiating elements [4]	7
Figure 2.2	Basic geometry of a MRA	8
Figure 2.3	Differential spatial phase delay of reflectarray [4]	13
Figure 2.4	Coordinate system for pattern analysis of RAs	15
Figure 3.1	Waveguide one-port with the TEM mode propagation boundary conditions to determine the amplitude and phase of the reflected wave from a minkowski unit cell	19
Figure 3.2	Geometry of minkowski shape	20
Figure 3.3	6 x 5= 30 minkowski configuration set for each substrate ($\epsilon_r = cont, h$) and frequency (f) sampling couple	21
Figure 3.4	Black-box analysis model of a minkowski radiator A: $\mathfrak{M}\{\mathfrak{R}^4\} \Rightarrow \phi\{\mathfrak{R}^1\}$	22
Figure 3.5	The Structure of MLP NN model for minkowski patch including 4 input and 1 output neurons with 2 hidden layers both of 10 neurons	23
Figure 3.6	Mean squared error variation of the MLPNN model of the minkowski RA	24
Figure 3.7	Linear regression scattering plot for minkowski ANN model (a)training and (b) testing, (training MSE error = 3.5992×10^{-4} , testing MSE error = 4.0192×10^{-4})	25
Figure 3.8	Reflection phase characteristics of the minkowski patch radiator against the patch length due to the $f = 11$ GHz, $\epsilon_r = 3.54$ (Taconic RF-35) and, $h = 1.25$ mm, taking different the iteration factor n values.	26
Figure 3.9	Reflection phase characteristics of the minkowski patch radiator against the patch length at the $f = 11$ GHz, $\epsilon_r = 3.54$ (Taconic RF-35), taking parameters; iteration factor n for the substrate thickness $h = 1.5$ mm; ...	26
Figure 3.10	Reflection phase characteristics of the minkowski patch against the patch length due to the $f = 11$ GHz, $\epsilon_r = 3.54$ (Taconic RF-35) and, $h = 1.75$ mm, taking different the iteration factor n values.	27
Figure 3.11	Reflection phase characteristics of the minkowski patch against the patch length due to the $f = 11$ GHz, $\epsilon_r = 3.54$ (Taconic RF-35) and, $n = 0.45$, taking different the substrate thickness h values.	27
Figure 3.12	Reflection phase characteristics of the minkowski patch radiator against the patch length at the $f = 11$ (GHz), $\epsilon_r = 3.54$ (Taconic RF-35), taking parameters; the substrate thickness h for the iteration factor $n = 0.75$	28

Figure 3.13	Testing performance of MLP NN in comparison between target and reconstructed data	29
Figure 3.14	Comparison of reflection phase values w.r.t m (patch variation) and η (iteration factor) for $h = 1.52$ (mm), $f = 10.5$ GHz with (a) the target data; (b) the reconstructed data	30
Figure 3.15	Comparison of reflection phase values w.r.t m (patch variation) and η (iteration factor) for $h = 1.524$ mm, $f = 11.5$ GHz with (a) the target data; (b) the reconstructed data	31
Figure 3.16	Flow chart of the PSO Algorithm [51]	33
Figure 3.17	Convergence curve for the PSO of the minkowski element ($n_{opt} = 0.7891$, $h_{opt} = 1.4516$ mm) with the resulted value of the objective 4.2×10^{-8}	34
Figure 3.18	According to optimum parameters $f = 10.875$ GHz $n = 0.7891$ ($h = 1.4516$ mm) reflection characteristics of the minkowski Reflectarray element by comparison with square patch on the Taconic RF-35 ($\epsilon_r = 3.54$) substrate	34
Figure 3.19	A General design procedure for a minkowski reflectarray antenna	35
Figure 3.20	2-D view of the center feed reflectarray antenna geometry [53].....	36
Figure 3.21	Phase compensation variation with respect to the radial distance for $F/D = 0.8$ at various operation frequencies	37
Figure 3.22	The 15×15 microstrip reflectarray antenna (a) minkowski (b) square with the optimum parameters ($n_{opt} = 0.789$, $h_{opt} = 1.4516$ mm, $FD = 0.8$) on 20×20 cm, $\epsilon_r = 3.54$ (Taconic RF-35).....	38
Figure 3.23	Effect of the feed movement on the max. gain variations of the 15×15 minkowski RA with the optimum parameters $n_{opt} = 0.789$, $h_{opt} = 1.4516$ mm on $\epsilon_r = 3.54$ (Taconic RF-35) for different F/D ratios within the X-band frequency range	38
Figure 3.24	Effect of the feed movement on radiation pattern of the 15×15 minkowski RA at 11 GHz with the optimum parameters $n_{opt} = 0.789$, $h_{opt} = 1.4516$ mm on $\epsilon_r = 3.54$ (Taconic RF-35).....	39
Figure 3.25	Comparative radiation patterns of the optimized and non-optimized 15×15 minkowski RAs for the various values of (h, n) sets for $F/D = 0.8$ at 11 GHz.....	40
Figure 3.26	Comparison of radiation patterns for the 15×15 minkowski, square reflectarray and the parabolic reflector antennas for parameters; $h_{opt} = 1.4516$ mm, $n_{opt} = 0.7891$ mm, $\epsilon_r = 3.54$ (Taconic RF-35).....	41
Figure 4.1	Black-box model II.....	45
Figure 4.2	The MLP NN structure	46
Figure 4.3	Linear regression scattering plots for the complete minkowski MLP model (a) Training (MSE= 9.9564×10^{-5}) and (b) Validation (MSE= 1.7264×10^{-4}).	46
Figure 4.4	Reflection phase characteristics taking dielectric property as parameter for (a) $h = 1$ mm, $n = 0.60$, $f = 11$ GHz; (b) $n = 0.90$, $\epsilon_r = 3$, $f = 11$ GHz; (c) $\epsilon_r = 3$, $h = 1.5$ mm, $f = 11$ GHz.	48
Figure 4.5	3-D reflection phase variations versus the patch width m and the relative permittivity of substrates, ϵ_r for the fixed conditions of $h = 1.5$ mm, $n = 0.6$, $f = 11$ GHz for (a) target and (b) reconstructed data.	49
Figure 4.6	Convergence performances of the genetic and memetic optimization.....	52

Figure 4.7	Reflection characteristics of the optimum minkowski reflectarray element with the parameters of $\epsilon_r = 3.1694$, $h_{opt} = 1.7916$ mm, $n_{opt} = 0.8438$ at $f=11$ GHz as compared with the square patch's values having the same resonance frequency.	53
Figure 4.8	Sensitivity analysis results for the optimum dielectric constant for the standard deviation (sigma) values: (a) $\sigma = 0.01$, (b) $\sigma = 0.05$ (c) $\sigma = 0.1$ at $f=11$ GHz.	55
Figure 4.9	Comparison of the reflection phase responses for unit cell element designed with optimized parameters and two equivalent commercially available substrates	56
Figure 4.10	Required compensation phases for 15x15 minkowski RA with $F/D= 0.8$ at 11 GHz.....	57
Figure 4.11	A general design procedure for a minkowski reflectarray antenna.....	58
Figure 4.12	(a) Fully-optimized RA with $\epsilon_{r,opt} = 3.1694$, $h_{opt} = 1.7916$ mm, $n_{opt} = 0.8438$; (b) Non-optimized RA with $\epsilon_r = 2.2$, $h = 1.5$ mm, $n = 0.90$	59
Figure 4.13	Realized gain versus frequency graphs for the fully optimized RA and the other RAs on the different substrates with the optimized parameters (n_{opt}, h_{opt})	61
Figure 4.14	Realized gain versus frequency variations for the comparison of fully optimized RA with only patch geometry n_{opt} optimized RAs on the given dielectric permittivity ϵ_r and substrate thickness h	61
Figure 4.15	Vector illustration of circular slant polarization.....	62
Figure 4.16	Circular polarization characteristics of optimized minkowski RA at 11 GHz for slant angle= 15°	63
Figure 4.17	Circular polarization characteristics of fully-optimized minkowski RA at 11 GHz for slant angle= 30°	63
Figure 4.18	Circular polarization characteristics of fully-optimized minkowski RA at 11 GHz for slant angle= 45°	64

LIST OF TABLES

		Page
Table 3.1	Typical results for comparison of target and reconstructed data.....	28
Table 3.2	Reflection phase with optimum parameters; $f = 10.875$ GHz, $\epsilon_r = 3.5$ (Taconic RF-35), $n_{opt} = 0.7891$, $h_{opt} = 1.4516$ mm,	35
Table 3.3	Typical phase compensation values at various operation frequencies	37
Table 3.4	Radiation pattern characteristics of the 15x15 minkowski reflectarray antenna with the optimum parameters: $n_{opt}=0.789$, $h_{opt} = 1.4516$ mm ..	39
Table 3.5	Comparison of the radiation pattern characteristics of the 15x15 minkowski, square reflectarray and the parabolic reflector antennas	41
Table 4.1	Comparison for reconstructed data by ANN with the simulated data for conditions $f=11$ GHz, $n = 0.75$, $h=1.524$ mm, $\epsilon_r=3.54$ (Taconic RF-35) and the measured results in [41].....	47
Table 4.2	3-D EM simulated reflection phases of the optimum MRA and constructed phases by the complete ANN response at $f=11$ GHz	53
Table 4.3	Performance comparison of the fully optimized reflectarray with a non-optimized reflectarray.....	60
Table 4.4	Comparison of the fully optimized RA and the other RAs designed on the different substrates with same optimized parameters (n_{opt} , h_{opt})	60
Table 4.5	Comparison of the Fully Optimized RA and RAs with the optimized minkowski shapes on the traditional substrates.....	62
Table 4.6	Circular polarization characteristics of fully-optimized minkowski RA...	64

ABSTRACT

ANALYSIS AND SYNTHESIS OF REFLECTARRAY ANTENNA

Selahattin NESİL

Department of Electronics and Communication Engineering

PhD. Thesis

Adviser: Prof. Dr. Filiz GÜNEŞ

Co-adviser: Prof. Dr. Bahattin TÜRETKEN

In this thesis, a design, optimization and analysis methodology, which is a novel, robust and systematic, is presented for an X-band microstrip reflectarray antenna (MRA). In this work, the two microstrip reflectarray designs have been carried out. The purpose of this thesis is to design a microstrip reflectarray, which has better radiation performance by determining the optimal geometry for the reflective patch element and dielectric substrate properties. In the designing of MRA, the most important and critical stage is the selection of patch element and its design optimization. In this work, the minkowski shape, which is from the first iteration of fractals, has been utilized as the radiating element, because of it has wider phase range in the linear region. In the first design, the reflection phase characterization of the minkowski unit element, which is placed at the end of the H-wall waveguide simulator on the substrate Taconic RF-35 ($\epsilon_r=3.54$, $\tan\delta=0.018$), has been generated as a nonlinear variation function. This function was generated by 3-D EM simulations based on Computer Simulation Technology Microwave Studio (CST MWS) for the continuous domain of the patch geometry and substrate sizes within X-band region centered at resonant frequency. Thereafter, the Multi-Layer Perceptron Neural Network (MLP NN) model have been created to characterize the minkowski RA unit element. Following that, the Particle Swarm Optimization (PSO) has been utilized to optimize the minkowski reflectarray with simplified multi-objective functions to determine the phase calibration characteristic having the maximum phase range and the slower gradient. In the design stage, the MLP NN model has been used as reverse model to determine the variable-size of each reflectarray element by providing the necessary phase delay with the adaptive iterative step. Thus, the minkowski reflectarray antenna, which is designed with optimum parameters, has been analysed using the 3-D CST simulations and has been compared with the counterpart square and parabolic reflector antennas. In the second design, a novel multi-objective design optimization procedure is generated for the

minkowski reflectarray using a complete 3-D CST MWS- based MLP NN model including the dielectric constant of substrate, ϵ_r via hybrid combination of Genetic (GA) and Nelder-Mead (NM) algorithms. Herein, the performed MLP NN model has been an accurate and fast model to get the reflection phase of minkowski RA element as a continuous function with the input domain including the substrate characteristics ($1 \leq \epsilon_r \leq 6$; $0.5 \text{ mm} \leq h \leq 3 \text{ mm}$), within the X-band frequency region. Finally, a design of a fully optimized X-band 15×15 minkowski RA is performed and so compared with the both optimized and non-optimized RAs on selected traditional substrates. In addition to optimization process, the tolerance analysis has been performed in order to specify the tolerance limits of optimized design and the commercially available substrate options. Consequently, this design approach enables a designer to obtain not only the most optimum minkowski RA design all throughout the X-band, at the same time the optimum minkowski RAs on the selected substrates.

Key words: ReflectarrayAntenna, Microstrip ReflectarrayAntenna, H-wall Waveguide Simulator, Artificial Neural Network, Multilayer Perceptron Neural Network, Minkowski Shape, Particle Swarm Optimization, Genetic and Nelder–Mead Algorithms, Antenna Optimization.

YANSITICI DİZİ ANTEN ANALİZ VE SENTEZİ

Selahattin NESİL

Elektronik ve Haberleşme Mühendisliği Anabilim Dalı

Doktora Tezi

Tez Danışmanı: Prof. Dr. Filiz GÜNEŞ

Eş Danışman: Prof. Dr. Bahattin TÜRETKEN

Bu tezde, bir X-band mikroşerit yansıtıcı dizi anten (MRA) için özgün, sağlam, sistemli bir tasarım, optimizasyon ve analiz yöntemi sunulmuştur. Bu çalışmada, iki tane mikroşerit reflectarray tasarımı gerçekleştirilmiştir. Bu tezin amacı; en uygun yansıtıcı yama elemanı geometrisi ve dielektrik alt-tabaka özelliklerinin belirlenmesi ile daha iyi radyasyon performansına sahip bir mikroşerit yansıtıcı dizi anten tasarlamaktır. MRA tasarımında, en önemli ve kritik aşama yama elemanın seçimi ve tasarım optimizasyonudur. Bu çalışmada, standart yansıtıcı dizi yama elemanı (kare yama) ile karşılaştırıldığında doğrusal bölgede daha geniş bir faz aralığına sahip olduğundan dolayı birinci fraktaller iterasyondan olan minkowski şekli yansıma elemanı olarak kullanılmıştır. İlk tasarımda, bir H-wall dalga kılavuzu simülatörü sonunda Taconic RF-35 ($\epsilon_r=3.54$, $\tan\delta=0.018$) üzerine yerleştirilen minkowski birim elemanının yansıma faz karakterizasyonu, doğrusal olmayan bir varyasyon fonksiyonu olarak elde edilmiştir. Bu fonksiyon, X-bandı bölgesi içinde rezonans frekansı merkezli yama geometrisi ve alt tabaka boyutlarının sürekli etki alanı için Computer Simulation Technology Microwave Studio (CST MWS) programına dayalı 3-D EM simülasyonlarla elde edilmiştir. Daha sonra, Çok Katmanlı Algılayıcı Yapay Sinir Ağı (MLP NN) modeli minkowski yansıtıcı dizi birim elemanını karakterize etmek için oluşturulmuştur. Bunu takiben, Parçacık Sürü Optimizasyonu (PSO) maksimum faz aralığı ve daha yavaş bir değişim ölçüsüne sahip faz kalibrasyon özelliğini saptanması için basitleştirilmiş çok amaçlı işlevleri ile minkowski yansıtıcı dizi anteni optimize etmek için kullanılmıştır. Tasarım aşamasında, MLP NN modeli uyarlanabilir iteratif adım ile gerekli faz gecikmesini sağlayarak yansıtıcı dizi antenin her bir elemanının değişken boyutunu belirlemek için ters model olarak kullanılmıştır. Böylece, optimum parametrelerle tasarlanmış minkowski reflectarray anten, 3-D CST simülasyonları kullanılarak analiz edilmiş ve muadili kare ve parabolik yansıtıcı antenler ile karşılaştırılmıştır.

İkinci tasarımda, minkowski yansıtıcı dizi anten için alt-tabakanın dielektrik sabiti, ϵ_r de dahil olmak üzere 3-D CST MWS tabanlı bütün bir MLP NN modeli kullanılarak için Genetik (GA) Nelder ve Mead (NM) algoritmalarının hybrid kombinasyonu ile yeni çok amaçlı bir tasarım optimizasyonu prosedürü oluşturulmuştur. Burada gerçekleştirilen MLP NN, minkowski yansıtıcı dizi elemanın yansıma fazını elde etmek için X-bant frekans bölgesinde alt-tabaka karakteristikleri ($1 \leq \epsilon_r \leq 6$; $0.5 \text{ mm} \leq h \leq 3 \text{ mm}$) dahil olmak üzere giriş alanı ile sürekli bir fonksiyon olarak doğru ve hızlı bir model olmuştur. Son olarak, tamamıyla optimize edilmiş bir 15×15 X-band minkowski yansıtıcı dizi anten tasarımı gerçekleştirilmiş ve de seçilen geleneksel alt-tabakalar üzerinde hem optimize edilmiş hem de optimize edilmemiş yansıtıcı dizi antenler ile karşılaştırılmıştır. Optimize tasarımın limitlerini ve ticari olarak elde edilebilir tabaka seçeneklerini belirlemek için optimizasyon işlemine ilave olarak tolerans analizi gerçekleştirilmiştir. Sonuç olarak, bu tasarım yaklaşımı bir tasarımcı için sadece tüm X-bandı boyunca en optimum minkowski yansıtıcı anten tasarımı değil aynı zamanda seçilen yüzeylerde de optimum tasarım yapma imkanı sunmaktadır.

Anahtar Kelimeler: Yansıtıcı Dizi Anten, Mikroşerit Yansıtıcı Dizi Anten, H-Wall dalga kılavuzu simülatörü, Yapay Sinir Ağı, Çok Katmanlı Algılayıcı Sinir Ağı, Minkowski, Parçacık Sürü Optimizasyonu, Genetik ve Nelder-Mead Algoritmalar, Anten Optimizasyonu.

INTRODUCTION

1.1 Literature Review

High-gain antennas are more important part of the telecommunications systems that require a significant amount of size and mass [1]. Several satellite communication and radar systems are in need of high gain antennas. In general, parabolic reflectors and array antennas have been used for high gain applications from past to present [2], [3]. But, the production of parabolic reflector with its curved surface has been complex and difficult at higher microwave frequencies. Moreover, the parabolic reflector does not have capable of wide-angle electronic beam scanning. On the other hand, the high gain array antennas enable the electronically wide-angle beam scanning with the controllable phase shifters [4]. But they generally have been very expensive with high-cost amplifier modules and complicated beam former circuits. In the early 1960s, the academic researches focused to eliminate the disadvantages of the parabolic reflector and the array antennas. As a result, the reflectarray antenna (RA) concept has been introduced in 1963 by Berry, Malech and Kennedy [5]. The studies conducted up to the present shows that the reflective array antenna has a chronological change and development process with three different main approaches as the basis of the light of technological developments on the other sciences. Short-ended waveguide elements with variable-length waveguides were used to demonstrate the capability of achieving co-phase reradiated far-field beams [4], [6]. The electromagnetic waves from the feed horn illuminate and couple into the waveguides from the open ends and travel as in transmission lines down to the other shorted ends. The shorted ends reflect all signals and reradiate out from the open ends. By controlling the lengths of individual waveguide elements, the phases of the reradiated signals could be appropriately adjusted to form a desired beam in the far-field distance. But using waveguide array

antenna reflector design, even in low-frequency applications in the wireless communication antenna structure consists of bulky in size, which has sustained the validity of a maximum of ten years.

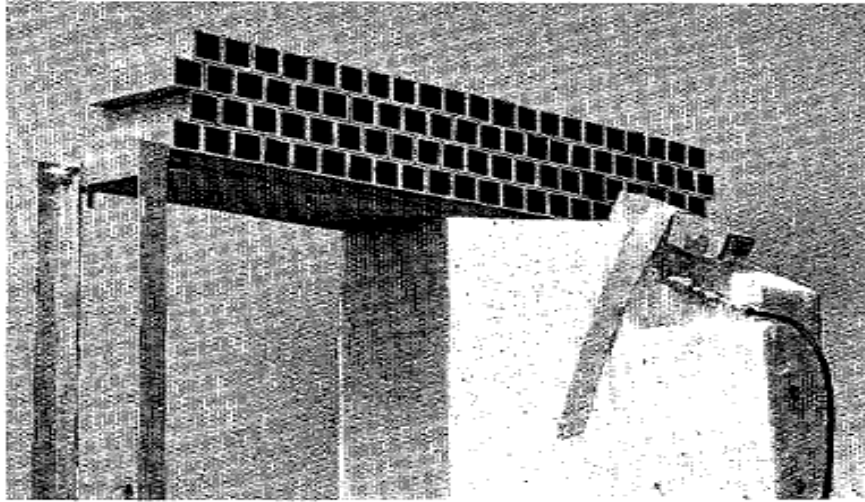


Figure 1.1 Waveguide reflectarray antenna with staggered rows [5]

As the second reflectarray antenna approach, in the mid - 1970s, a very clever concept of “spiral phase ” reflectarray was developed by Phelan [4], [7], where switching diodes, as illustrated in, were used in a four - arm spiral or cross - dipole element of a circularly polarized reflectarray to electronically scan its main beam to large angles from the broadside direction. To activate different pairs of spiral arms by switching diodes, can be adjusted to create a co-phases not-only far-field beam phase, but it is also possible to electronically scan a wide beam angles. But, the spiral phase reflectarray was still bulky and heavy because of its thick spiral cavity and large components. Because of these disadvantages, the interest in this approach did not last more than ten years, and recent studies have not been performed.

The third main and final approach for the RAs is that the reflector element can be used as a microstrip patch. In 1978, the first M. Hajian has proposed that this approach could be applied [7]. In the same year, the first analysis of MRA was realized by Montgomery using an infinite array approach. But, the real interest for this type antenna began with the development of the printed circuit board technology in the late 1980s. Munson et al. have received a patent in 1987 by designing a MRA for satellite communications and radar applications [4], [6]. In this design, the planar reflecting surface is comprised of an array of microstrip patches, loaded with stubs of varying lengths for adjusting the reflection phase.



Figure 1.2 Reflectarray using a 4-arm spiral as element with switching diodes at center to achieve a 2-bit phase-shift system for circular polarization [4]

The interest in MRAs began to increase in the early 1990s. In the early 1990s, to reduce the antenna size and weight was carried out various applications. The printed RA in various structures was obtained by using the flat surface, low profile, light weight reflective surfaces [8]-[14]. The identical patch elements or open-circuit elements having different phase delays have been used in the first implementations. The side-lines for phase delay were in size up to half a wavelength or less. These side-lines are used to supply to the elements that create the different path lengths to compensate the phase differences. The RA can be formed co-phase radiation beam in the far-field in accordance with concordantly design of all the side-lines [1], [4]. In 1993, the applied second method was that the printed dipoles with different lengths were used as the reflective element. This development in the RA had shown that this application can be set an equivalent efficiency as an identical RA comprising variable-length of lines.

In 1995, Huang obtained and developed co-phase radiation beam in the far field by applying the angular rotation technique in identical RA with the circular polarized microstrip patch elements [4]. Along with the beginning of the 2000s, the developments in reflectarray antennas began to accelerate. Some new techniques have been applied to improve the antenna performance. The stacked patches were used on the multilayer surface for improving the bandwidth of RA [15].

Nowadays, the studies have been carried out to optimize the reflective element of RA [16]. In this way, the overall efficiency of the antenna can be improved. The most critical component of RA is its reflector element. This element may vary depending on a number of different parameters. These parameters are features such as the electrical conductivity of reflective surface, the thickness of the substrate, the element size, the incident angle, the main beam direction and bandwidth. The optimization of the antenna gain and side lobe level (SLL) may be provided with the some optimization methods by considering all these parameters. However, the applications oriented with optimization of MRA in the literature are limited and do not include the broad scope. So, the activities to be undertaken in this area are of great importance in terms of the future for the development of MRA.

1.2 Objective the Thesis

In this thesis, it is aimed to design a microstrip reflectarray, which has better radiation performance by determining the optimal geometry for the reflective patch element and dielectric substrate properties. In the designing of MRA, the most important and critical stage is the selection of patch element and its design optimization. If the element design is not optimized, the reflectarray will not scatter the signal from the feed effectively to form an efficient far-field beam. Thus, “phasing” is very important process in designing reflectarray [1], [4], [17]-[22]. In literature different approaches of compensating the phase of each element have been proposed, however phasing method using the variable size patches is preferable choice in many designs due to its simplicity [9]-[13], [23]. Furthermore, it is needed to perform a model as fast as a coarse and as accurate as so that they can be utilized efficiently within an optimization procedure to determine the calibration phasing characteristic belonging to the resultant optimum patch geometry and substrate. The necessary phase shift at each element is obtained by varying one of the geometrical parameters in the reflectarray element [24]-[26].

Since it is simple to manufacture the MRA on a single layer, in order to satisfy requirements as the capability to radiate a shaped beam or multi-beams, or also to enhance the frequency behavior and bandwidth, the advanced patch configurations are necessary to be worked out in which the structure has a lot of degrees of freedom and all concur to the performances of the whole antenna. The management of different parameters and the need of satisfying requirements that could be also in opposite each

other could however make the design of a reflectarray quite complex. Therefore first of all for a computationally efficient optimization process, an accurate and rapid model for the reflection phase of a unit element is needed to establish it as a continuous function in the input domain of the patch geometry and substrate variables.

1.3 Hypothesis

This thesis is organized in three parts which include the main steps for designing MRA. The first part of thesis consists of Chapter 1 and 2. A brief review of the literature about reflectarray antennas is given in Chapter 1. A detailed development history of the reflectarray since its invention is hereafter, the objective and structure of the thesis are presented on the other hand. The second part consisting of Chapter 3 and 4 is dedicated to design and analysis stage of the thesis. Finally, the third part covers the Chapter 5 and summarizes the accomplishments acquired from the design approaches in this thesis.

The organization of the thesis is briefly explained as follows: in Chapter 2, an overview of the reflectarray antenna is given. The advantages and disadvantages of microstrip reflectarray antennas are discussed in more detail. This chapter will help to the readers who are strange about the thesis topic for understanding the reflectarray system. Chapter 3 presents the first design application of this thesis. In this chapter, a systematic design optimization procedure and analysis is presented for a minkowski reflectarray. This chapter introduces a new design and analysis concept for the microstrip reflectarray antennas. Chapter 4 deals with the design and analysis of a fully optimized 15x15 minkowski reflectarray antenna. A robust methodology for design optimization of the microstrip RAs is presented. The first stage of the chapter is to build a rapid and accurate ANN model for the reactive impedance behavior of a minkowski unit element. The next is the design stage of the reflectarray having 15×15 minkowski interspaced by half-wavelengths at 11 GHz using again its MLP NN model. In this stage, the different designs are made corresponding to the fully or partially optimized antenna parameters. In the final stage, performance analyses of the designed RAs are made employing the 3-D CST MWS simulations, compared, and discussed. Finally, conclusions, achievements and observations acquired by the thesis, are addressed in Chapter 5.

FUNDAMENTALS OF REFLECTARRAY ANTENNAS

2.1 Reflectarray Antenna Concept

The concept of reflectarray antenna has been around for several decades. Reflectarray antenna that emerged as a result of the researches oriented to eliminate the disadvantages of the parabolic antennas and planar array antennas [4], [5]. Reflectarray antennas designed with microstrip patch elements provide low profile reflection surface, a smaller antenna size, and low cost. The printed reflectarray can be designed to have very high gain with relatively good efficiency, as well as to have its main beam tilted/scanned to large angles from its broadside direction.

Reflectarray antennas regarded as new generation antenna type having the reflective elements on a flat reflection surface [1], [4], [6]. On the reflecting surface, there are many isolated microstrip patch elements without any power division network. This surface reflects the incident EM waves in the desired certain direction as co-phase by forming the appropriate phase delay. The total re-radiated energy will be non-co-phase if all the elements and their terminations are identical. This is because the fields that propagate to the elements from the feed have different path lengths, and thus form different phases. The required path delay-compensating phases from the elements are achieved primarily via the differing lengths of the dipoles. Different lengths yield different input impedances (complex quantity) at a particular frequency, which in turn give different phases.

Each patch is attached a short segment of phase-adjusting transmission line to compensate for the phase delay over the path from the illuminating feed. Because of the phase adjustment capability of the patch elements, the reflecting surface can be flat or conformal to its mounting structure and still maintain a constant phase aperture field.

Planar reflectarray antennas are manufactured on a plate using printed circuit technology [1], [4], [6]. The radiating elements of the reflectarray antenna are placed as series on the reflective surface. These elements can be open or short circuit termination waveguides, printed microstrip patches, dipoles, ring or dielectric resonator antennas (Figure 2.1). The prime feature of this antenna is that have the ability of adjusting the phase of the reflected wave with a variety of methods.

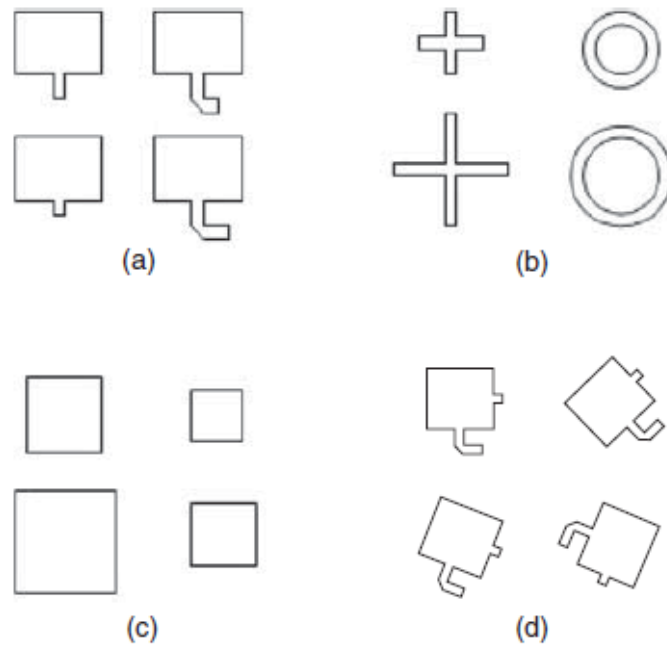


Figure 2.1 Reflectarray radiating elements [4]

2.2 Microstrip Reflectarray Antennas (MRA)

The printed MRA applications can be considered as fairly new research area for antenna community [4], [27], [28]. The rapid development in microstrip antenna technology has led to the use of microstrip antennas in a variety of reflectarray configurations. The MRAs have many advantages that can be categorized into two points of view which are from electromagnetically and mechanically. From an electromagnetically perspective, they are high gain antennas, low side lobes, capable of beam steering, and from a mechanically perspective, they have lightweight structures, easy to fabricate and manufacture and robust. Microstrip elements are frequency sensitive and for large apertures, distance differential delays between the feed and points on the surface can reach several wavelengths. It is well known that when a required antenna gain is given at a particular frequency, the antenna aperture size is more or less fixed. The only

significant size reduction that may be achieved for an antenna is its profile thickness. The flat-plate microstrip reflectarray offers such an advantage of profile size reduction as compared to a conventional parabolic reflector.

The MRA, being one of the printed low-profile antenna technologies, consists of a very thin, flat reflecting surface and an illuminating feed (Figure 2.2). There are many isolated microstrip patch elements on the reflecting surface without any power division network. They are designed to reflect the incident wave independently with a phase shift proportional to the distance by the phase center of the feed–horn to form a pencil beam in a specified direction (θ_0, ϕ_0) as is well-known from the classic phased array theory. Alternatively, contoured beams can be generated by implementing the appropriate phase distribution, obtained by a phase-only synthesis method. For the design of the reflectarray, any possible value of the phase-shift must be implemented by varying one parameter in the unit cell, such as the patch resonant dimensions, stub length, or patch rotation angle.

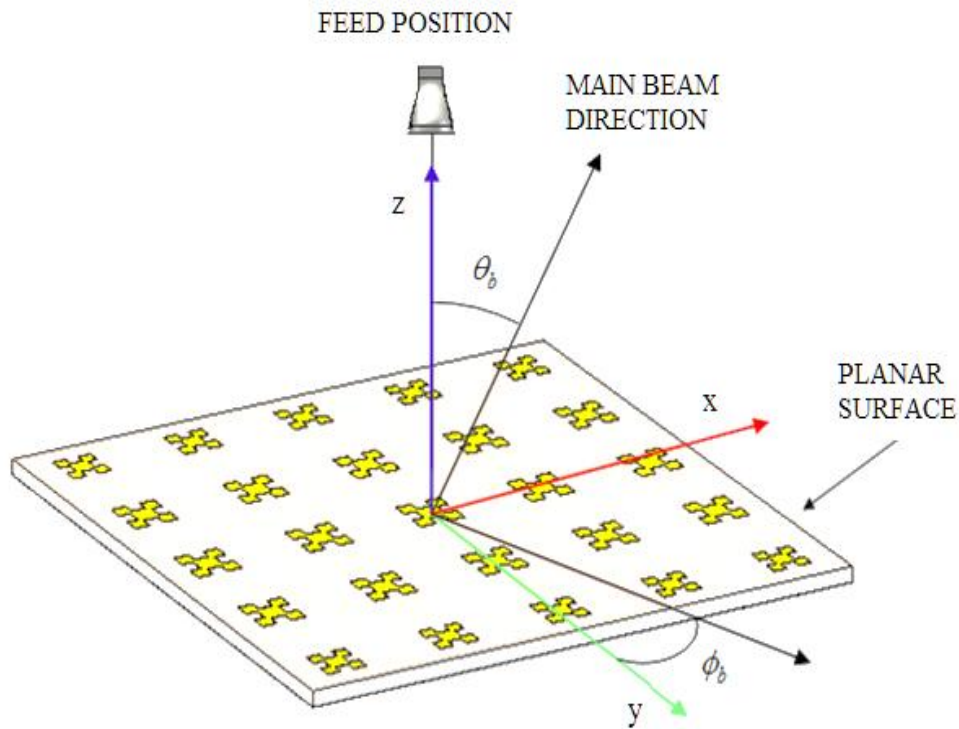


Figure 2.2 Basic geometry of a MRA

2.2.1 Advantages of MRA

Microstrip Reflectarray Antenna provides a low profile reflection surface, smaller size and low cost specifications when it is designed with printed reflective elements [4], [10]-[16]. because of its thin and flat reflecting surface, the antenna can be mounted more easy onto a vehicle, spacecraft, building walls. In particular, the MRAs are aesthetically pleasing in appearance, lightweight and compact, and have good efficiencies and high gains. One of the significant advantages due to the large antenna aperture is required curved parabolic reflector according to a flat structure easier and more reliable mechanism can be formed is manufactured. Thus, The phase variation caused by the curved structure can be compensated by a number of techniques. The reflectarray provides very good efficiency (>50%) like as a parabolic reflector for a very large aperture since no power divider is needed and thus very little resistive insertion loss is encountered here [4], [6], [8]. On the other hand, the reflectarray can have its main beam designed to tilt at a large angle (>50°) from its broadside direction same as a phased array antenna. The elements on the MRA consists low-loss electronic phase shifters for wide-angle electronic beam scanning. One specific advantage of the printed reflectarray is that the flat surface of the reflectarray allows a much simpler and reliable folding mechanism compared with that required for the doubly curved surface of a parabolic reflector when a large aperture (e.g., 10 m size) antenna requires a deployment mechanism. The flat reflecting surface of the reflectarray also lends itself for flush mounting onto an existing flat structure without adding significant amount of mass and volume to the overall system structure. A reflectarray with hundreds or thousands of elements, being in the form of a printed microstrip antenna, can be fabricated with a simple and low-cost. Another major feature of this antenna is that, with a large number of elements in a reflectarray having elemental phase adjustment capability, it can achieve very accurate contour beam shape by using a phase synthesis technique. Multiple-beam capability can also be performed by placing multiple feed elements at the focal area of the antenna like as the parabolic reflector. As well as at the millimeter-wave frequencies, the reflectarray technology can be applied throughout the microwave spectrum, [4], [8], [9].

2.2.2 Disadvantages of MRA

The most critical disadvantage of MRA is the bandwidth limitation. The bandwidth of MRA is mainly related and determined by the bandwidth of the single element. This is its inherent characteristic of microstrip patches. In general, it cannot exceed much beyond ten percent depending on its element design, aperture size, focal length, etc. [4]. For a printed microstrip reflectarray, its bandwidth is primarily limited by two factors. One is the narrow bandwidth of the microstrip patch elements on the reflectarray surface and the other is the differential spatial phase delay. The microstrip patch element generally has a bandwidth of about 3-5%. To achieve wider bandwidth for a conventional microstrip array, techniques such as using thick substrate for the patch, stacking multiple patches, and using sequentially rotated sub-array elements have been employed. The second reflectarray limiting factor, the differential spatial phase delay [29]. This will be discussed in detail in section 2.3.2.

2.3 MRA Design and Analysis Techniques

For each MRA element, the characteristic of the electric field depends on the position of the feed and radiation pattern. Generally, in practice the horn antenna is preferred for feeding network of MRA, because the horn antenna has high efficiency, less loss, high gain and also it is not affected by external noises. For a horn antenna, the radiation pattern its radiation is modeled as a $\cos^q(\theta)$ function [30]-[36] in the feed coordinate system as given in (2.1) and (2.2).

For an x-polarized ideal feed, the radiated field is given by (2.1) and for a y-polarized feed by (2.2):

$$E^{Fx}(\theta, \varphi) = \frac{jke^{-jkr}}{2\pi r} \left[(\cos^{qE}(\theta) \cos \varphi) \vec{a}_\theta - (\cos^{qH}(\theta) \sin \varphi) \vec{a}_\varphi \right] \quad (2.1)$$

$$E^{Fy}(\theta, \varphi) = \frac{jke^{-jkr}}{2\pi r} \left[(\cos^{qE}(\theta) \cos \varphi) \vec{a}_\theta - (\cos^{qH}(\theta) \sin \varphi) \vec{a}_\varphi \right] \quad (2.2)$$

An axial symmetric pattern is usually desirable, and the same q power is chosen in both planes, $q^E = q^H = q$.

In general, the feed may be positioned at center focal distance or an arbitrary angle from reflectarray surface. It is assumed to be far enough from the reflectarray so that the incident field can be approximated by a plane wave. Linear, dual and circular

polarization can be obtained. Since it is desired to form a planar phase surface in front of the aperture, one of the key feature of MRA is how the individual elements can be made to scatter with a desired phase. There are a number of different techniques to control the phase. One method is to use identical elements with variable length stubs to control the reflection phase [1], [4], [5]. Usually this is not the optimal approach since the delay lines require space and as its length increases it becomes part of the radiating process. A better and successful approach is done by using patches with variable sizes [1], [4]-[12]. Another method is done by rotating the antenna element. The feeding techniques of MRA are similar to the parabolic reflector antennas. In general, a horn- or waveguide feed antennas are used for MRA measurements. The feed is placed at the focal point of the antenna which is usually is at the far-field of MRA. Thus, the MRA is illuminated with the plane waves.

Reflectarray antenna efficiency is determined by the two primary factors very similar to the parabolic reflector [1], [4]. The efficiency of MRA is formed by the aperture illumination and the feed spillover efficiency efficiencies. The aperture illumination efficiency is caused by the unequal illumination of the array aperture due to the feed's tapered pattern. For this feed pattern the spillover and amplitude taper efficiencies can be found in closed-form expressions. The illumination efficiency for a center-fed reflectarray can be obtained in a closed form as given in (2.3) [1]:

$$\eta_i = \frac{\left[\left(\frac{1 - \cos^q \theta_e}{q} \right) + \left(\frac{1 + \cos^{q+1} \theta_e}{q+1} \right) \right]^2}{2 \tan^2 \left[\left(\frac{1 - \cos^{2q+1} \theta_e}{2q+1} \right) \right]}, \quad (2.3)$$

and the spillover efficiency is given in (2.4) [1]:

$$\eta_s = 1 - \cos^{2q+1} \theta_e, \quad (2.4)$$

The feed pattern is assumed as $\cos^q(\theta)$ function to illustrate the spillover and illumination efficiencies. θ_e is half of the subtend angle from the feed to the reflectarray aperture.

2.3.1 H-wall waveguide simulator technique

For the design of the reflectarray, any possible value of phase-shift must be implemented by varying one parameter in the unit cell, such as the patch size, stub length, or patch rotation angle [1], [4], [10]-[14]. To compose the reflection phase of the

radiating elements, using an H-wall waveguide simulator is the very popular approach, also called parallel-plate waveguide simulator, where the top and bottom surfaces of the waveguide are electric conducting walls, while the right and left walls are magnetic field walls. Vertically polarized waves in the direction element will be scattered from the end of the waveguide edge and the amplitude and phase information of a specific sequence back to the broadside direction. This H-wall waveguide simulator, however, can only calibrate the reflectarray element for the normal incident case. Although this is adequate, more accurate results could be achieved by calibrating the element with various incident angles. Each waveguide can only simulate one incident angle at one frequency. Several different waveguides need to be constructed in order to calibrate the element with several sets of calibration data for several different incident angles. Techniques are used to derive the phase-versus-element-change curve, which is generally an S-shaped curve with nonlinear relationship.

To achieve a larger phase shift, techniques such as using thin substrate for the patch, stacking multiple patches and proposing a new kind of patch have been employed. However, multilayer configurations are costly and generally impractical. By decreasing the substrate thickness, a larger phase variation can be achieved. However, the bandwidth becomes narrower. Therefore, novel, complicated patch configurations are needed to be worked in which the structure to be optimized presents a lot of degrees of freedom and all concur to the performances of the whole antenna.

2.3.2 Infinite Array Approach

Infinite array approach was carried out to analyze the microstrip reflectarray element by Montgomery [4], [6]. The infinite array approach can be used in principle for any type of phase delay element. In this approach, the current distribution on a single radiator element in the array is first obtained. From the current coefficients obtained, the reflection phase and the scattered fields of the reflectarray are then approximated. Mutual coupling between array elements is accounted for through Floquet modal formulations. A similar infinite periodic array approach was employed by Johansson in his analysis and design of quasi-periodic planar reflectors, but with additional formulations included for first-order diffracted fields [37]-[39]. For multilayered microstrip reflectarray, on the other hand, the generalized scattering matrix for analyzing periodic structures may be utilized, as proposed by Encinar [4], [6].

2.3.3 Path Length and Phase Shift

The gain bandwidth of a microstrip reflectarray is dependent on the compensation mechanism for unequal path delay between its feed and the elements across its flat reflector that is used to convert the spherical wave into a plane wave. The path lengths from the feed to all radiating elements are all different. They have different phase delays. These elements must have corresponding phase advancements designed in accordance with its uniquely calibrated phase design curve to compensate for the phase delays. This curve will be different for different types of elements used. But, they generally have an S-shaped curve. The differential spatial phase delay, ΔS , is graphically represented in Figure 2.3.

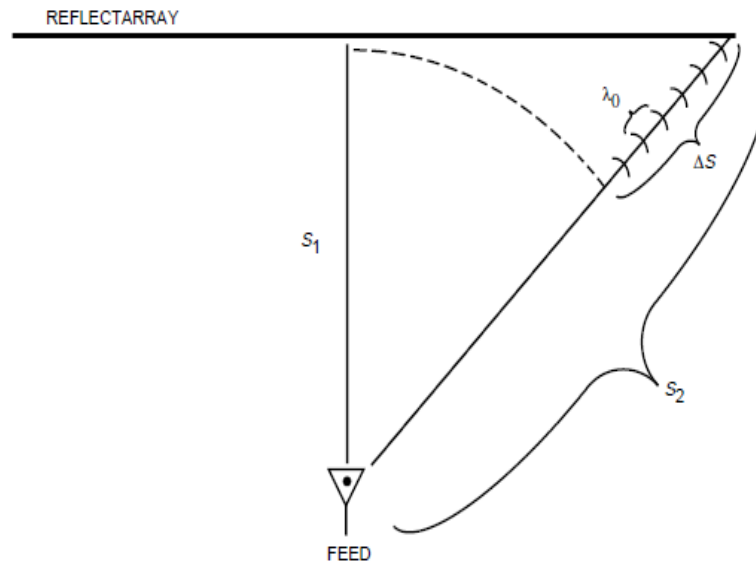


Figure 2.3 Differential spatial phase delay of reflectarray [1]

The differential spatial phase delay is the phase difference between the two paths S_1 and S_2 from the feed to the reflectarray elements. At the center frequency, the many multiples of the wavelength (λ) give us this ΔS . This phase delay can be expressed as $\Delta S = (N + d)\lambda$. In here, N refers as integer and d is a fractional number of a free-space wavelength, λ . At each element location, d is compensated by an appropriate phase delay achieved by the reflectarray element design (achieved by variable patch size, variable phase delay line length, etc.). As the frequency changes, the factor $(N + d)$ becomes $(N + d)(1 + \Delta)$. Since the design and the compensating phase for each element are fixed for the center frequency, a frequency excursion error will occur in the reradiated phase front. The amount of phase change in each path when compared with a

reference path, say SI , is $(N + d) \Delta \lambda$ which can be a significant portion of a wavelength or 360° [1], [4]-[8].

The differential path length for each element is given as [4]:

$$\Delta L_{m,n} = L_{m,n} - L_{0,0} \quad (2.5)$$

where $L_{m,n}$ is the path length between the feed and the m th element, which can be obtained by a simple geometry calculation. $L_{0,0}$ is the distance between the feed and a reference point on the reflectarray surface. $\Delta L_{m,n}$ is thus the differential feed path length for the m th element. To achieve a collimated radiation, the phase advancement $\Delta \phi_{mn}$ needed for the m th element is given by [4]

$$\Delta \phi_{mn} (\text{°}) = \left[\frac{\Delta L_{m,n} - \text{integer of } (\Delta L_{m,n})}{\lambda_0} \right] \times 360 \quad (2.6)$$

The above indicates that the compensating phase can be repeated every 360° and the portion that is integer multiple of a wavelength or 360° can be deleted. It is difficult to convert a spherical wave generated by the feed into a plane wave over a large frequency band. In order to get this relation over a limited band, a suitable path length correction mechanism is required. One possible method to provide this compensation is through the phase shift that can be generated using its elements. The phase-shift that must be introduced at each element to produce a collimated beam in a given direction. Considering the coordinate system detailed in Figure 2.2, the progressive phase distribution on the reflectarray surface that produces a beam in the direction (θ_b, ϕ_b) , as known from array theory is referred as [1], [4]-[6]:

$$\phi(x_i, y_i) = -k_0 \sin \theta_b (\cos \phi_b x_i + \sin \phi_b y_i) \quad (2.7)$$

where k_0 is the propagation constant in vacuum, and (x_i, y_i) the coordinates of i^{th} element. The phase - shift required at each element is obtained [1], [4]:

$$\phi_{mn} (\text{°}) = k_0 (d_i - \sin \theta_b (x_i \cos \phi_b + y_i \sin \phi_b)) \quad (2.8)$$

where d_i is the distance from the phase center of the feed to the cell.

2.4 Radiation Pattern Analysis of Reflectarray Antennas

The innovative architectures and technologies have to control the radiation efficiently and to make reflectarrays more performing and competitive [6]. The accurate calculation method is required to get far-field radiation patterns of a reflectarray. So the main beam width and direction, side lobe level, cross-polarization level, and directivity can be accurately predicted for the system. Conventional array theory is usually used to calculate the radiation pattern of the reflectarray antenna in the far-field, where the radiations of all elements are summed together [1], [4], [8]. A sample planar array consisting of $M \times N$ elements that are non-uniformly illuminated by a low-gain feed is depicted in Figure 2.4.

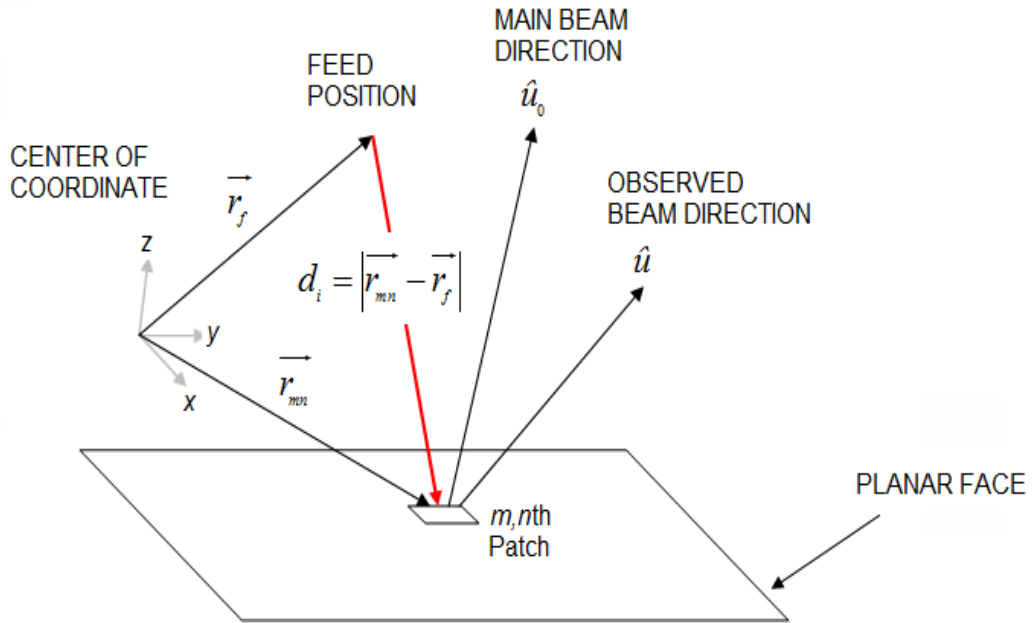


Figure 2.4 Coordinate system for pattern analysis of RAs

Thus, the far-field of the reflectarray in the \hat{u} direction will be of the generated as;

$$E(\hat{u}) = \sum_{m=1}^M \sum_{n=1}^N F(\vec{r}_{mn} \cdot \vec{r}_f) \cdot A(\vec{r}_{mn} \cdot \hat{u}_0) \cdot A(\hat{u} \cdot \hat{u}_0) \cdot \exp\left[-jk_0 \left(|\vec{r}_{mn} - \vec{r}_f| + \vec{r}_{mn} \cdot \hat{u}\right) + j\alpha_{mn}\right] \quad (2.9)$$

where F is the feed pattern function, A is the reflectarray element pattern function, r_{mn} is the position vector of the mn^{th} element, and α_{mn} is the required compensating phase of the mn^{th} element [1], [4], [38], [39]. In(2.9), only the number of array summation technique is used without taking into account the mutual coupling and scattering effects

between elements. The good main beam, beam direction, and general pattern shape can be calculated by this formula; but it does not give accurate side lobe and cross-polarization characteristics because there are numerous radiating elements on the reflectarray surface [4]. There are two radiation patterns calculation techniques as quite accurate. One of them is the infinite array approach that mentioned before in section 2.3.2. In this technique, firstly the single element pattern of the reflectarray is calculated by assuming it is in an infinite array environment with all surrounding elements identical. This single element pattern is then summed together for all the elements by using the formula similar to generate a far-field pattern. Thus, the element function, A in (2.9) will contain mutual coupling effects with some approximation in an infinite array environment. In the second technique, the single element pattern is calculated by including all mutual coupling effects of only the nearby surrounding elements. The Method of Moments solution is used. The range of nearby elements number changes from several to 50. It is depending on the type of used elements and the main beam angle. These elements are not identical but are the actual on the reflectarray. The resulting single element pattern is then summed together by using (2.9) to calculate a far-field pattern. This method, although more accurate, is more simple because all elements with unique surrounding elements throughout the entire array need to be calculated [1], [4]-[10].

DESIGN AND ANALYSIS OF MINKOWSKI RA USING PARTICLE SWARM OPTIMIZATION BASED ON MLP NN

3.1 Introduction

In this chapter, a systematic design optimization procedure and analysis is presented for a Minkowski reflectarray. It has been also working out for a 3-D EM simulation based ANN model of reflective phasing of the Minkowski radiator. Minkowski shape is from the first iteration of fractals and the Minkowski radiator is shown to have an optimum phasing characteristic with the large linear region and easy fabrication [40]-[42]. Thus, it can briefly be summarized in the following stages:

The first stage is the analysis stage of the reactive impedance behavior of a reflectarray element. Thus, its reflection phase is established as a highly nonlinear function within the continuous domain of the element geometry and substrate parameters in a defined bandwidth centered the resonant frequency employing the 3-D Computer Simulation Technology Microwave Studio (CST MWS)-based Multi-Layer Perceptron Neural Network (MLPNN);

The second stage is the optimization stage where the phase calibration characteristic is determined among the phasing characteristics established in the first stage, as the one having slower gradient with respect to the geometry and substrate thickness and the wider range to achieve a wider operational bandwidth and smaller susceptibility to manufacturing errors. In this process PSO algorithm is employed and thus the optimum geometry and substrate parameters are resulted for the synthesis of the reflectarray antenna;

The third stage is the design stage of the reflectarray having 15×15 Minkowski radiators with n_{opt} and interspaced by 0.5 wavelengths at frequency 11 GHz on the Taconic RF-

35 with $\varepsilon_r = 3.5$, $\tan\delta = 0.0018$ and the optimum thickness (h_{opt}). This stage may be considered to be consisting of the following steps: first step, the phase distribution is obtained throughout the reflectarray evaluating the necessary phase compensation for each element depending on its position for a certain F/D ratio where F and D values are respectively, the focal feed length and array diameter [20], [21]. In the following step, the variable size of each reflectarray element is determined to meet the necessary phase delay by the reversing the MLP NN analysis model where the other input parameters are fixed to their optimal values; In the final step, radiation features of the designed reflectarray are obtained employing the 3-D Computer Simulation Technology Microwave Studio (CST MWS).

3.2 Reflectarray Element Design Analysis

3.2.1 Generation of the Training and Validation Data

The fine discretization training and validation data set for the reflection phase φ_{11} of a reflectarray element, being a function of the element's geometry (m, n) and the substrate parameter (h). It is obtained by the 3-D EM simulator CST MWS considering a unit cell equivalent of an infinite periodic array of identical elements on which a plane wave of given polarization is incident [8], [10]-[15]. In order to work out the phase characteristics, only the case of a vertically polarized (in-Y direction) TEM plane wave (Figure 3.1) that is normally incident on an infinite periodic array of identical elements is considered. Restricting these considerations to the TEM case is motivated by the fact that it provides a good approximation to the phase range and slope for the cases of TEM, TE and TM wave incidence for an angle up to 30° from the reflectarray bore sight direction [10-18].

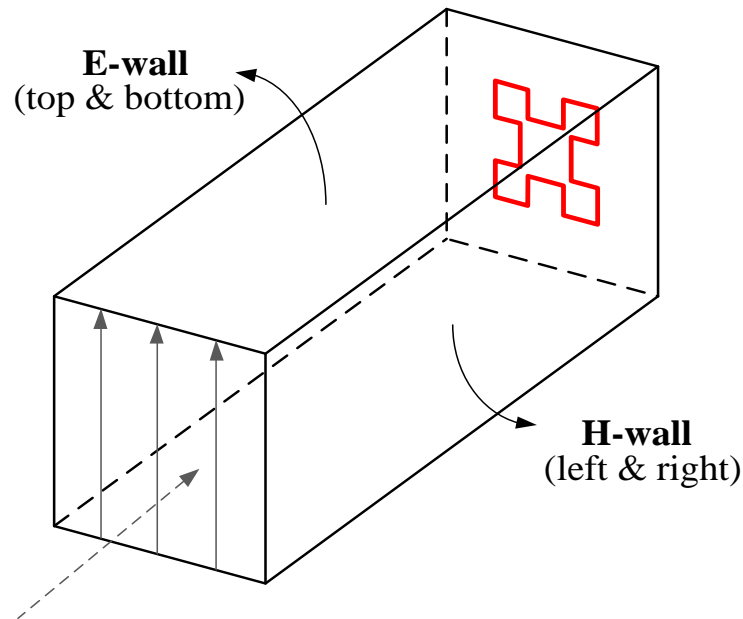


Figure 3.1 Waveguide one-port with the TEM mode propagation boundary conditions to determine the amplitude and phase of the reflected wave from a minkowski unit cell

Figure 3.1 shows the rectangular waveguide one-port that has been used to design and analysis a reflectarray element and the boundary conditions in the simulation set up for TEM-mode propagation subject to the infinite array approach. The sidewalls of the waveguide are formed by a perfect magnetic conductor while its bottom and top walls are composed of a perfect electric conductor. The vertically polarized incoming waves will see the element at the end of the waveguide at the broadside direction and then scattered back at the broadside direction with a set of amplitude and phase information [8-15].

Thus, the amplitude and phase of the reflected wave at each element is determined as the amplitude and phase of the scattering parameter S_{11} for the waveguide one-port containing this element. The structure is analyzed and simulated using the 3-D CST MWS.

The goal of the training process is to find the set of weight values that will cause the output from the neural network to match the target values as closely as possible. There are several issues involved in designing and training a multilayer perceptron network. First we need to select how many hidden layers to use in the network. Second we have to decide how many neurons to use in each hidden layer. After that we need to be found a globally optimal solution that avoids local minima. Then we can converge to an

optimal solution in a reasonable period of time and finally validate the neural network to test for over fitting.

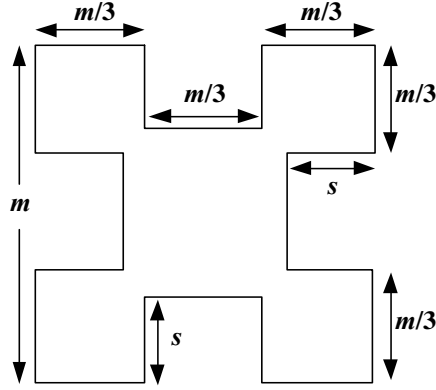


Figure 3.2 Geometry of minkowski shape

The iteration factor n is defined as the ratio between the geometry parameters of the minkowski patch as in [40]:

$$n = \frac{s}{m/3}, \quad 0 \leq n \leq 1 \quad (3.1)$$

where m is the patch length, s is the cavity parameter of the patch in Figure 3.2.

Sampling process can briefly be explained as follows: The operation bandwidth is swept as the intervals of 1 GHz and the resulted number of the sample frequencies is $f_s = 5$. Similarly, the substrate thickness is sampled as the intervals of 0.25 mm between the 0.5 and 3 mm range and the total number of the thickness sampling is $h_s = 11$. Simultaneously, $n_s \times m_s$ minkowski configurations are generated for each sampled substrate ($\epsilon_r = const, h$) at each sampling frequency where $n_s = 6$ and $m_s = 5$ are the number of samples for the iteration factor and patch width, respectively. Figure 3.3 depicts $n_s \times m_s$ minkowski configuration set with respect to the relation in (3.1) for each substrate ($\epsilon_r = const, h$) and frequency sampling couple, where m is swept by %10 around the resonant length which is $m = 5.41$ mm while n is swept by an interval of 0.15 between 0.15 and 0.90. Thus, the entire minkowski space is discretized totally into the $f_s \times h_s \times m_s \times n_s = 1650$ minkowski configurations.

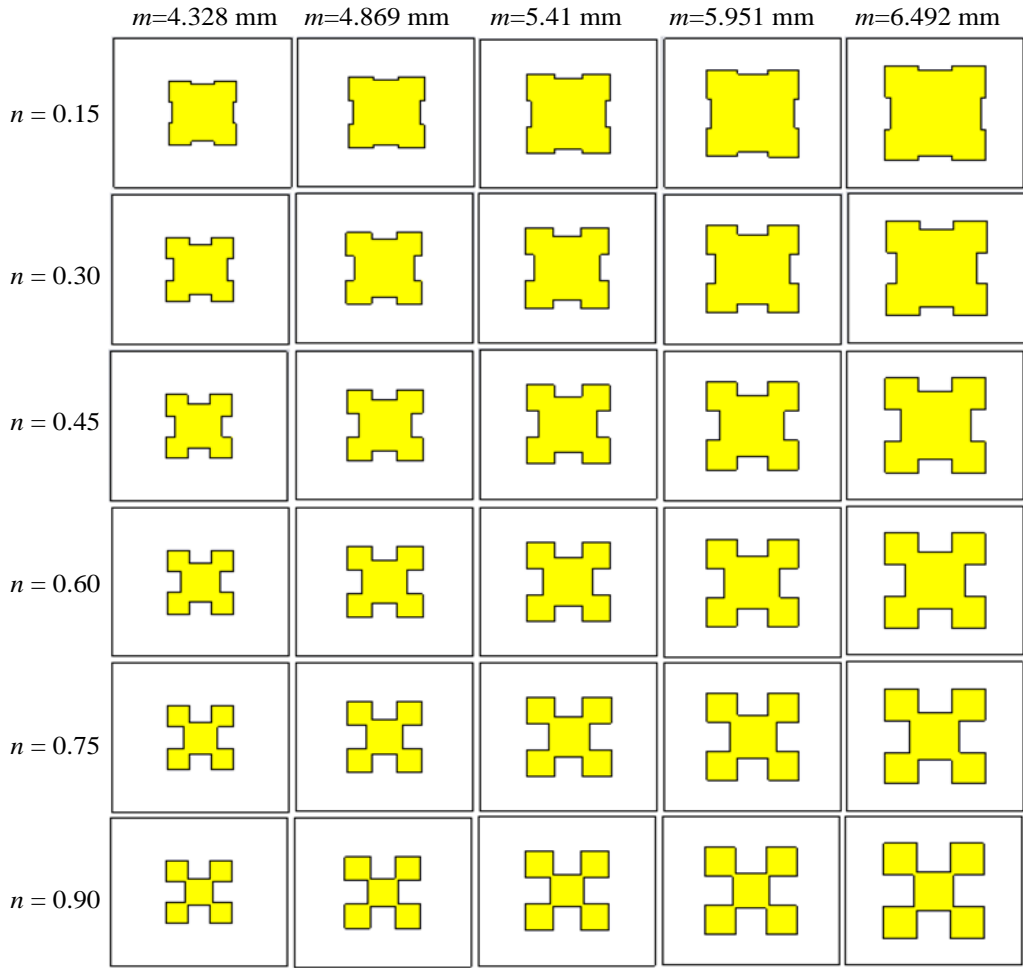


Figure 3.3 6 x 5= 30 minkowski configuration set for each substrate ($\epsilon_r = cont, h$) and frequency (f) sampling couple

3.2.2 Black-Box Model

In this work, the MLP is employed as a universal function approximator to express the reflection phase (ϕ_{11}) of a single element as a continuous function in the design variable domain defined by the element's geometry parameters (m, n), the substrate thickness (h), and frequency (f) within their given limitations. Thus, the 4-dimensional minkowski space is mapped into the one-dimensional reflection phase space by this MLP black-box analysis model in Figure 3.4.

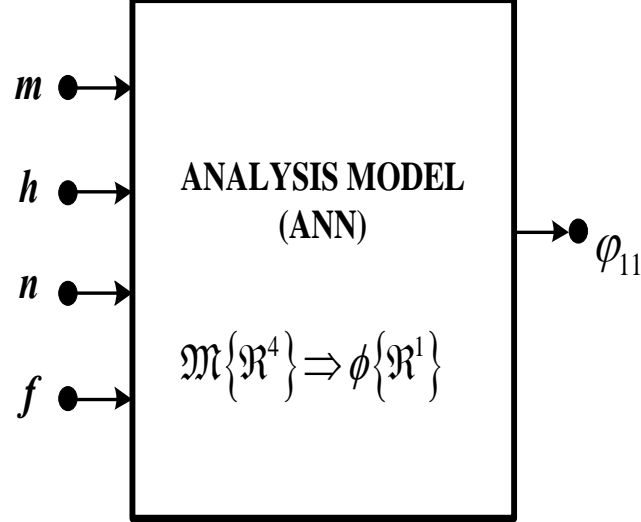


Figure 3.4 Black-box analysis model of a minkowski radiator A: $\mathfrak{M}\{\mathfrak{R}^4\} \Rightarrow \phi\{\mathfrak{R}^1\}$

Typically, a Multilayer Perceptron (MLP) is a feed forward distributed information processing system consisting of an input layer, one or more hidden layers and an output layer. The processed information is available at the output end of the neuron. The processing mechanism of a MLP can be found in the pioneer works in [43]-[49].

Let n and m number of the input and output neurons, thus let \vec{x} be n - vector containing the external inputs to the neural network and \vec{y} be an m -vector containing the outputs from the output neurons and \vec{w} be a vector containing all the weight parameters representing the connections in the neural network. The function $\vec{y} = \vec{y}(\vec{x}, \vec{w})$ mathematically represents a neural network [45], [46].

During the training process, the neural network performance is evaluated by computing the difference between the actual neural network outputs and desired outputs for all the training samples [45], [49]. The difference, also known as the error is quantified by

$$E = \sum_{k \in T_r} \sum_{j=1}^m (y_j(\vec{x}_k, \vec{w}) - d_{jk})^2 \quad (3.2)$$

where d_{jk} is the j th element of the \vec{d}_k , $\vec{y}_j(\vec{x}_k, \vec{w})$ is the j th neural network output for the input \vec{x}_k , and T_r is an index set of the training data. The weight parameters \vec{w} in (3.2) are taken account as the optimization variables during the optimization process with the use of either gradient or non-gradient optimization algorithm such that the error given by (3.2) is minimized.

Thus, the modeling problem,

$$\vec{x}=[m,n,h,f]^t, \quad \vec{y}=[\varphi_{11}]^t \quad (3.3)$$

In (3.3), the input \vec{x} is a 4-dimensional vector consisting of the geometry parameters (m,n) , the substrate thickness (h) and the operation frequency (f) , and the output vector \vec{y} has a unique element, which is the reflection phase (φ_{11}) of the unit cell element. Moreover, the MLPNN model of the unit minkowski element has two hidden layers, each of which has 10 neurons (Figure 3.5). The first hidden and the second hidden layer neurons are activated by the logarithmic sigmoid function and tangent sigmoid function respectively.

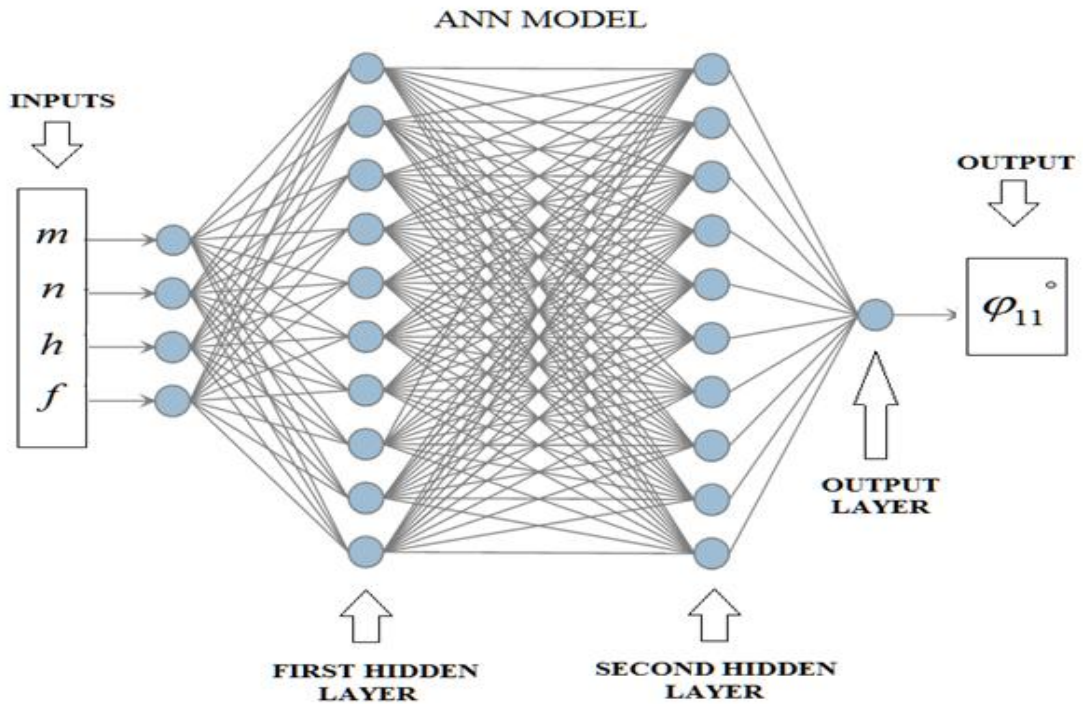


Figure 3.5 The Structure of MLP NN model for minkowski patch including 4 input and 1 output neurons with 2 hidden layers both of 10 neurons.

The Levenberg Marquart algorithm is employed in determination of the weight parameters \vec{w} of the MLPNN. Total 1650 (\vec{x}_k, \vec{d}_k) data samples are obtained by 3-D EM simulator CST MWS using the minkowski unit cell within the 8-12 GHz bandwidth with respect to the geometry parameters of the patch (m,n) and thickness (h) of the selected substrate to be utilized as the 990 data for training and 660 data for validation.

3.2.3 Performance of the MLP Black Box Model

The overall performance of the MLP NN for Black Box Model is measured by the mean square error (MSE) expressed by:

$$mse = \frac{1}{N} \sum_{p=1}^{N_v} E_p = \frac{1}{N} \sum_{p=1}^{N_v} \sum_{i=1}^M (t_p(i) - y_p(i))^2 \quad (3.4)$$

E_p corresponds to the error for the P^{th} pattern, N_v refers training data set, t_p is the desired output and, y_p corresponds to the M -dimensional output vector from the trained network for the P^{th} pattern. Figure 3.6 gives the MSE evaluated by the (3.4) versus with the epoch number for the training and validation processes where the best performance has been obtained rapidly within 16 epochs and the MSE values are 3.5992×10^{-4} and 4.0192×10^{-4} for the training and validation processes, respectively. Moreover, the resulted respective linear scattering graphics are given by the Figure 3.7.

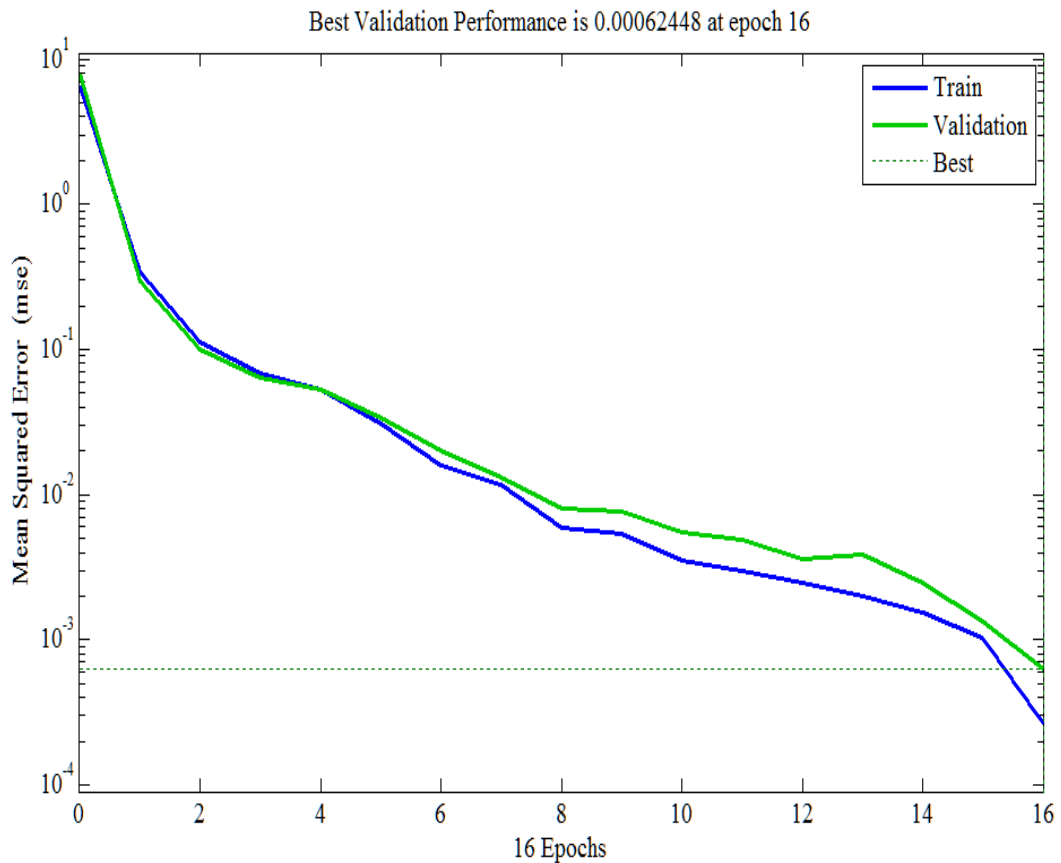


Figure 3.6 Mean squared error variation of the MLPNN model of the minkowski RA

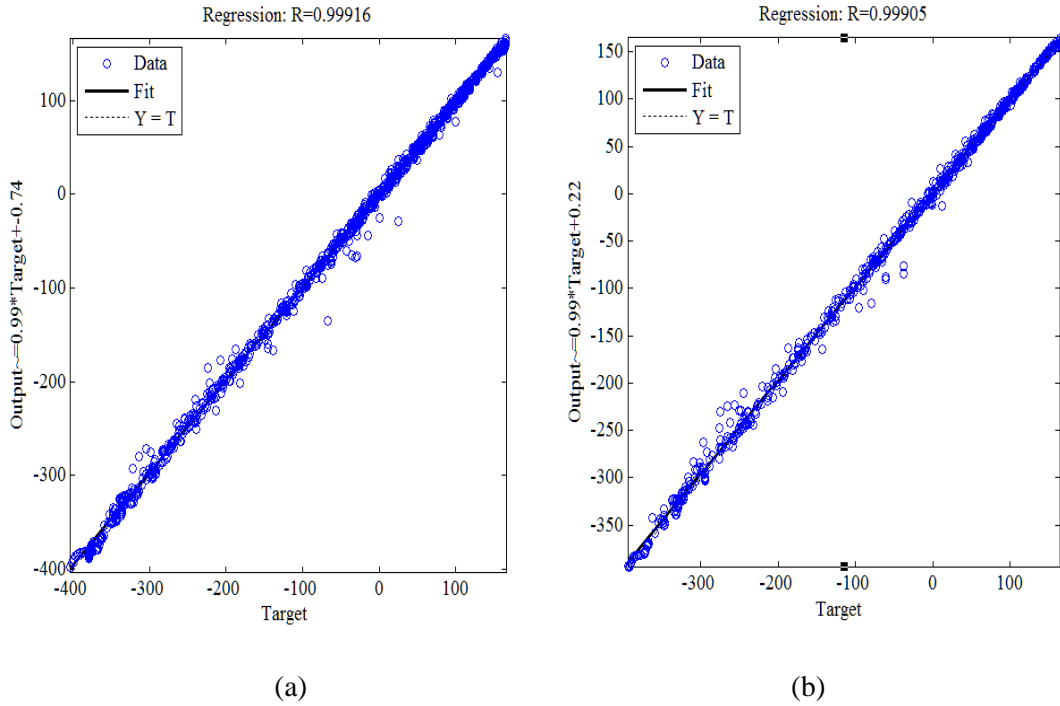


Figure 3.7 Linear regression scattering plot for minkowski ANN model (a)training and (b) testing, (training MSE error = 3.5992×10^{-4} , testing MSE error = 4.0192×10^{-4})

The reflection phase characteristic of a minkowski patch radiator is given in Figure 3.8 and Figure 3.9 by taking the different iteration factors, n for the fixed substrate thicknesses $h = 1.25$ mm and $h = 1.5$ mm respectively with respect to the patch length variations on the Taconic RF-35 with $\epsilon_r = 3.54$ at the resonance frequency $f = 11$ GHz. In comparison, the minkowski patch has a lower phase range when the iteration factor, $n = 0.15$, while it has a larger phase range when the iteration factor, $n = 0.90$. However, it has slower gradient and larger phase range when the iteration factor, $n = 0.75$. In addition, the reflection phase characteristic of minkowski patch is also given in Figure 3.10 and Figure 3.11 for the various substrate thicknesses, h with the iteration factors, $n = 0.45$ and $n = 0.75$ respectively. It can be observed that, the phase of the reflection coefficient undergoes the usually performed change of less than 360° when the element size is changed. Furthermore, Table 3.1 gives typical phase values for $n = 0.75$ and $h = 1.5$ mm at $f = 11$ GHz for comparison the reconstructed data with the target data and the corresponding values found and measured by Zubir [41]. It is observed that reconstructed data are especially agreed with the measured values.

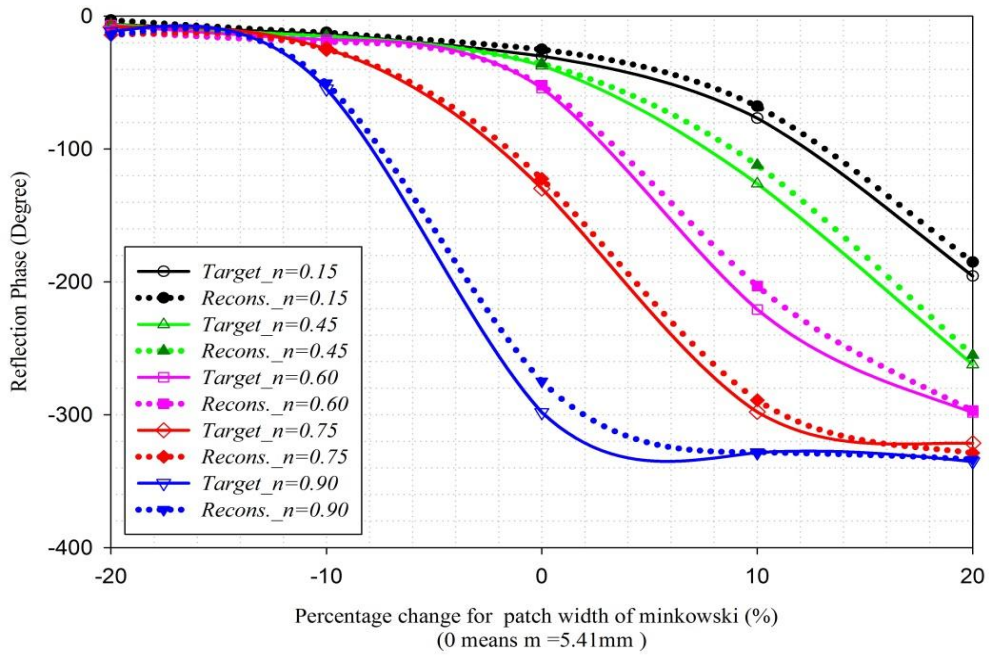


Figure 3.8 Reflection phase characteristics of the minkowski patch radiator against the patch length due to the $f = 11$ GHz, $\epsilon_r = 3.54$ (Taconic RF-35) and, $h = 1.25$ mm, taking different the iteration factor n values.

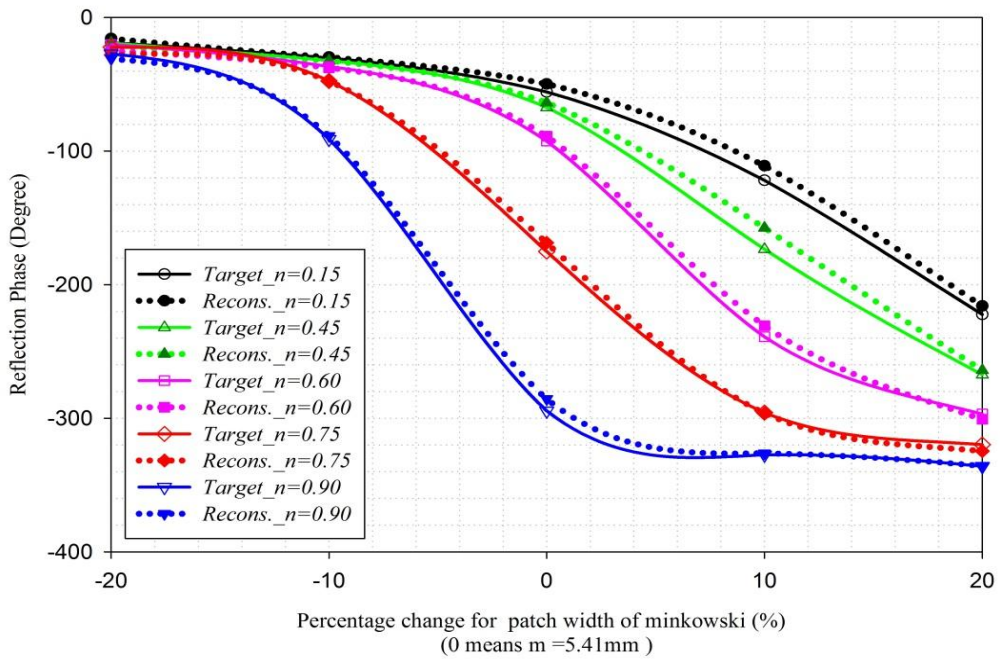


Figure 3.9 Reflection phase characteristics of the minkowski patch radiator against the patch length at the $f = 11$ GHz, $\epsilon_r = 3.54$ (Taconic RF-35), taking parameters; iteration factor n for the substrate thickness $h = 1.5$ mm;

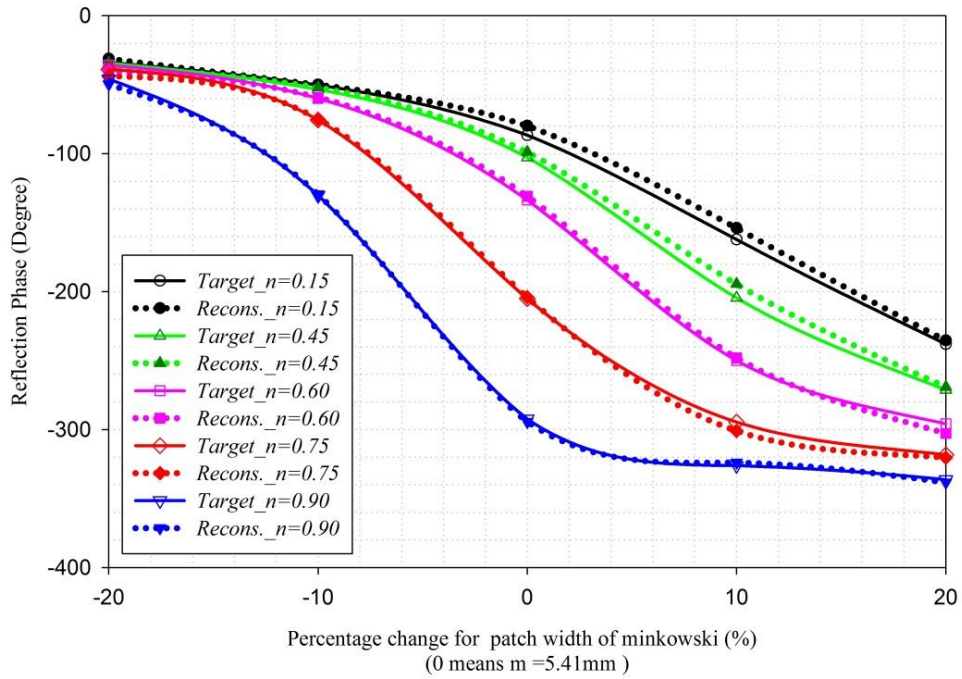


Figure 3.10 Reflection phase characteristics of the minkowski patch against the patch length due to the $f = 11$ GHz, $\epsilon_r = 3.54$ (Taconic RF-35) and, $h = 1.75$ mm, taking different the iteration factor n values.

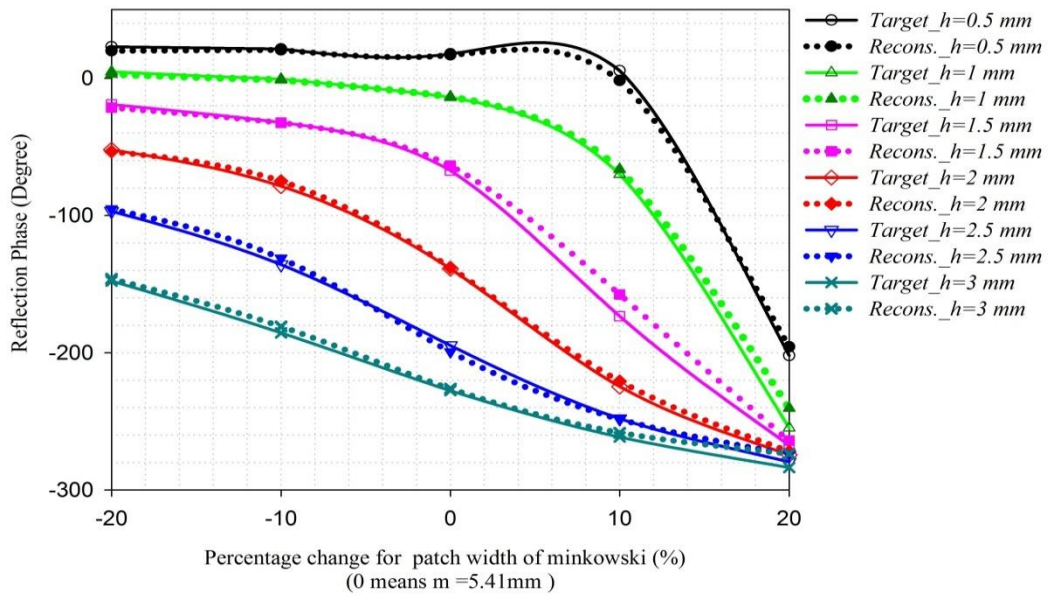


Figure 3.11 Reflection phase characteristics of the minkowski patch against the patch length due to the $f = 11$ GHz, $\epsilon_r = 3.54$ (Taconic RF-35) and, $n = 0.45$, taking different the substrate thickness h values.

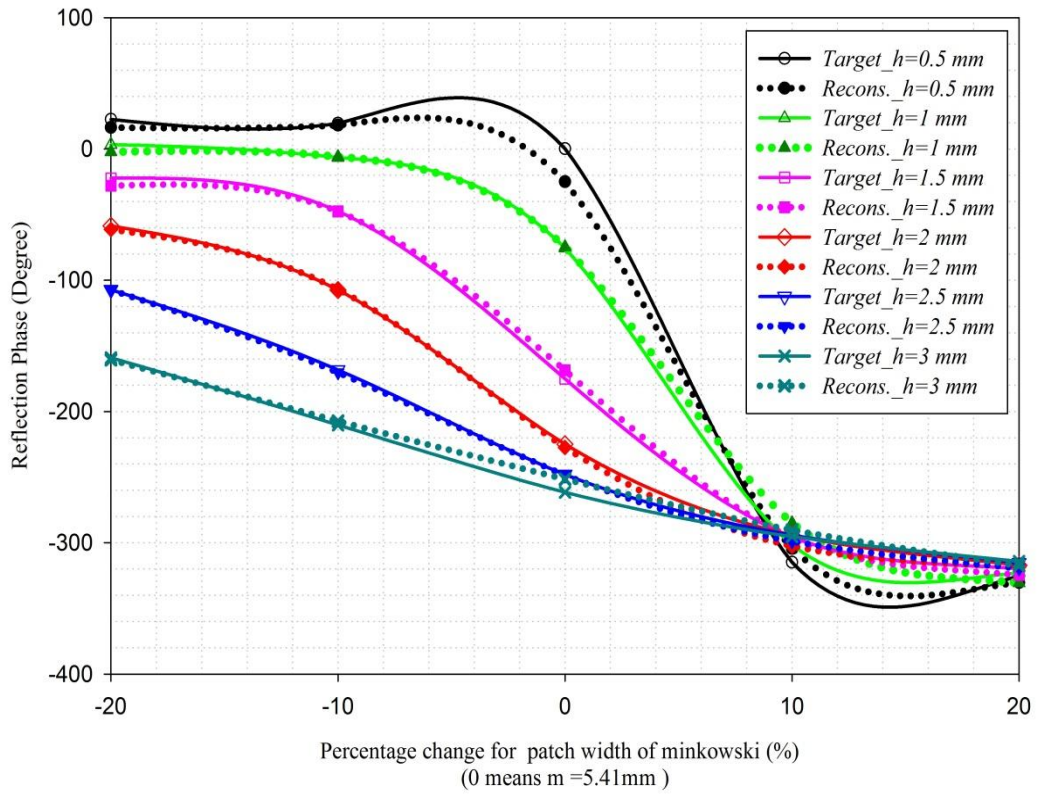


Figure 3.12 Reflection phase characteristics of the minkowski patch radiator against the patch length at the $f=11$ GHz, $\epsilon_r=3.54$ (Taconic RF-35), taking parameters; the substrate thickness h for the iteration factor $n = 0.75$

Table 3.1 Typical results for comparison of target and reconstructed data

Percentage change (%)	Simulated and Reconstructed Data $f=11$ GHz, $n = 0.75$, $h=1.5$ mm, $\epsilon_r=3.54$ (Taconic RF-35)		Results of ZUBIR et al. [40]	
	Target Data ($^{\circ}$)	Reconstructed Data ($^{\circ}$)	Simulated Results ($^{\circ}$)	Measured Results ($^{\circ}$)
-20	-22,202	-27,93716508	6.4797	-16.5188
-10	-47,4357	-47,60231759	-19.0891	-39.6383
0	-175,011	-168,5417868	-178.9874	-196.3713
+10	-295,78	-296,3251307	-284.6809	-290.3985
+20	-319,752	-324,6011538	-304.348	-323.4595

The phase behavior of the reflected waves for the target and reconstructed data are given in Figure 3.13. Target and reconstructed data are matched by network. It can be clearly seen that outputs of network follow the real data. This means network can predict the reflected phase values with very small training and testing errors.

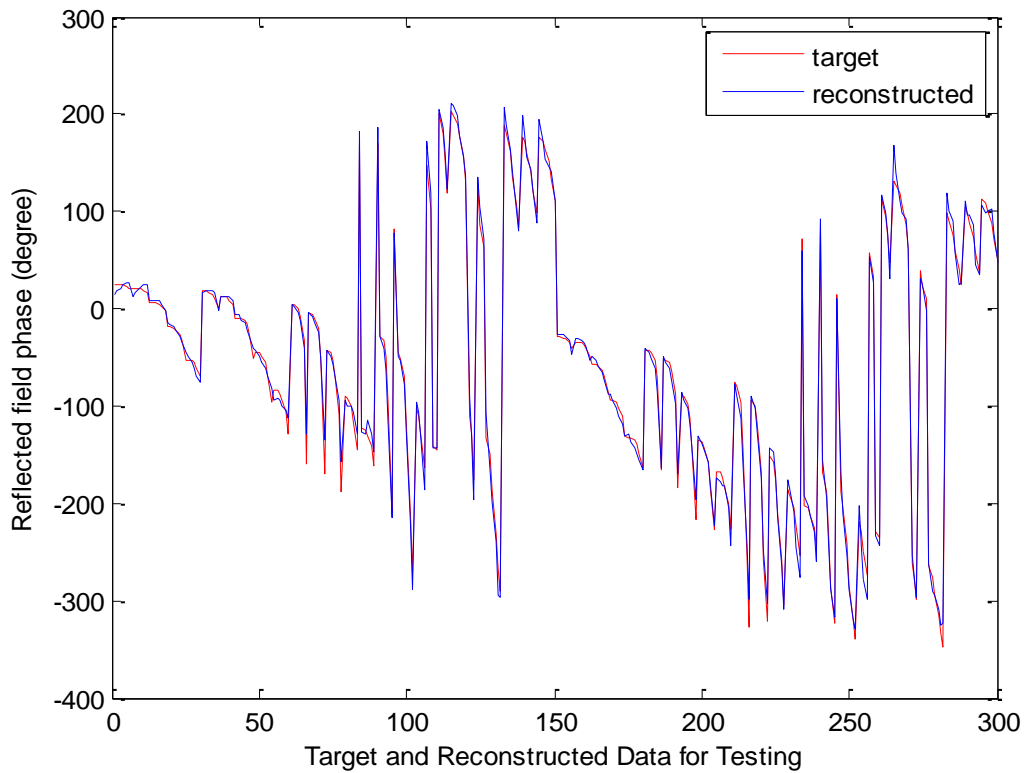


Figure 3.13 Testing performance of MLP NN in comparison between target and reconstructed data

Reflection phase variations for testing data at 10.5 and 11.5 GHz can be examined with respect to the percentage patch length variation and the fixed substrate thickness $h=1.524$ mm for different iteration factor value, η which is built up using the reconstructed data at the resonant frequency 11 GHz. These characteristics are shown in (Figure 3.14) and (Figure 3.15) as in 3-D view. When these phase variations of the reflected wave are compared the target and reconstructed data and recognized MLP NN model is very successful to predict the real phase values which are provided with simulations.

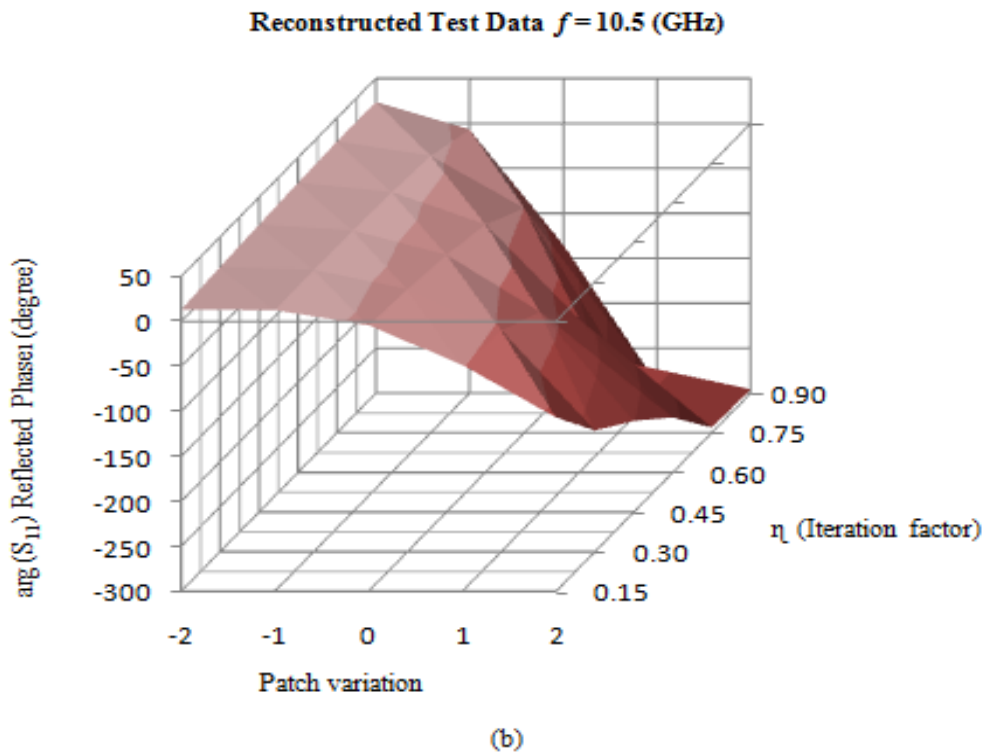
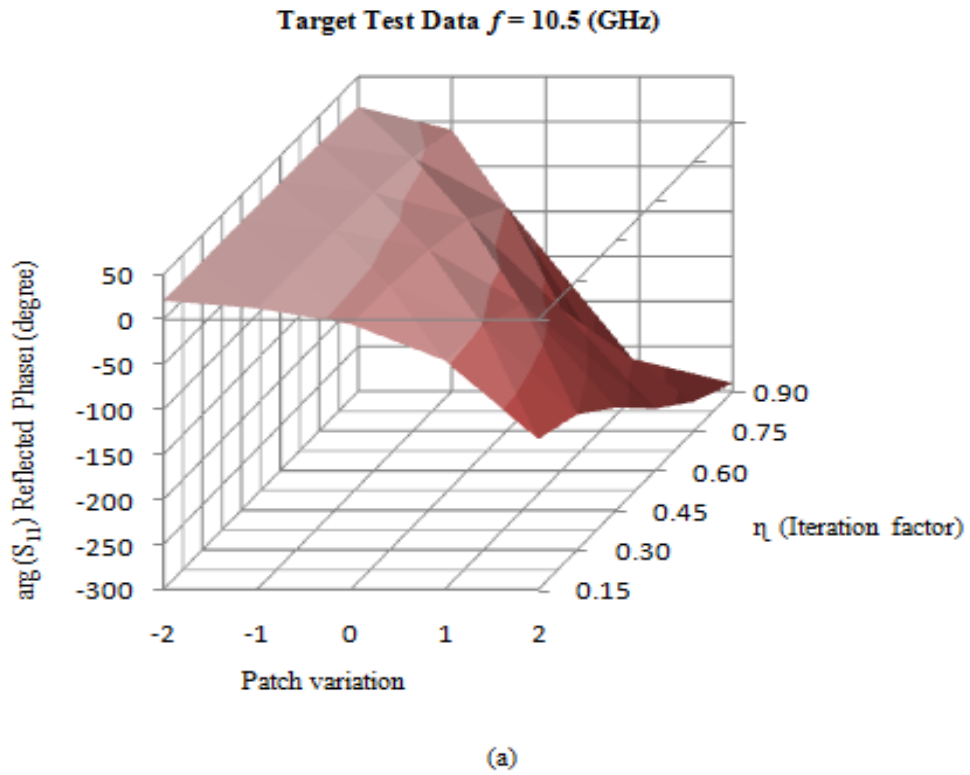
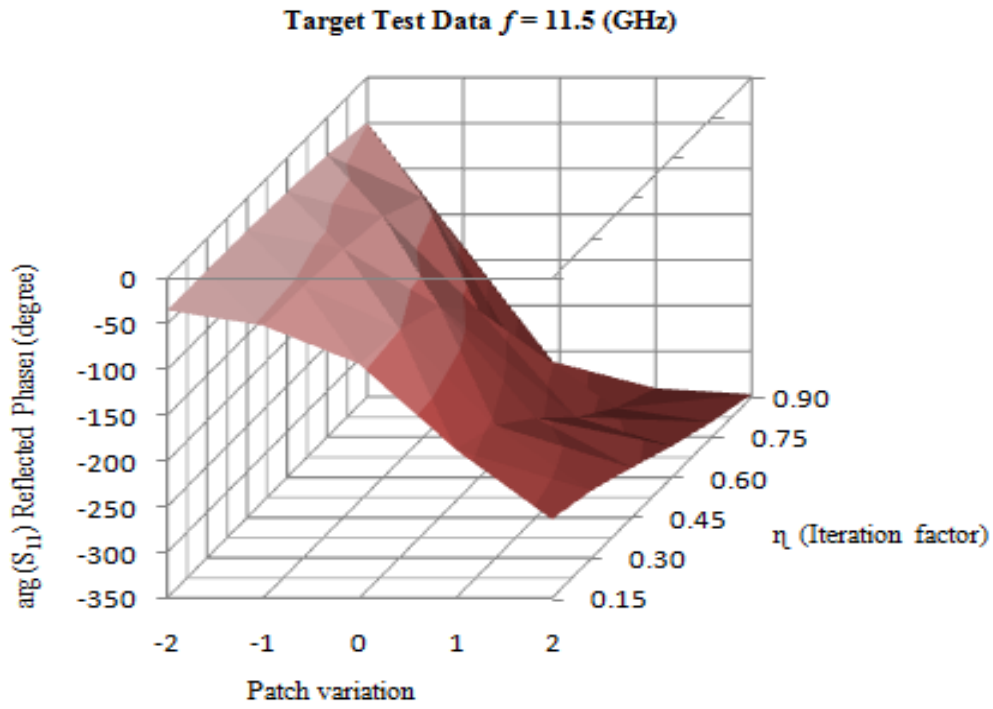
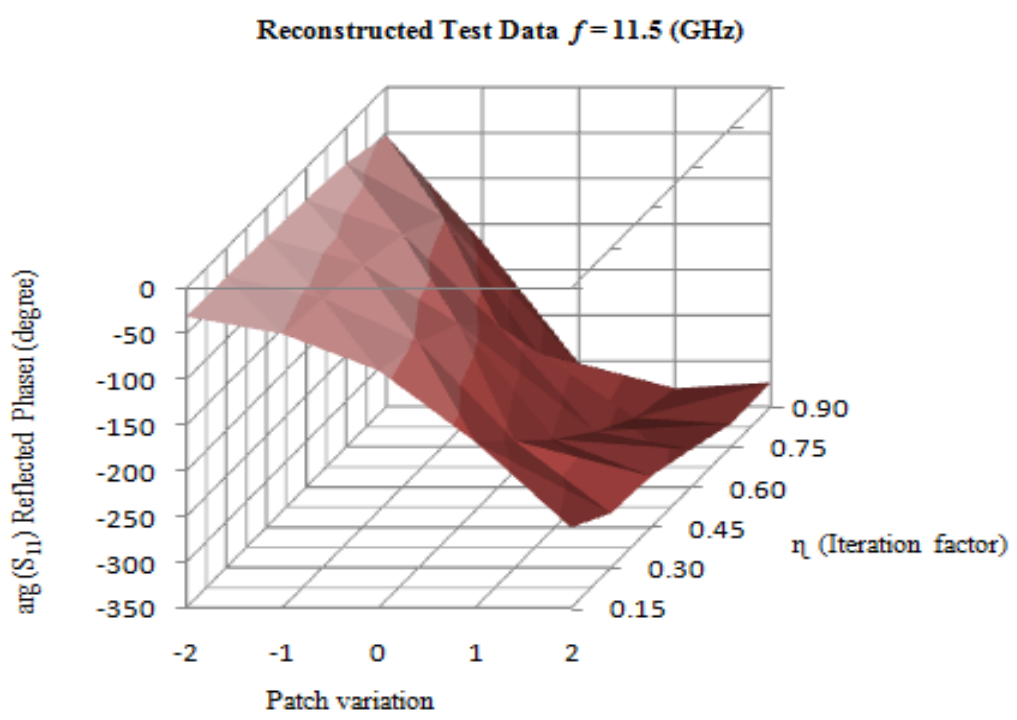


Figure 3.14 Comparison of reflection phase values w.r.t m (patch variation) and η (iteration factor) for $h = 1.52$ (mm), $f = 10.5$ GHz with (a) the target data; (b) the reconstructed data



(a)



(b)

Figure 3.15 Comparison of reflection phase values w.r.t m (patch variation) and η (iteration factor) for $h = 1.524$ mm, $f = 11.5$ GHz with (a) the target data; (b) the reconstructed data

3.3 The Optimization of the Minkowski Element with Particle Swarm Algorithm

In the design optimization, the patch length (m) is used as the phase (φ_{11}) variable size and among a lot of ($\varphi_{11} - m$) phasing characteristics identified by the discretized substrate thickness h and iteration factor n couples, the one is targeted with the slower gradient and wide range using the following objective function:

$$Objective = Min_{h,n} \left\{ \sum_{\substack{h=0.5\text{mm} \\ \Delta h=0.01\text{mm}}}^{3\text{mm}} \sum_{\substack{n=0.15 \\ \Delta n=0.01}}^{0.9} e^{-|\varphi_{\max} - \varphi_{\min}|_{h,n}} + \sum_{m=m_{\min}}^{m_{\max}} \frac{\Delta\varphi_{11}(m,n,h,f)}{\Delta m} \right\}_{h,n} \quad (3.5)$$

where φ_{11} is the reflection phase of the array element, obtained by its MLPNN model and $|\varphi_{\max} - \varphi_{\min}|_{h,n}$ is its phase range.

PSO algorithm in [50] is used to minimize the objective function given by (3.5) with respect to the iteration factor n and the substrate thickness h . For an N - dimensional problem, the position and velocity of each particle can be specified by $M \times N$ matrices, where M is the number of particles in the swarm.

In Figure 3.16, the flowchart of the PSO algorithm is presented [51]. At the first stage, physical and convergence parameters of the algorithm are assigned. Position, velocity, personal best and global best matrices are initialized randomly at the second stage. For each iteration, fitness function value is computed for each particle and these values are used to determine each particle's personal best and global best value of the swarm [52]. The algorithm ends when either the error or the iteration number reaches to its assigned value.

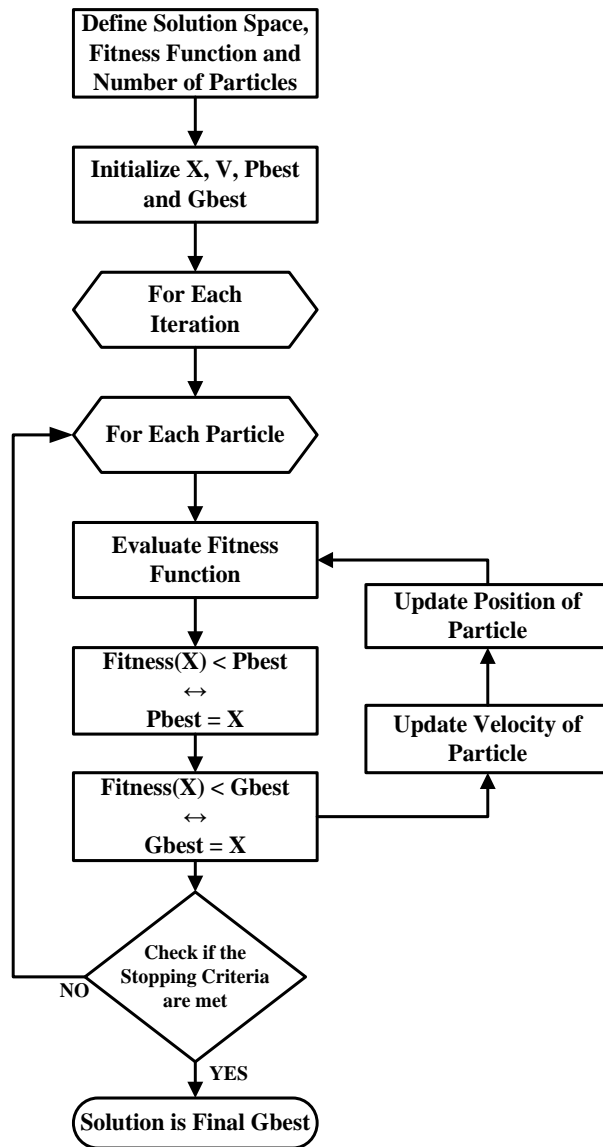


Figure 3.16 Flow chart of the PSO Algorithm [51]

In this section, convergence of PSO application occurs between 150 and 300 iterations depending on the initialization values taking 1 minute and 12 seconds and 2 minutes and 33 seconds, respectively using 75 particles with Core i7 CPU, 1.60 GHz Processor, 4 GB RAM. A typical convergence curve is given in Figure 3.17.

The optimum values are found as $n_{opt} = 0.7891$ and $h_{opt} = 1.4516$ mm and the corresponding phase calibration characteristic is given in Figure 3.18 together with the reflection magnitude together which remains above % 90 throughout the calibration range. The phase calibration can be used between (-25°) and (-335°) , therefore the range of 310° is achieved with the slope of $(1.8^\circ/\text{mm})$ at the middle point of the operation range.

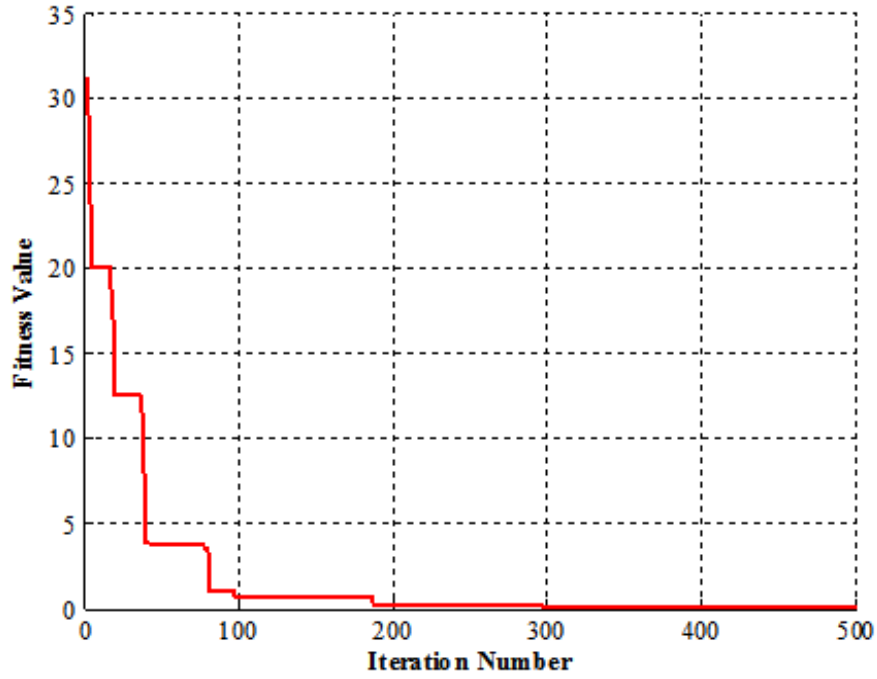


Figure 3.17 Convergence curve for the PSO of the minkowski element ($n_{opt} = 0.7891$, $h_{opt} = 1.4516$ mm) with the resulted value of the objective 4.2×10^{-8}

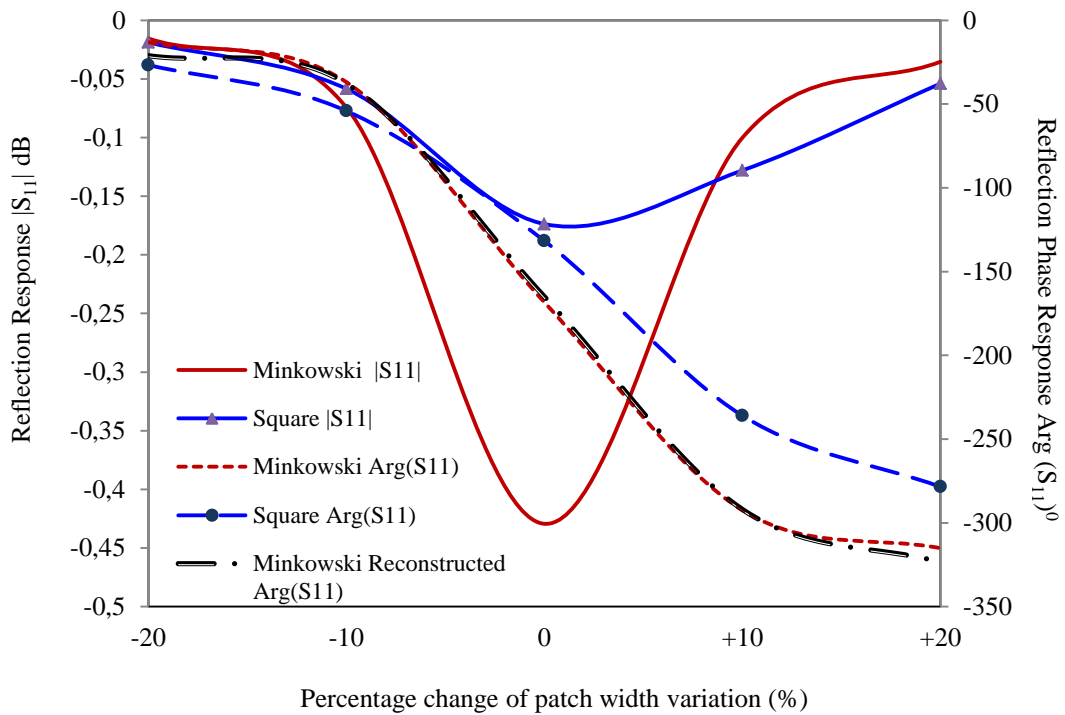


Figure 3.18 According to optimum parameters ($f = 10.875$ GHz $n = 0.7891$ $h = 1.4516$ mm) reflection characteristics of the minkowski Reflectarray element by comparison with square patch on the Taconic RF-35 ($\epsilon_r = 3.54$) substrate

Table 3.2 Reflection phase with optimum parameters; $f = 10.875$ GHz,
 $\varepsilon_r = 3.5$ (Taconic RF-35), $n_{opt} = 0.7891$, $h_{opt} = 1.4516$ mm,

Patch Width (mm)	$ S_{11} $ (dB)	Target Arg(S_{11}) ($^\circ$)	Recons. Arg(S_{11}) ($^\circ$)
4,328	-0,01543	-13,05736637	-21,0973
4,869	-0,0744	-36,90439224	-37,7558
5,41	-0,42936	-168,3211823	-164,9736
5,951	-0,10008	-292,4859619	-291,9791
6,492	-0,03528	-315,1140137	-323,4096

3.4 Design of Minkowski RA with Substantially-Optimized Parameters

A general design procedure for a reflectarray antenna is given in Figure 3.19 where the number of the element in the form of $M \times N$ and the uniform interspacing as electrical length are given as the input data. In the phase compensation unit, a coordinate system has been used to determine the progressive phase distribution on the microstrip reflectarray surface of $M \times N$ arbitrarily spaced patches with a centered focal point that will produce a pencil beam in a direction of normal to the surface.

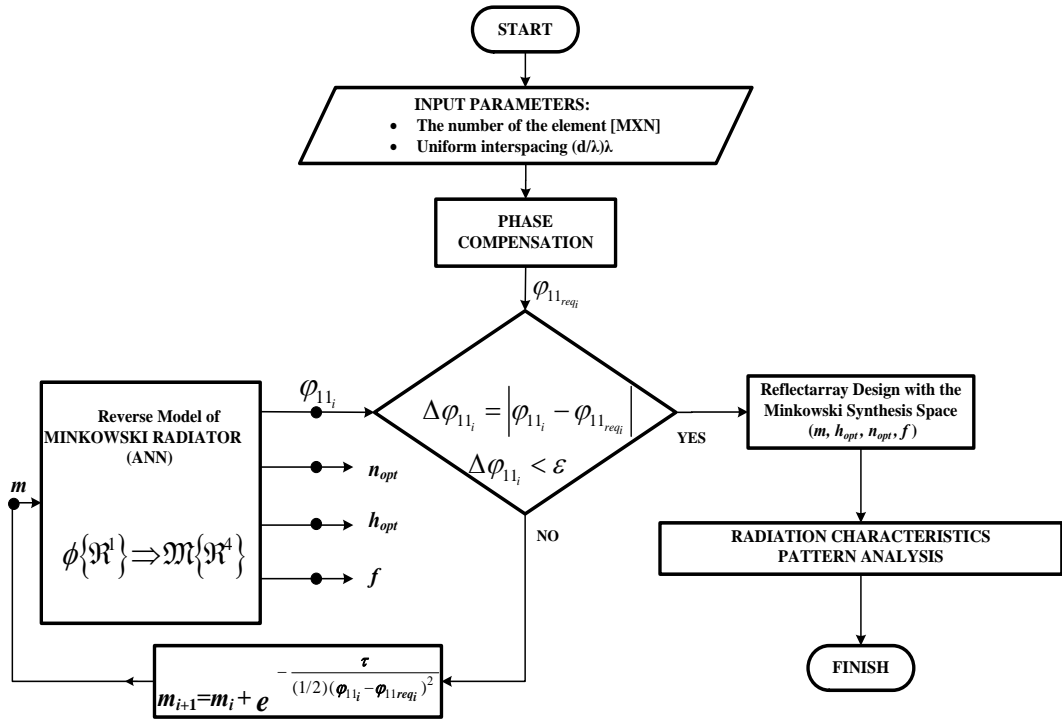


Figure 3.19 A General design procedure for a minkowski reflectarray antenna

In the reverse model of the minkowski element (Figure 3.19), the mapping $S: \phi\{\mathfrak{R}^1\} \Rightarrow \mathfrak{M}\{\mathfrak{R}^4\}$ is obtained using MLP NN analysis model, where the weight vector \vec{w} obtained in the analysis process remains constant while input m changes itself using the adaptable size Δm which get exponentially smaller with an adaptation parameter τ as decreasing the squared error.

Thus, the required phase to compensate path difference $\Delta R(x)$ for a reflectarray element can be given as a function of its radial distance (x) to the center and the operation frequency (f) as follows [53]:

$$\varphi(x, f) = -\beta(\Delta R_{\max} - \Delta R(x)) = -\frac{2\pi f F}{c} \left(\sqrt{1 + (D/F)^2 / 4} - \sqrt{1 + (x/f)^2} \right) \quad (3.6)$$

where the minus sign expresses delay, c is the velocity of light. In, D and F are the diameter and the focal length of the feed to the array center, respectively (Figure 3.20).

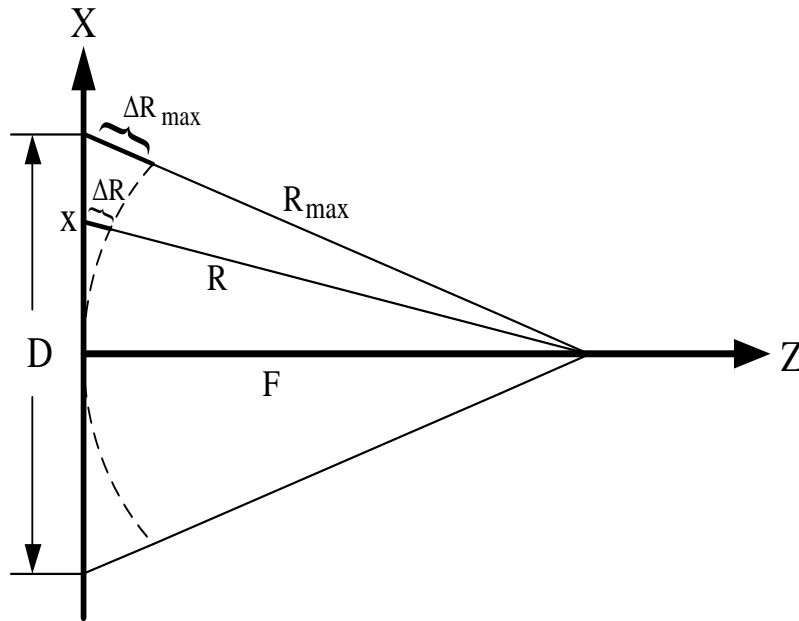


Figure 3.20 2-D view of the center feed reflectarray antenna geometry [53]

Quadrature symmetry characteristic of the phase compensation with respect to the element position is given in for the 15x15 Reflectarray where frequency is considered as the parameter and F/D is taken as 0.8. Furthermore, typical phase compensation values at various operation frequencies take place in Figure 3.21 and Table 3.3.

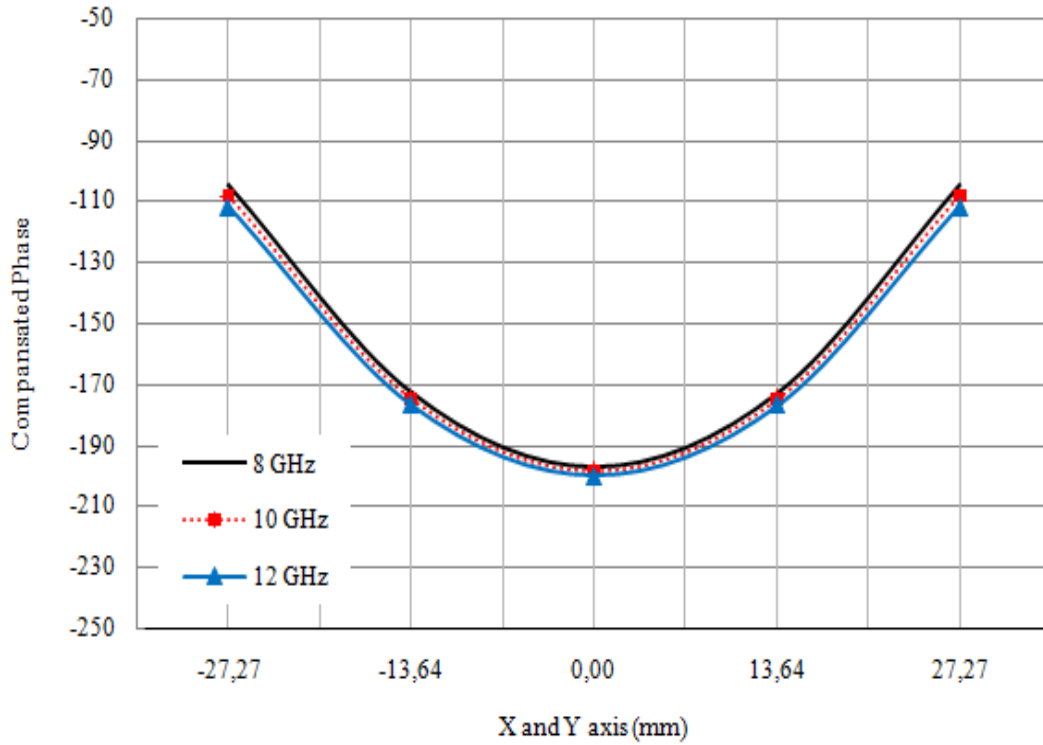


Figure 3.21 Phase compensation variation with respect to the radial distance for $F / D = 0.8$ at various operation frequencies

Table 3.3 Typical phase compensation values at various operation frequencies

x and y axis (mm)	Frequency (GHz)				
	8 GHz	9 GHz	10 GHz	11 GHz	12 GHz
-27,27	-104,58	-106,46	-108,334	-110,207	-112,078
-13,64	-172,80	-173,82	-174,869	-175,931	-177,008
0,00	-197,11	-197,80	-198,506	-199,242	-200,002
13,64	-172,80	-173,82	-174,869	-175,931	-177,008
27,27	-104,58	-106,46	-108,334	-110,207	-112,078

3.5 Results and Discussion for the Optimum Minkowski Reflectarray Antenna

In this work, the 15×15 variable- size minkowski and square RA s with half- wave spacing at frequency of 11 GHz are designed on the Taconic RF-35 with $\epsilon_r = 3.54$. The radiation analysis is implemented using available full-wave simulation tool CST MWS.

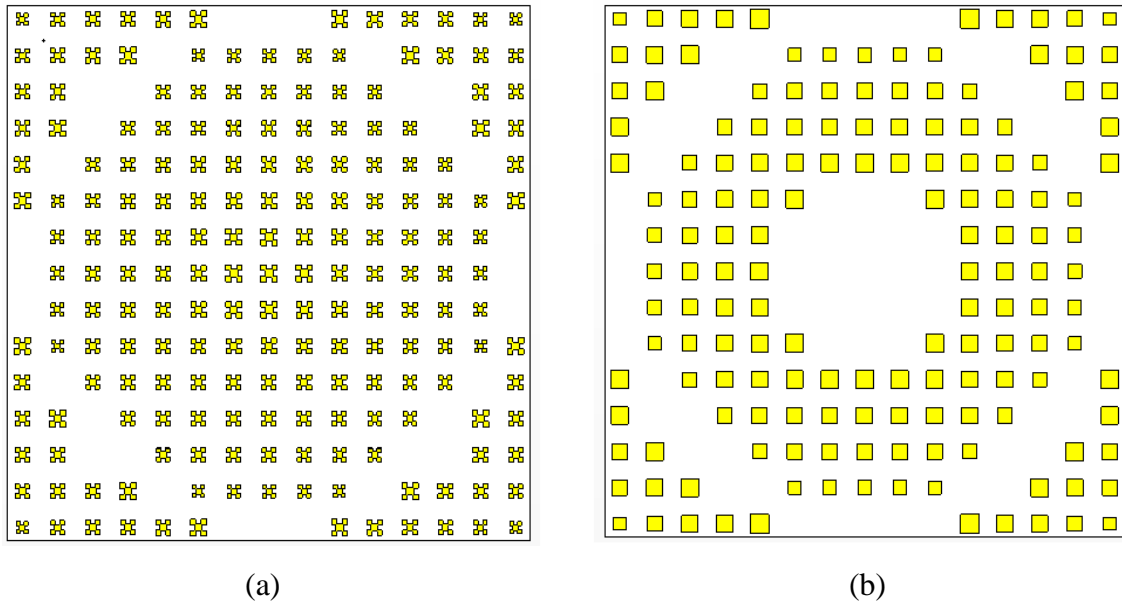


Figure 3.22 The 15×15 microstrip reflectarray antenna (a) minkowski (b) square with the optimum parameters ($n_{opt}=0.789$, $h_{opt}=1.4516\text{mm}$, $F/D=0.8$) on 20×20 cm, $\epsilon_r = 3.54$ (Taconic RF-35)

In order to investigate the effect of the feed movement along the focal length on the radiation features, gain variations with respect to the frequency and radiation patterns of the 15×15 optimum minkowski RA are given in Figure 3.23 and Figure 3.24, respectively for the various F/D values and the resulted pattern characteristics and 3-dB bandwidths are also given in Table 3.4.

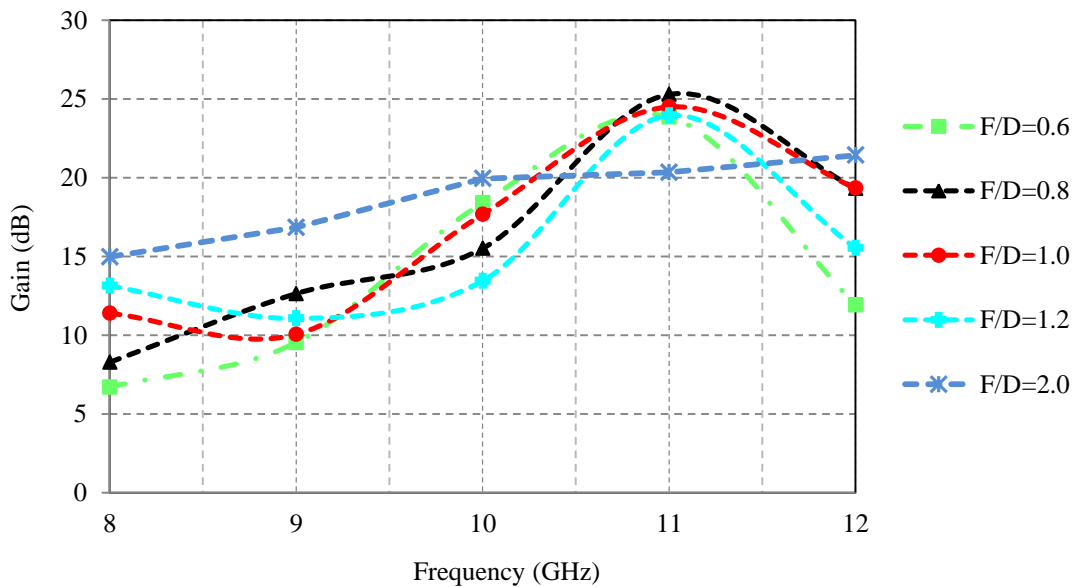


Figure 3.23 Effect of the feed movement on the max. gain variations of the 15×15 minkowski RA with the optimum parameters $n_{opt}=0.789$, $h_{opt}=1.4516$ mm on $\epsilon_r = 3.54$ (Taconic RF-35) for different F/D ratios within the X-band frequency range

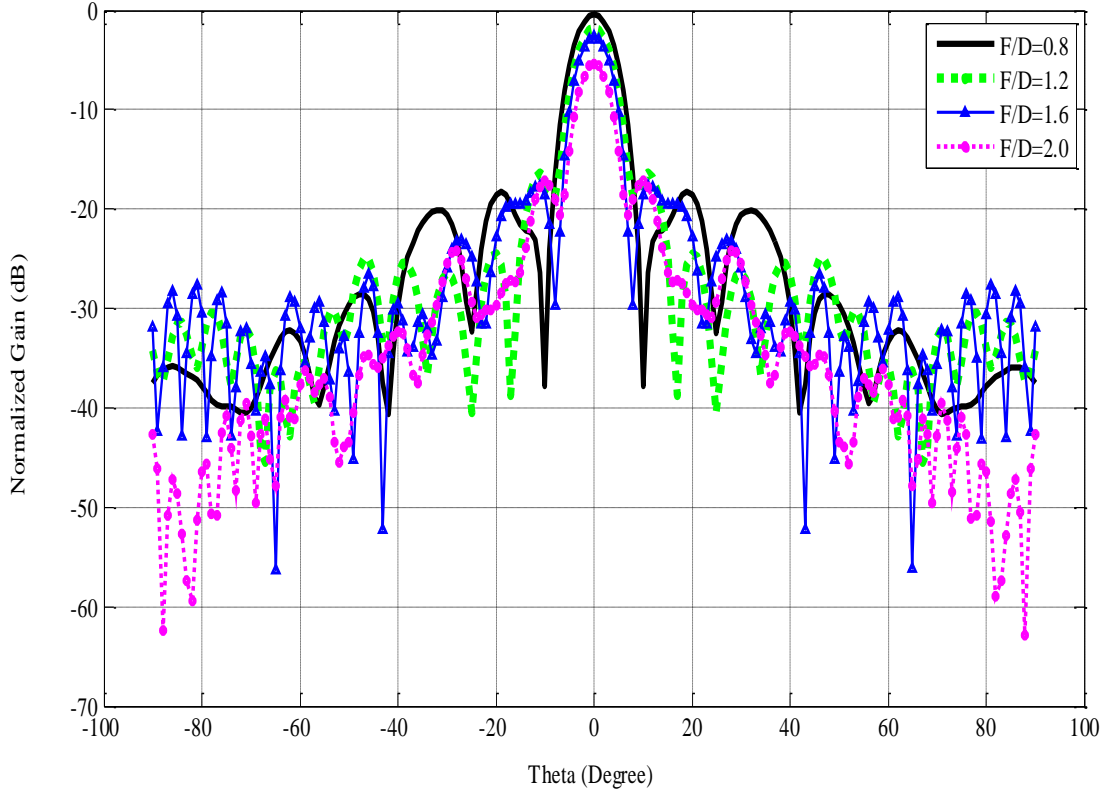
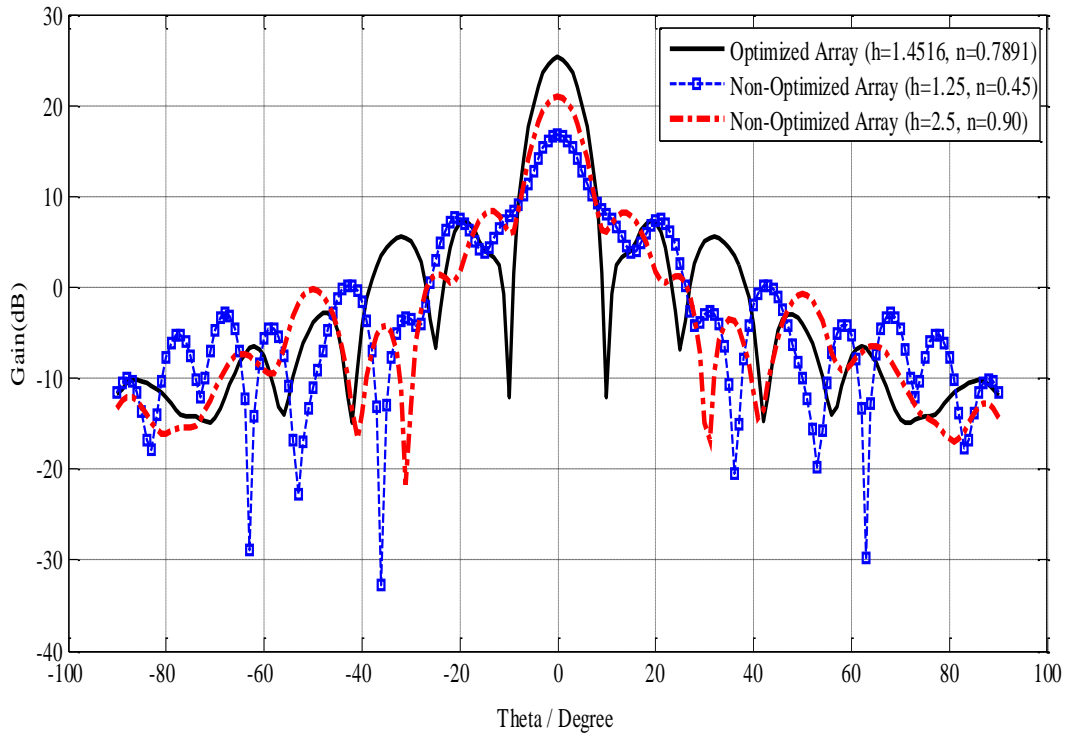


Figure 3.24 Effect of the feed movement on radiation pattern of the 15×15 minkowski RA at 11 GHz with the optimum parameters $n_{opt}=0.789$, $h_{opt}=1.4516$ mm on $\epsilon_r = 3.54$ (Taconic RF-35)

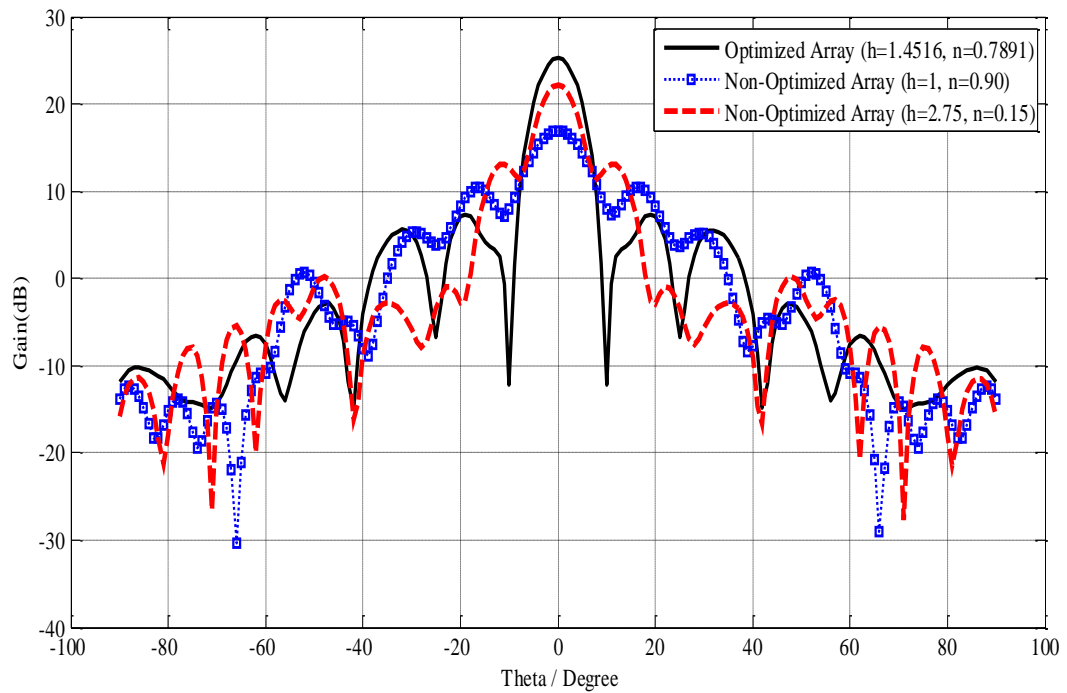
Table 3.4 Radiation pattern characteristics of the 15×15 minkowski reflectarray antenna with the optimum parameters: $n_{opt}=0.789$, $h_{opt}=1.4516$ mm

F/D ratio	Array Directivity (dBi)	Realized Gain (dB)	Side Lobe Level (dB)	Angular Beam width (3dB) (Deg.)	Radiation Efficiency	Total Efficiency	3-dB Bandwidth (GHz)
0.6	24.6	23.9	-16.6	7.8	0.962585	0.838301	0.75599
0.8	25.7	25.3	-17.9	7.7	0.948496	0.914878	0.79763
1.0	24.8	24.5	-16.5	7.2	0.950772	0.937088	0.98485
1.2	24.2	24.0	-14.7	6.8	0.974969	0.936913	1.1455
1.6	23.3	23.1	-12.8	6.5	0.981158	0.952549	1.367
2.0	20.6	20.3	-9.6	6.1	0.979080	0.942615	1.5

In order to demonstrate merit of the optimization, comparative radiation patterns of the optimized and non-optimized minkowski RAs are depicted in Figure 3.25 for the various values of (h, n) sets at 11 GHz.



(a)



(b)

Figure 3.25 Comparative radiation patterns of the optimized and non-optimized 15×15 minkowski RAs for the various values of (h, n) sets for $F/D=0.8$ at 11 GHz

Moreover, radiation features of the optimum minkowski RA for $F/D=0.8$ are compared with its counterpart square RA with the resonance size 6.06 cm at frequency of 11 GHz and parabolic reflector with the same diameter and the comparative patterns can be seen as graphics in Figure 3.26 and examined as the numerical values from the Table 3.5. It can be observed that the RA with minkowski shape radiating element has better performance than the conventional RA with square shape of radiating element.

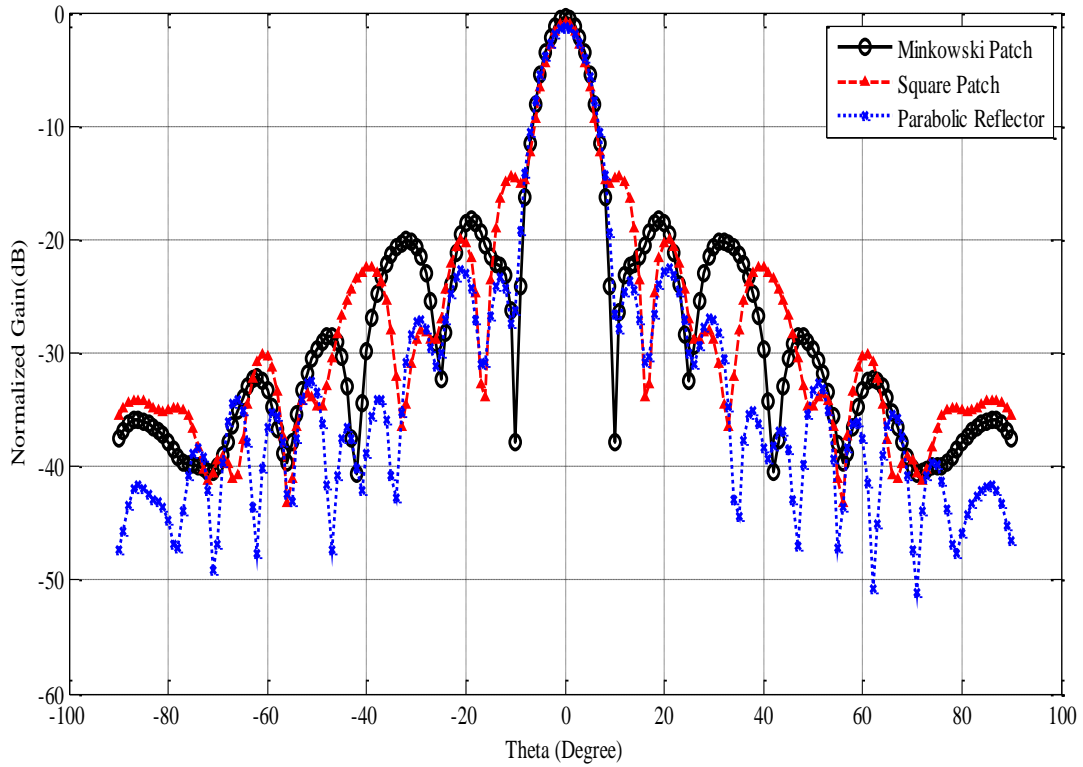


Figure 3.26 Comparison of radiation patterns for the 15×15 minkowski, square reflectarray and the parabolic reflector antennas for parameters; $h_{opt}=1.4516$ mm, $n_{opt}=0.7891$ mm, $\epsilon_r=3.54$ (Taconic RF-35)

Table 3.5 Comparison of the radiation pattern characteristics of the 15×15 minkowski, square reflectarray and the parabolic reflector antennas

<i>Array Type</i>	<i>Array Directivity (dBi)</i>	<i>Realized Gain (dB)</i>	<i>Side Lobe Level (dB)</i>	<i>Angular Width (3dB) (°)</i>	<i>Total Efficiency</i>
Minkowski Shape	25.7	25.3	-17.9	7.7	0.914878
Square Patch	25.2	24.4	-13.6	7.3	0.823479
Parabolic Reflector	24.4	24.1	-17.0	8.4	0.915983

Thus the RA with Minkowski shape radiating element is able to provide higher realized gain, good total efficiency as well as very low SLL due to its wider reflection phase range (310°) compared to the RA with the square element (250°), since the wider reflection phase range facilitates larger number of radiating elements to the RA by comparison with the narrow phase range. Furthermore, the blanks on the RA surface will contribute to phase error. The increase of phase error will significantly increase the side-lobe level and thus reduce the gain for the microstrip RA itself. Besides, the effect of feed movement along the focal length on the gain and radiation patterns is also worked out and demonstrated.

A NOVEL DESIGN APPROACH USING HYBRID GA-NM OPTIMIZATION BASED ON COMPLETE MLP ANN MODEL

4.1 Introduction

This chapter puts forward a robust methodology for design optimization of the microstrip RAs. It has been worked with the minkowski shape [40], [41] that is from the 1st iteration of fractals and the minkowski radiator is shown to have an optimum phasing characteristic with the large linear region and easy fabrication.

In this part, a complete model is built mapping the 5-dimensioned minkowski space $M(5)$ to the 1-dimensioned reflection phase space $R(1)$ to be used in the design optimization of the minkowski RAs for the X-band applications. Here, the 5-dimensioned minkowski space $M(5)$ consists of the minkowski geometry parameters m, n and the substrate dielectric, ϵ_r and thickness, h and the operation frequency f . Thus, the designer will be able to obtain the optimum minkowski geometry not only on a selected substrate, at the same time, on the most suitable substrate with the optimum dielectric property ϵ_r and thickness h within the X-band.

The systematic design optimization procedure presented in this chapter can be considered consisting of the following stages: The first stage is to build a rapid and accurate model for the reactive impedance behavior of a minkowski radiator. For this purpose, a MLP NN is optimized by the Levenberg-Marquardt algorithm using the training and validation data sets obtained by varying the geometrical parameters m, n for each substrate ϵ_r, h around the resonance frequency, f of the 3-D CST simulation of a unit minkowski reflective element placed at the end of a standard X-band waveguide. Thus the reflection phase of an independent minkowski radiator is established as a highly nonlinear function within the continuous domain of the element

geometry m, n and substrate parameters ϵ_r, h in a defined bandwidth centered the resonant frequency of the microstrip patch. In the second stage, a hybrid GA–NM algorithm is used to obtain the most proper phasing characteristic as the calibration characteristic for the gain and bandwidth optimization using the MLP NN model and thus the optimum patch geometry on the optimum substrate (ϵ_r, h) within the X-band is determined for the design of the minkowski RA.

The organization of the chapter is as follows: The next section is devoted to the discretization of the 5-D minkowski space of (m, n, ϵ_r, h, f) to obtain the training and validation data for MLP NN. The MLP NN modeling is given in the third section. In the fourth section gain and bandwidth, optimization will be presented using the hybrid combination of Genetic and Nelder-Mead algorithms with respect to the input variables. Design and performance analysis of the minkowski RA s with the optimized or non-optimized antenna parameters will be taken place in the fifth and sixth sections, respectively. Finally, the paper ends the conclusions.

4.2 Reflection Phase Characterization of Minkowski Unit Element

The form of reflection phase characterization for minkowski element was mentioned before in chapter 3. The generation of training and validation is performed by the 5-dimensional discretized minkowski space of (m, n, ϵ_r, h, f) , which are constructed by totally 5400 samples to be used in the training and validation data using the H-wall waveguide simulator analyzed by 3-D CST MWS as follows:

The operation bandwidth of 8-12 GHz is swept as the intervals of 1 GHz and the resulted number of the sample frequencies is $f_s = 5$. Then, minkowski sampling matrix is generated as $n_s \times m_s$ for each sampled substrate properties (ϵ_r, h) at each sampling frequency where $n_s = 6$ and $m_s = 5$ are the number of samples for the indentation factor and patch width within the ranges of $0.15 \leq n \leq 0.90$ and $m \pm (\Delta m / m)_{\max} = m \pm \% 20$ where m is the resonant length at 11 GHz, respectively. Simultaneously the substrate thickness h , is sampled $0.5 \text{ mm} \leq h \leq 3 \text{ mm}$ as the intervals of 0.5 mm between them and the total number of the thickness sampling is $h_s = 6$. In addition, dielectric permittivity of substrate ϵ_r is totally sampled as 6 times between $1 \leq \epsilon_r \leq 6$. Thus, the

entire minkowski space is discretized totally into the $\varepsilon_s \times f_s \times h_s \times m_s \times n_s = 5400$ minkowski configurations.

4.3 MLPNN Black-box modeling in the analysis

The black-box model of a minkowski radiator is depicted in Figure 4.1 where the MLPNN is employed for the generalization process that is already given in Figure 4.2. The MLP NN has the two hidden layers each of which consists of 10 neurons activating by the tangential sigmoid functions. The input \vec{x} and output \vec{y} vectors are 5-and 1-dimensional, respectively and can be expressed as

$$\vec{x} = [m \ n \ \varepsilon_r \ h \ f]^t, \quad \vec{y} = [\varphi_{11}]^t = \varphi_{11}(\vec{x}, \vec{w}) \quad (4.1)$$

where \vec{w} is the weighting vector of the MLP NN given in Figure 4.2 and the output function $\varphi_{11}(\vec{x}, \vec{w})$ can be built using the MLPNN theory [8]. \vec{w} is determined by the optimization with the following mean-squared error function over the training data using the Levenberg- Marquardt algorithm [9]:

$$E = \sum_{k \in T_r} (\varphi_{11k} - d_k)^2 \quad (4.2)$$

where T_r is an index set of the training data which consists of 3240 (\vec{x}, φ_{11}) data pairs corresponding to all the patch lengths of 4.328 mm, 5.41mm and 6.491mm, the rest 2160 (\vec{x}, φ_{11}) data pairs are used to validate the MLP NN model.

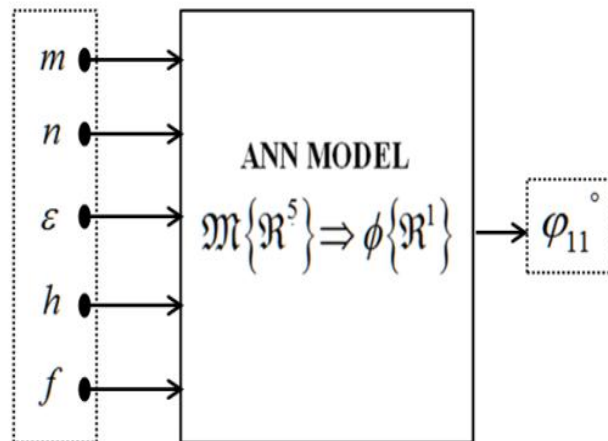


Figure 4.1 Black-box model II

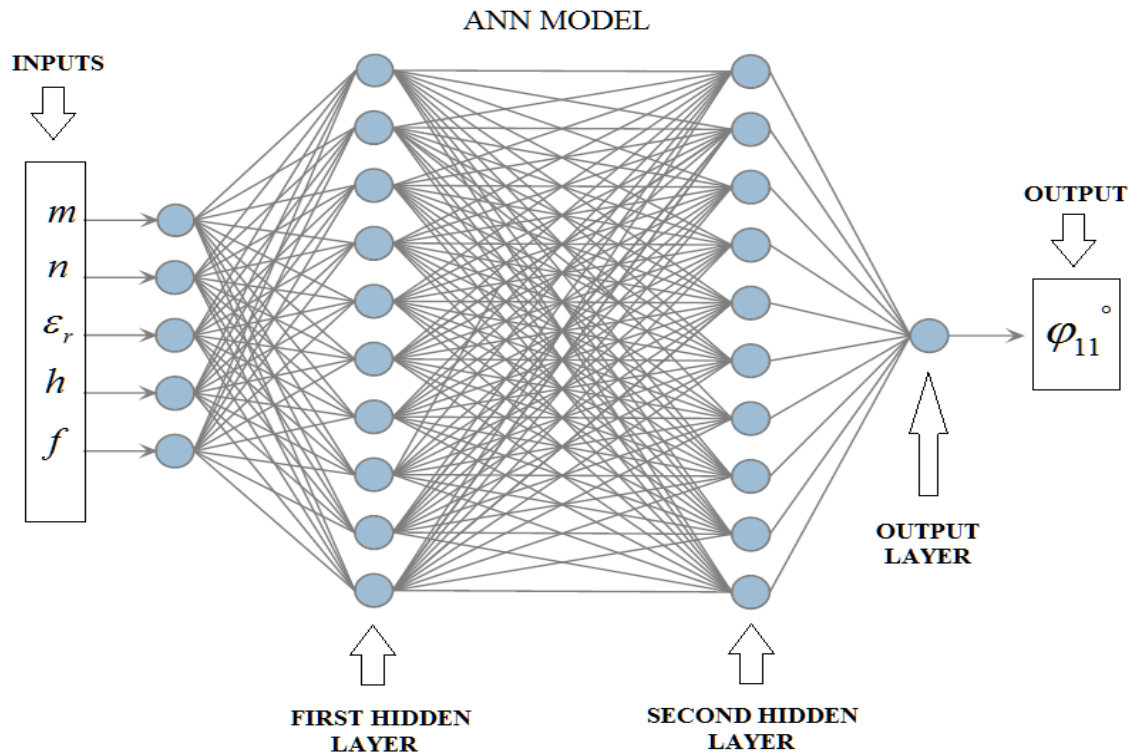


Figure 4.2 The MLP NN structure

The Linear Regression scattering plots for the training and the validation process are given in Figure 4.3 respectively with their Mean Squared Error (MSE).

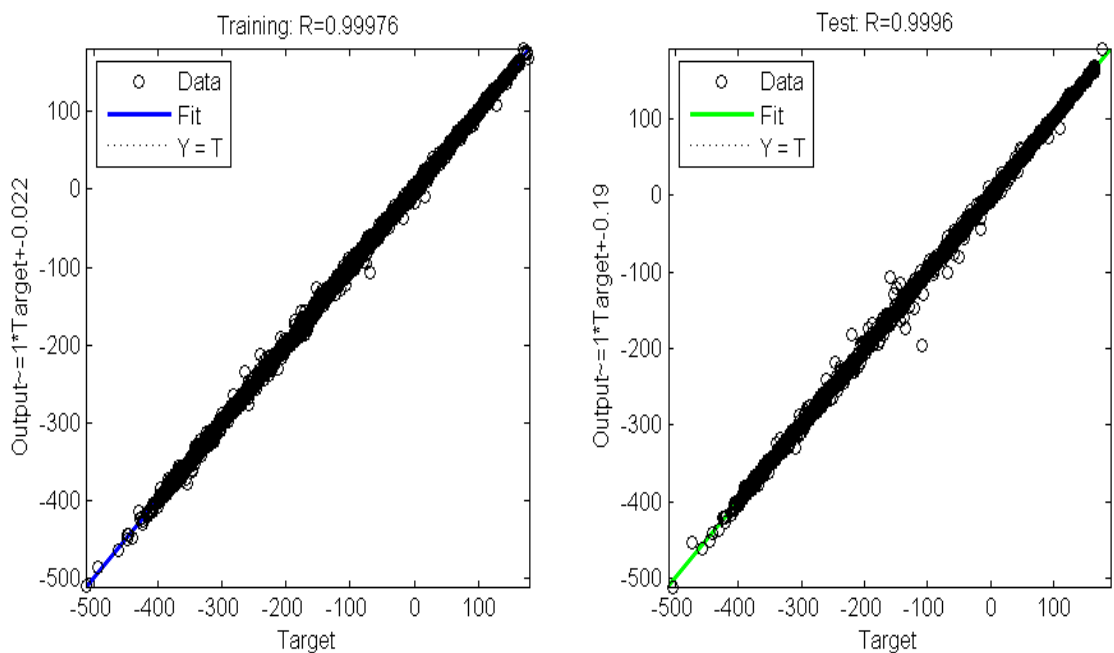
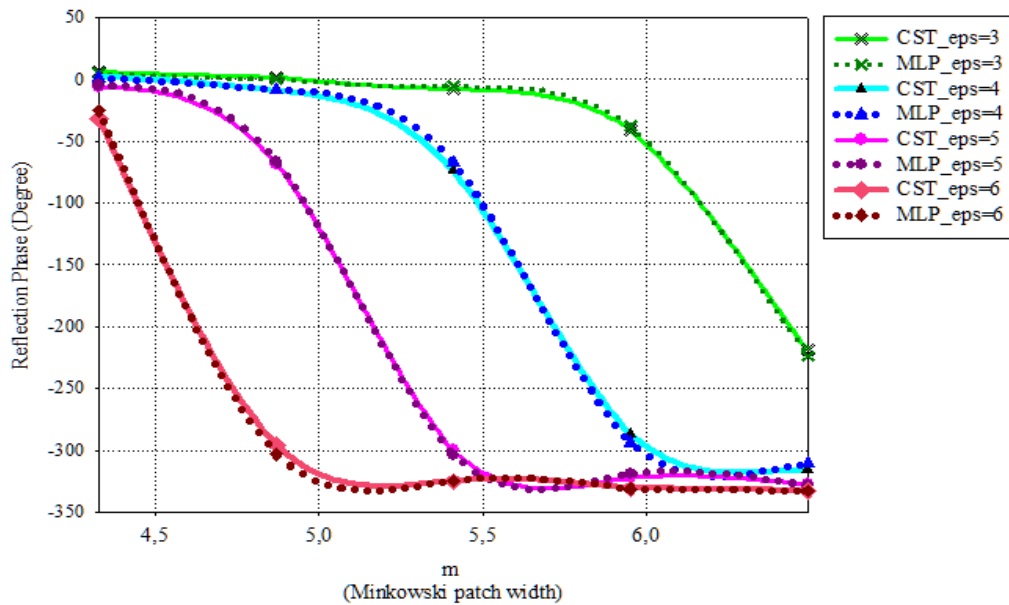


Figure 4.3 Linear regression scattering plots for the complete minkowski MLP model (a) Training ($MSE= 9.9564 \times 10^{-5}$) and (b) Validation ($MSE= 1.7264 \times 10^{-4}$).

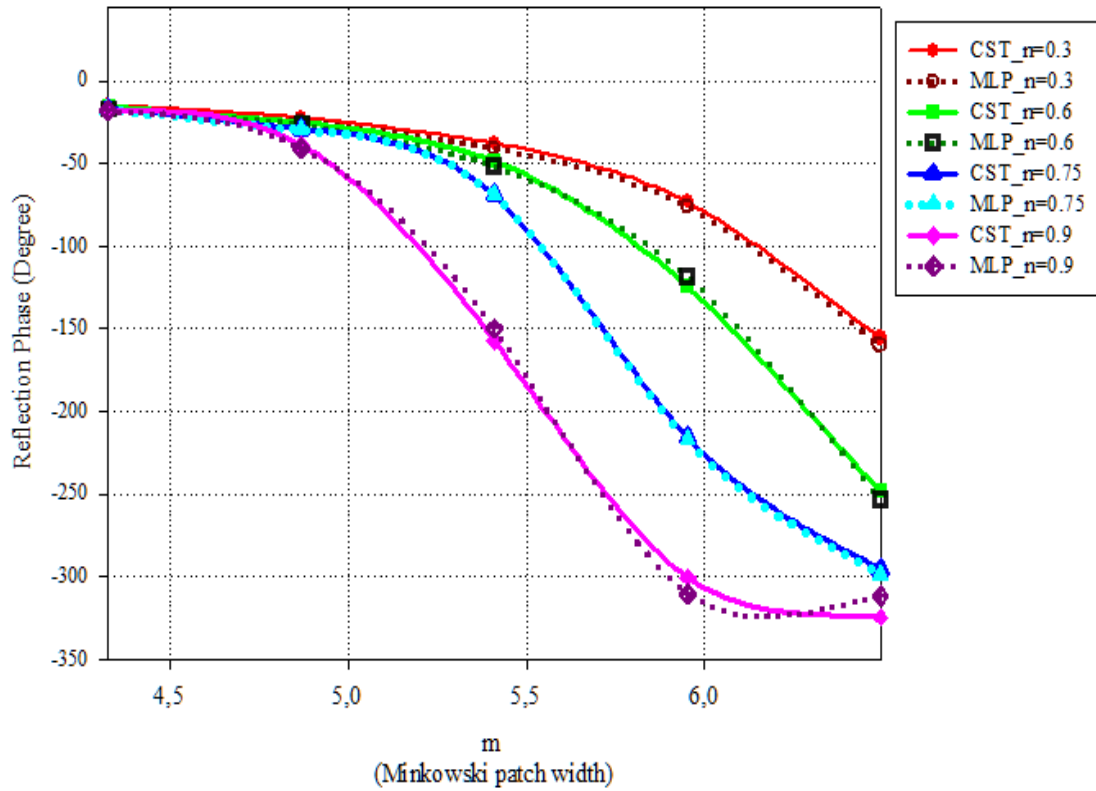
Some examples of modeling performances are depicted in Figure 4.4 where the constructed phasing characteristics are compared with the targets. Furthermore, Figure 4.5 gives the three dimensional view of the reflection phase variations with the patch width m and the relative permittivity of substrate value, ϵ_r for the constructed and targeted data at the fixed conditions of $h=1.5 \text{ mm}$, $n=0.6$, $f=11 \text{ GHz}$. Thus, it can be inferred that the MLP NN model works very well in generalization of the 5400 (\vec{x}, φ_{11}) data pairs to the entire domains to obtain the continuous minkowski reflection phasing function $\varphi_{11}(\vec{x})$. In next section, this $\varphi_{11}(\vec{x})$ function will be used directly to determine the phase calibration characteristic and later by reversing to synthesize the minkowski RA in the Memetic optimization procedure.

Table 4.1 Comparison for reconstructed data by ANN with the simulated data for conditions $f=11 \text{ GHz}$, $n = 0.75$, $h=1.524 \text{ mm}$, $\epsilon_r=3.54$ (Taconic RF-35) and the measured results in [41].

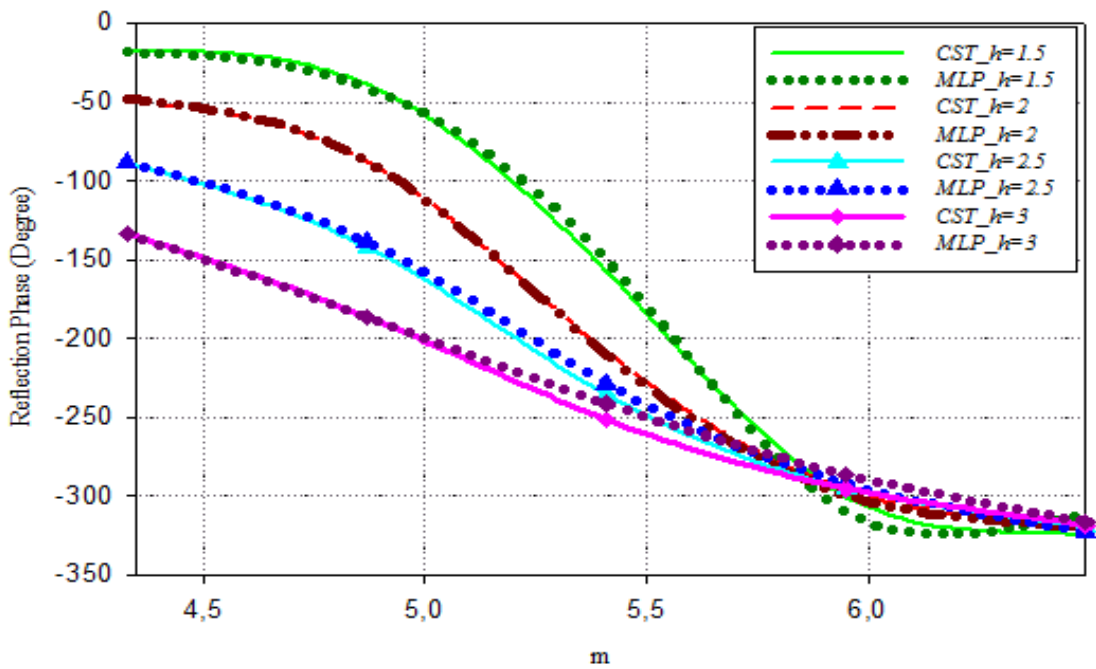
Patch Size Change (%)	Results of this study		Results of ZUBIR et al. [41]	
	Target Data (°)	Reconstructed Data (°)	Target Data (°)	Measured Data (°)
-20	-24,228	-23,776	6.4797	-16.5188
-10	-50,994	-53,195	-19.0891	-39.6383
0	-176,368	-170,462	-178.9874	-196.3713
+10	-292,906	-295,782	-284.6809	-290.3985
+20	-317,745	-309,813	-304.348	-323.4595



(a)



(b)



(c)

Figure 4.4 Reflection phase characteristics taking dielectric property as parameter for
 (a) $h = 1 \text{ mm}, n = 0.60, f = 11 \text{ GHz}$; (b) $n = 0.90, \epsilon_r = 3, f = 11 \text{ GHz}$;
 (c) $\epsilon_r = 3, h = 1.5 \text{ mm}, f = 11 \text{ GHz}$.

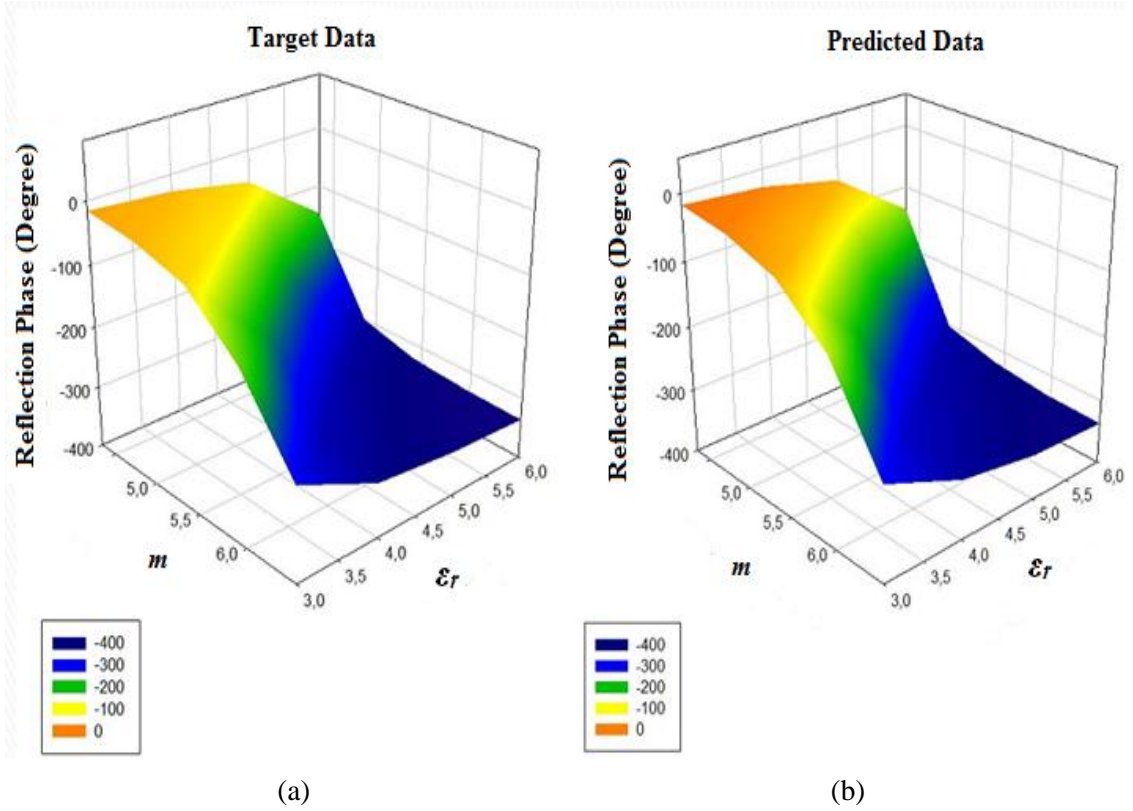


Figure 4.5 3-D reflection phase variations versus the patch width m and the relative permittivity of substrates, ϵ_r , for the fixed conditions of $h = 1.5$ mm, $n = 0.6$, $f = 11$ GHz for (a) target and (b) reconstructed data

4.4 The Optimization of Minkowski Element using the Memetic Algorithm

4.4.1 Objective Function

In this section, a multi- objective optimization procedure is established where the phase calibration characteristic is selected among the phasing characteristics obtained in the previous section as the one having the slower gradient and the wider range with respect to the indentation (n) and substrate (ϵ_r , h) to achieve the wider band and smaller susceptibility the manufacturing errors. Thus, this target is expressed as the sum of the three ingredients as follows:

$$Objective = Min \left\{ \sum_{i=l,c,u} \mathcal{G}_i(n, h, \epsilon_r) \right\} \quad (4.3)$$

with the following objective, \mathcal{G}_i at the frequency, f_i :

$$\mathcal{G}_i = \left\{ \sum_{\substack{\epsilon_r=1 \\ \Delta\epsilon_r=0.01}}^6 \sum_{\substack{h=0.5\text{mm} \\ \Delta h=0.01\text{mm}}}^{3\text{mm}} \sum_{\substack{n=0.15 \\ \Delta n=0.01}}^{0.9} W_1 \cdot \epsilon_1(f_i) + W_2 \cdot \epsilon_2(f_i) + W_3 \cdot \epsilon_3(f_i) \right\} \quad (4.4)$$

where,

$$\epsilon_1 = e^{-\left(\frac{\varphi_{\max} - \varphi_{\min}}{360}\right)} \quad (4.5)$$

$$\epsilon_2 = \left| \varphi_{\max} - \varphi_{center} \right| - \left| \varphi_{\min} - \varphi_{center} \right| \quad (4.6)$$

$$\epsilon_3 = 1 - \left(\frac{\Delta \varphi_{center}}{\Delta m_{center}} \right) \quad (4.7)$$

In (4.4), ϵ_1 is used to maximize the phase range while ϵ_2 , ϵ_3 provide the centralization of the characteristic with the angle of $\pi/4$. In (4.5), (4.6), and (4.7), φ_{\max} , φ_{\min} and φ_{center} are the reflection phase values at m_{\max} , m_{\min} and m_{center} for a certain (n, ϵ_r, h) set, respectively at the f_i where ℓ , c , u stand for the lower, center and the upper frequencies. In the optimization process, the operation frequency range is defined as follows: $f_\ell = 10$ GHz, $f_c = 11$ GHz, $f_u = 12$ GHz.

In (4.5), the phase difference between φ_{\max} and φ_{\min} is normalized by dividing 360 and $(\Delta \varphi_{center} / \Delta m_{center})$ is the gradient of the phasing characteristic at the point of $(\varphi_{center}, m_{center})$ which is aimed at to be equal to unity corresponding to optimum angle $\pi/4$. All weighting coefficients in (4.4) have been taken as unity. Optimization process is completed as soon as the iteration number has reached to its maximum value or the predefined cost value. In our case, the optimization ends when the cost value reaches to 0.4353 with the optimized values of all the weighting coefficients.

4.4.2 The Memetic Algorithm

The Memetic algorithm (MA) used in the optimization procedure consists of a hybrid of a Genetic Algorithm (GA) and the Nelder-Mead (NM) algorithm that forms a type of metaheuristic that balances exploration and exploitation well to find the high quality solutions within all the possible solution space [54]-[56]. GA is a population-based global optimization algorithm and uses the evolution operations such as crossover and mutation and the concept of fitness. Population is built from the chromosomes each of which a solution candidate binary is encoded randomly varied as 0 and 1. Chromosomes are ranked from the lowest to the highest cost values of the objective function after evaluation for each of them [54]. Then, the unacceptable chromosomes

are discarded and the remaining chromosomes are paired at randomly selected crossover points. Mutation process prevents the solution from being trapped into local minima by transforming a small percentage of the bits in the chromosome from 0 to 1 or vice versa. The mutation process per iteration is applied for 1% of the chromosomes. In this work, a simple algorithm called Nelder-Mead [55] is used along with the GA for finding the local minima at the location obtained by global minima. Recently, the hybrid GA-NM and BSO-NM algorithms are successfully implemented to design of the low-noise microwave amplifier and Bow-Tie antennas in [56], [57], respectively.

The MA used in our work can be briefly described through the following abstract description [42]:

Begin

Population Initialization

Local Search

Evaluation

Repeat

Crossover

Recombination

Mutation

Local Search

Evaluation

Selection

Until termination criterion is satisfied

Return best solution

End

Here, the initial populations are usually generated in a random or controlled manner and then the evolution of these populations are carried out by the genetic operators such as crossover, mutation and recombination. Local search is utilized to reduce the cost of the resulted solution from the global optimization.

In our GA-NM application, convergence occurs very quickly typically within the 30 iterations shortening 5 times as compared with the 61 iterations GA process, which takes 1 min and 12 s and 5 min and 41 s with Core i7 CPU, 1.60 GHz Processor, 4 GB RAM depending on the initialization values. A typical convergence curve is given in Figure 4.6. According to objective function (4.3) and (4.4), parameters of the optimum

minkowski RA within X-band are found as $\epsilon_r = 3.1694$, $h_{opt} = 1.7916$ mm, $n_{opt} = 0.8438$ and the corresponding reflection characteristics and values are given in Figure 4.7 and, respectively as compared with the square radiator's reflection properties. Radiation analysis of the 15×15 variable-size minkowski RA with half-wave spacing at resonant frequency of 11 GHz and comparison with the designs both non-optimized and optimized on some traditional substrates are given in the following sections.

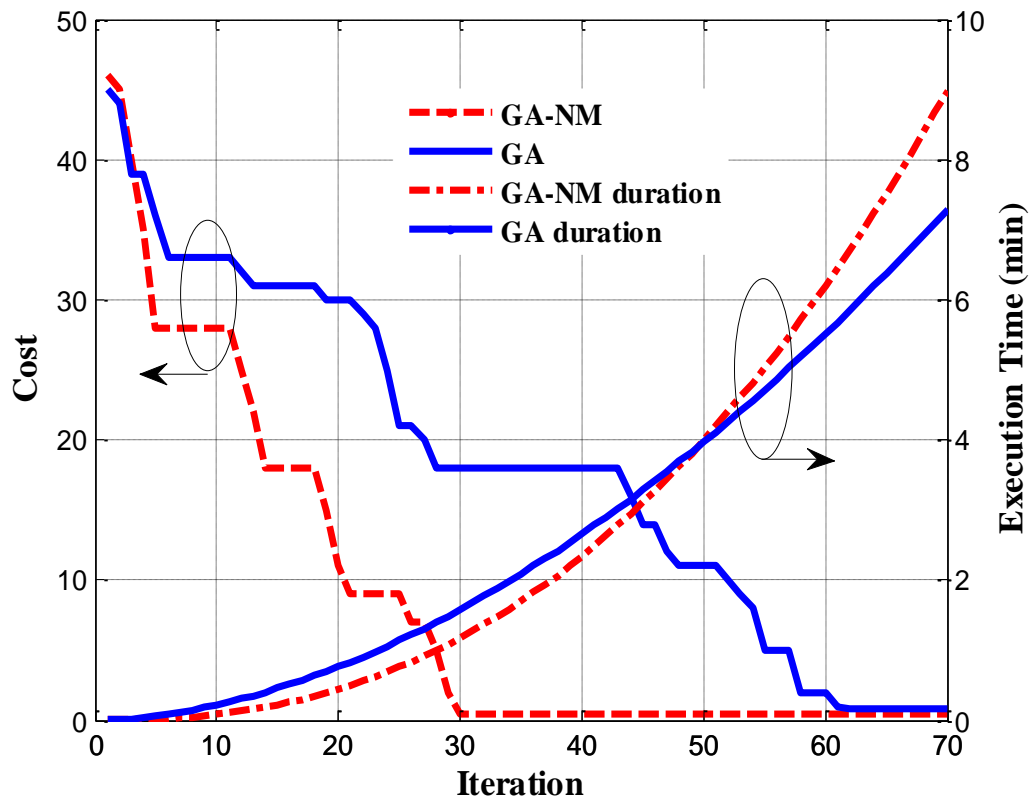


Figure 4.6 Convergence performances of the genetic and memetic optimization

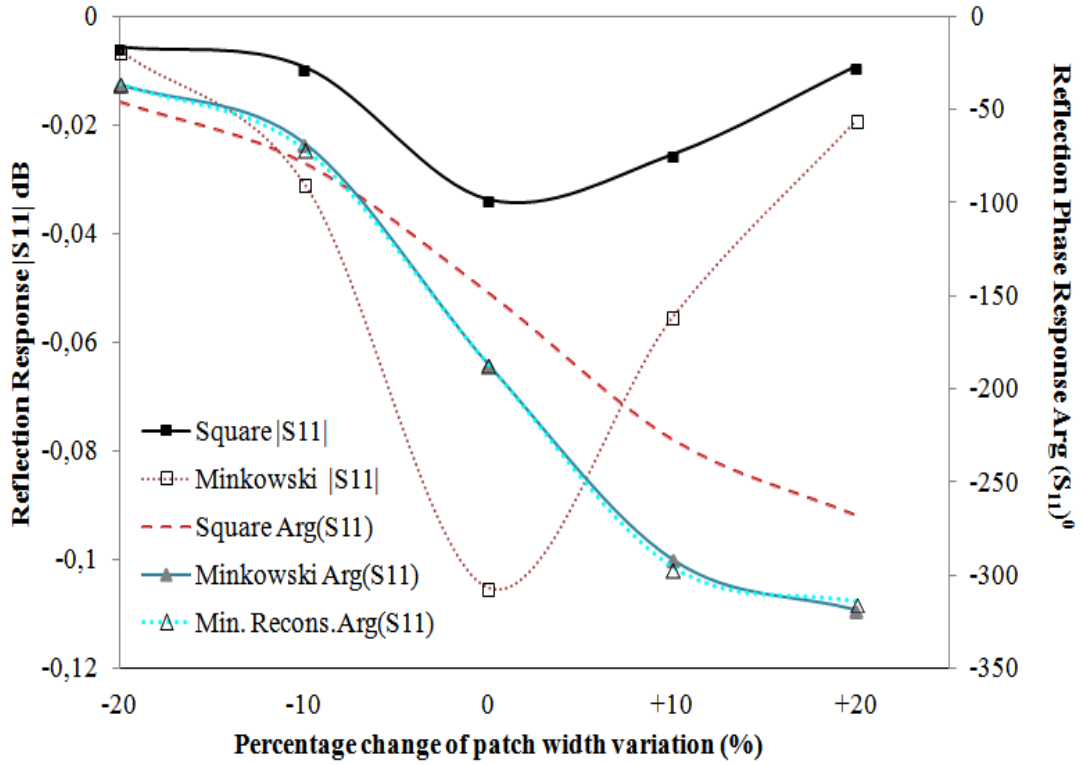


Figure 4.7 Reflection characteristics of the optimum minkowski reflectarray element with the parameters of $\epsilon_r = 3.1694$, $h_{opt} = 1.7916$ mm, $n_{opt} = 0.8438$ at $f=11$ GHz as compared with the square patch's values having the same resonance frequency.

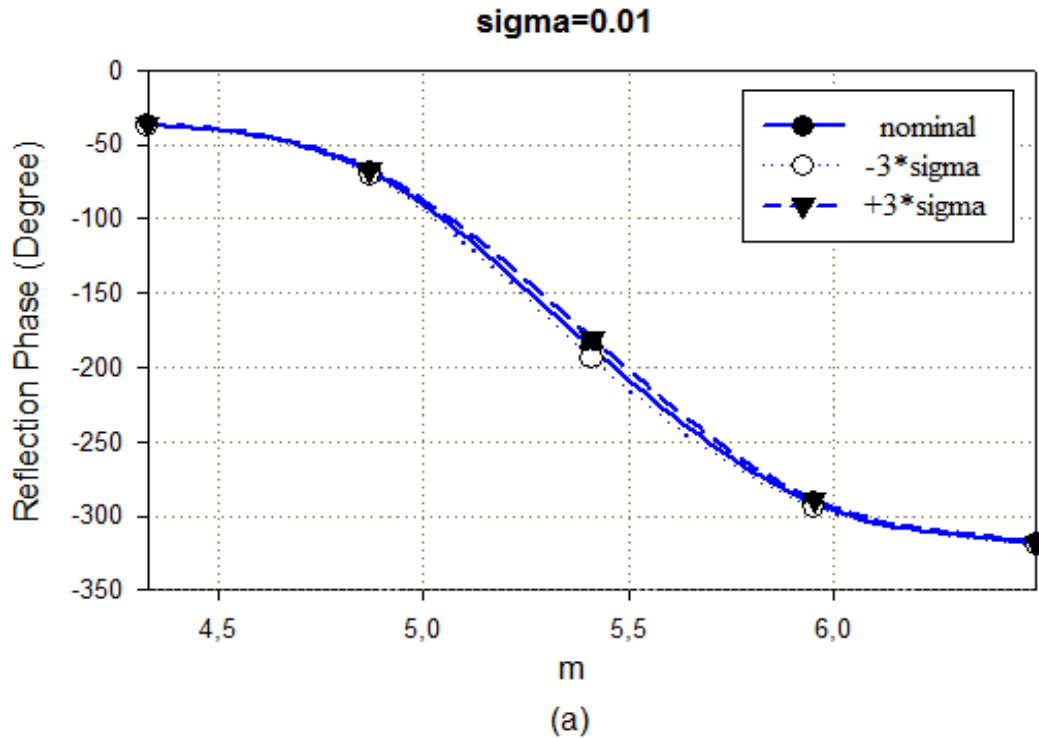
Table 4.2 3-D EM simulated reflection phases of the optimum MRA and constructed phases by the complete ANN response at $f=11$ GHz

Patch Width (mm)	Square Patch (Resonant size=6.06 mm)		Minkowski Patch (Resonant size=5.41 mm)		
	S ₁₁ (dB)	Target Arg(S ₁₁) (°)	S ₁₁ (dB)	Target Arg(S ₁₁) (°)	Recons. Arg(S ₁₁) (°)
-20	-0,00575	-46,4841112	-0,0064	-37,016407	-35,9411
-10	-0,00945	-79,192581	-0,03085	-68,385344	-70,9368
0	-0,03373	-148,82782	-0,10519	-187,0838	-186,72
10	-0,02543	-227,4055	-0,05529	-291,59329	-295,5879
20	-0,00919	-268,14059	-0,01901	-318,6572	-314,4403

4.4.3 Tolerance analysis of the optimization

The design parameters may usually change in a certain tolerance region during the manufacturing process. Thus, it is of interest to which percentage the design specifications are fulfilled. Thus the yield analysis is applied to compute an expected tolerance as percentage. In the implementation of yield analysis, variations in the design parameters are assumed to be small so that the linearization via the sensitivity analysis can be valid. For this reason a yield analysis can only be applied after a successful run of the sensitivity analysis. In the sensitivity analysis, the derivatives of output function (in our case it is reflection phase) with respect to geometric and/or material design parameters can be calculated without re-meshing the example. The first derivative of the network function with respect to a design parameter can be calculated with the information of the nominal value in a small neighborhood of that nominal value. Also the sensitivity information is used for a more efficient optimization.

In this study, sensitivity analysis is applied to the optimum dielectric constant $\epsilon_{r,opt}=3.164$ by rounding up the other parameters, as $n_{opt}=0.85$, $h_{opt}=1.8$. Then the yield analysis is applied to the results of the sensitivity analysis for the three values of the standard deviation belonging to the dielectric constant. The graphics for these results are shown in Figure 4.8.



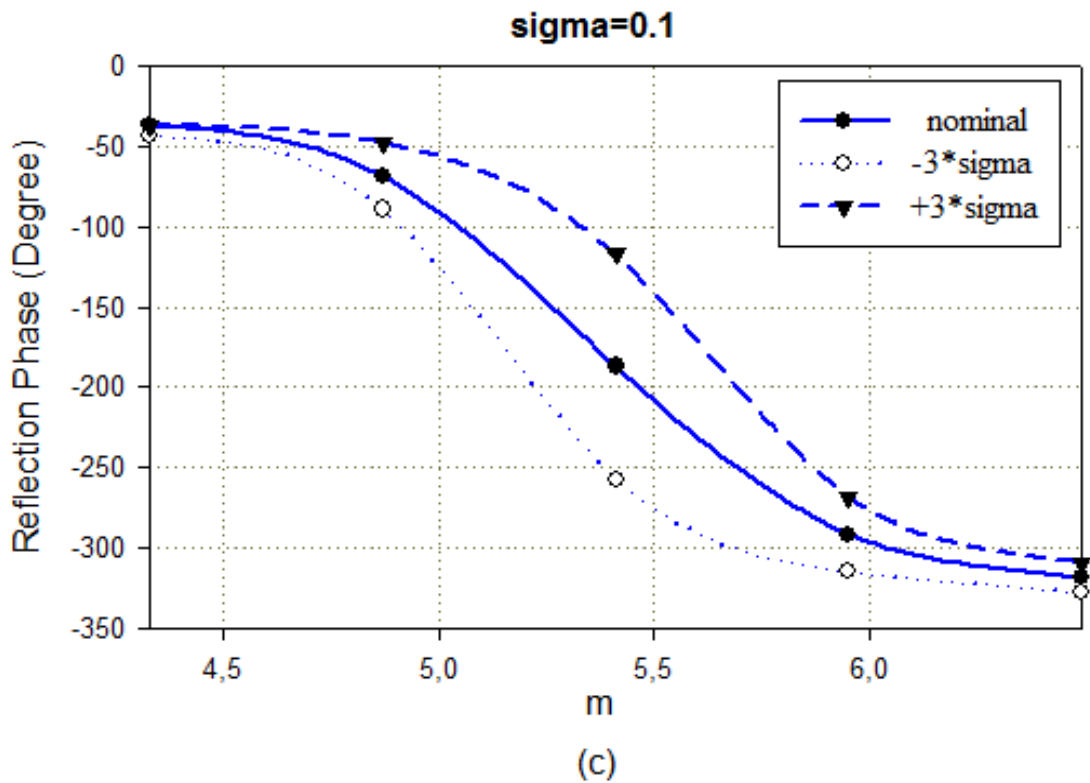
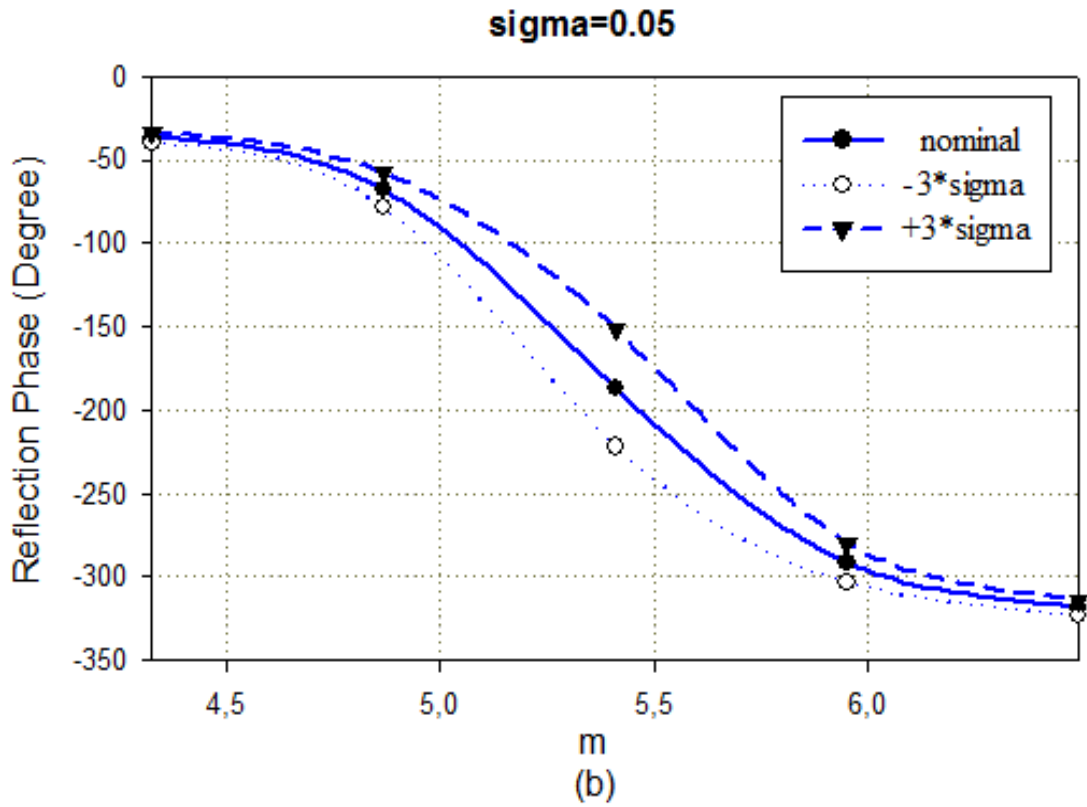


Figure 4.8 Sensitivity analysis results for the optimum dielectric constant for the standard deviation (σ) values: (a) $\sigma=0.01$, (b) $\sigma=0.05$ (c) $\sigma=0.1$ at $f=11$ GHz.

As is seen from Figure 4.8, the best tolerance is at the nominal design parameter value with a lower and upper bound (-3σ , $+3\sigma$) of the dielectric permittivity when the sigma is equal to 0.01. The upper and lower bound indicate as the worst case limits of the tolerance for the dielectric property of substrate. The substrate that has closest specifications to the optimized parameters had been searched, and the two commercially available substrates which are Rogers RO3003 and RO4232 has been found. As is seen from Fig. 9, RO4232 is the fittest substrate as commercially available for our optimized parameter result.

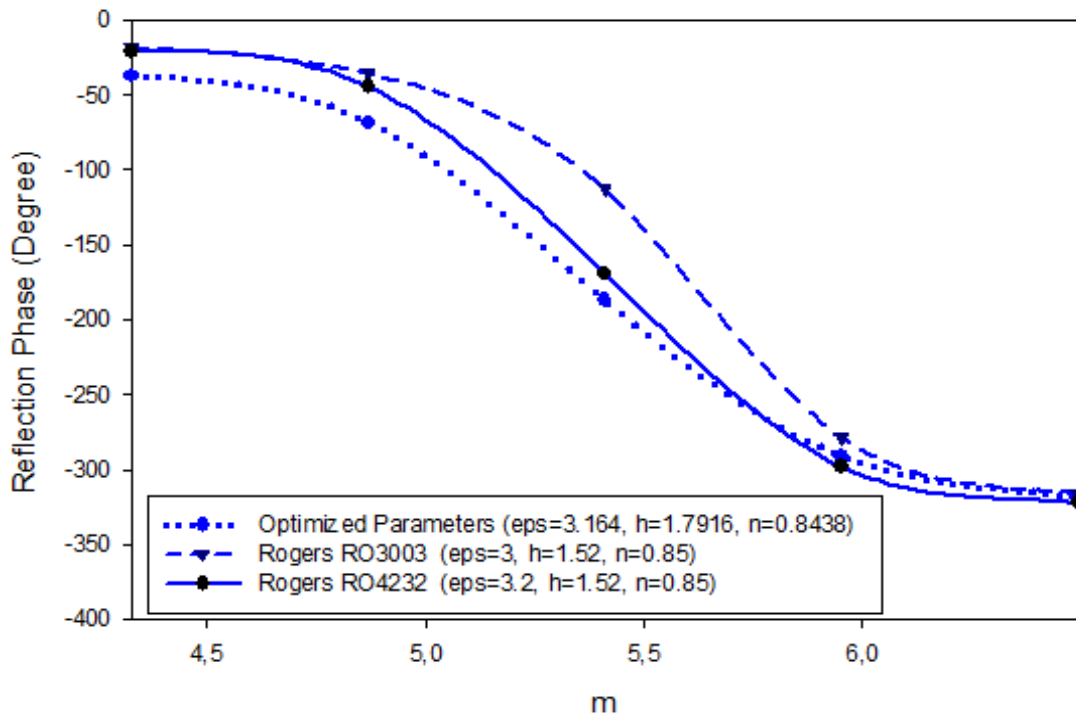


Figure 4.9 Comparison of the reflection phase responses for unit cell element designed with optimized parameters and two equivalent commercially available substrates

4.5 Design and Analysis of Minkowski RA with Fully-Optimized Parameters

4.5.1. Phase Compensation

In this work, the 15×15 variable-sizes minkowski RA with half-wavelength spacing at resonant frequency of 11(GHz) are designed. The radiation analysis has been generated using available full-wave simulation tool of CST MWS. In the phase compensation unit, a coordinate system has been used to determine the progressive phase distribution on the microstrip reflectarray surface of $M \times N$ arbitrarily spaced patches with a centered focal point that will produce a pencil beam in a direction of normal to the surface [8].

Thus, the required phase to compensate path difference $\Delta R(x)$ for a reflectarray element can be calculated as a function of its radial distance x to the center and the operation frequency f as given in the previous chapter in (3.6). The quadrature symmetry characteristic of 15×15 reflectarray for the phase compensation with respect to the element position where frequency is considered as the parameter and F/D is taken as 0.8 (Figure 4.10).

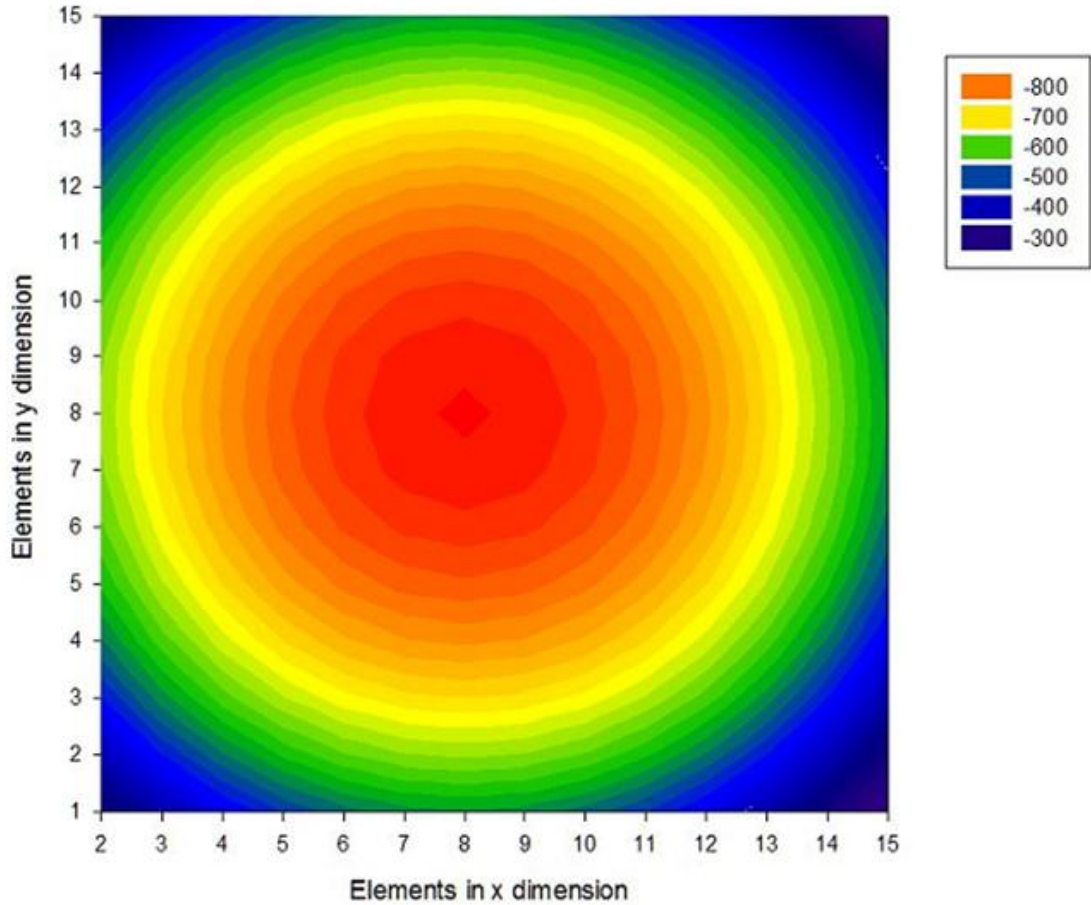


Figure 4.10 Required compensation phases for 15×15 minkowski RA with $F/D = 0.8$ at 11 GHz

4.5.2. Determination of Size for Each Minkowski Element

Size of each radiator is determined to meet the necessary compensation phase using the phase calibration characteristic. For this purpose, the established ANN model is reversed by inputting optimum values corresponding the phase calibration characteristic and while input m changes itself using the adaptable size Δm s which get exponentially smaller with an adaptation parameter τ as decreasing the squared error as given in Figure 4.11.

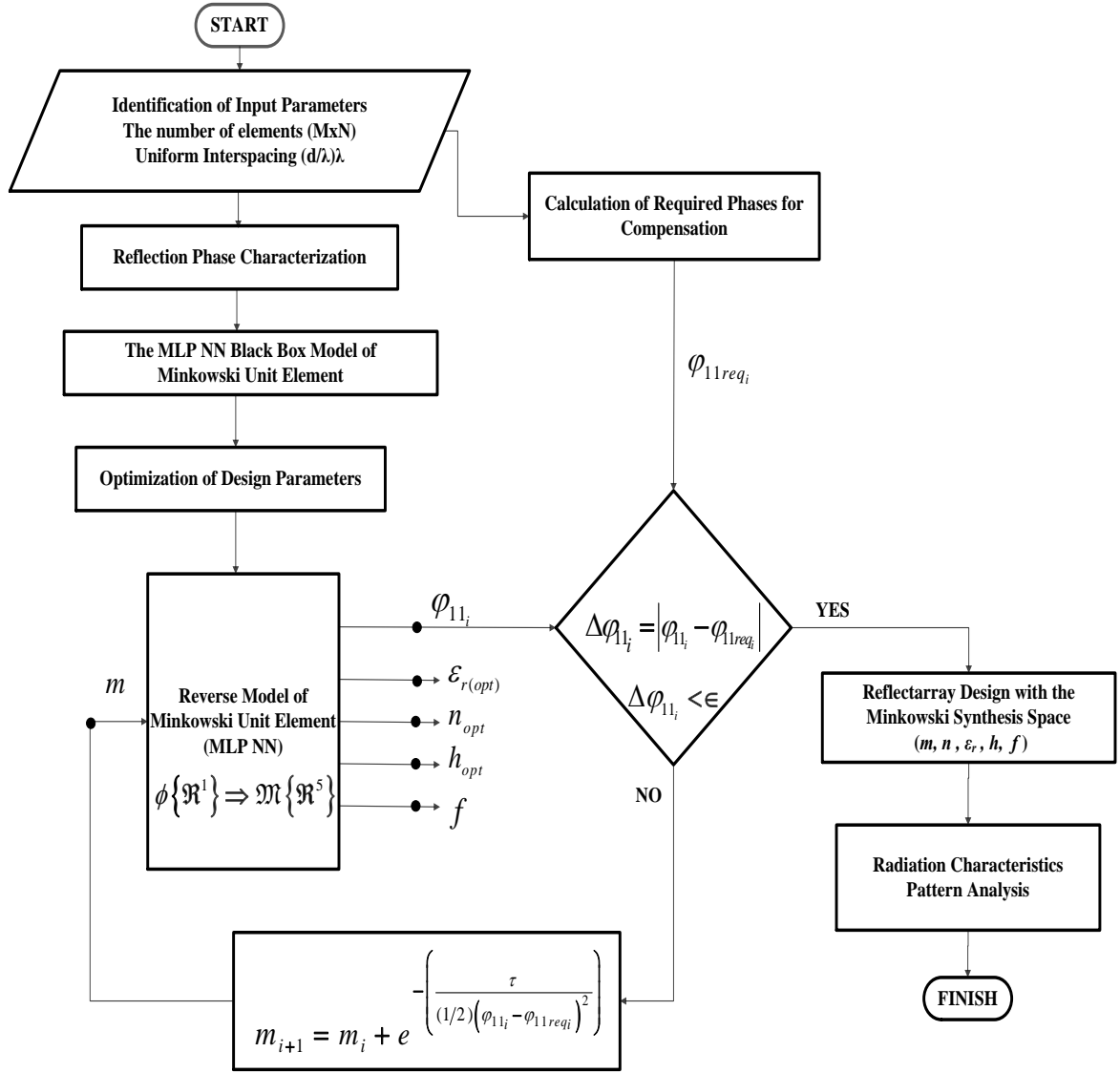
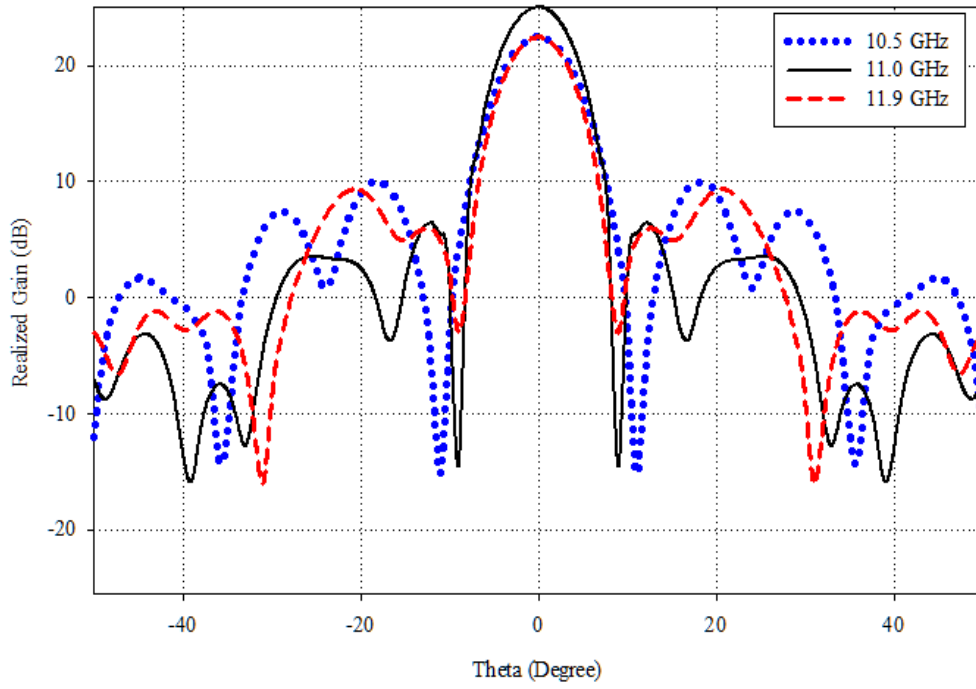


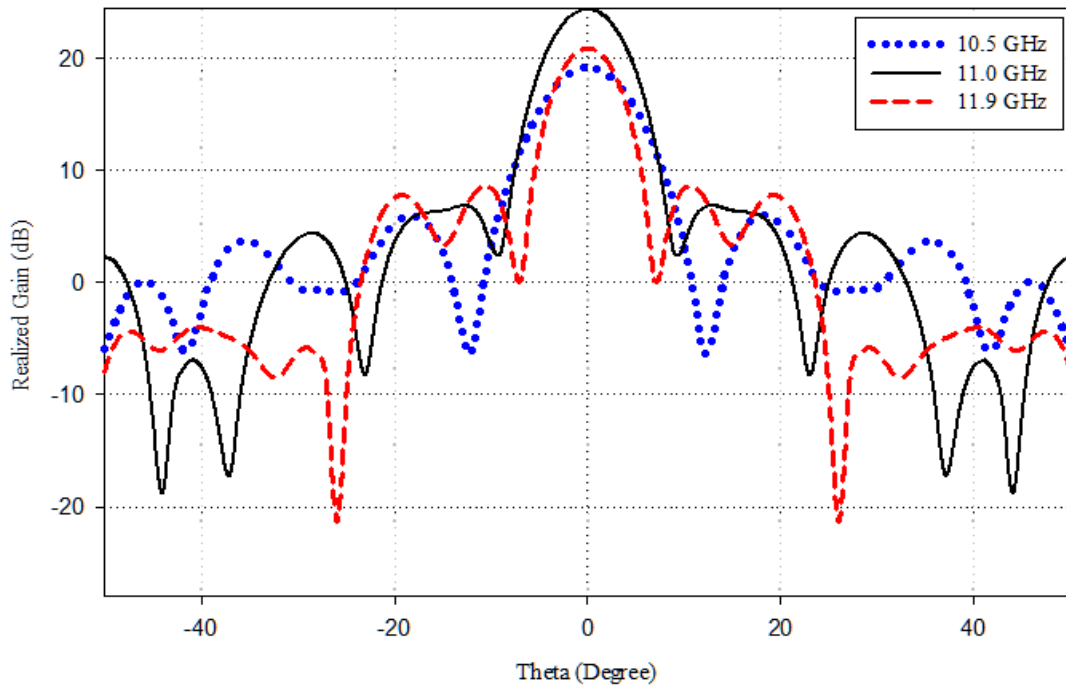
Figure 4.11 A general design procedure for a minkowski reflectarray antenna

4.5.3. Implementation of Reflectarray

In the implementation stage, all the radiation performance analyses are made using 3-D CST Microwave Studio. The fully optimized X-band minkowski RA with the parameters $\epsilon_{r_{opt}}=3.1694$, $h_{opt}=1.7916$ mm, $n_{opt}=0.8438$ is designed using the general design procedure and its realized gain patterns at the frequencies 10.5 GHz, 11 GHz and 11.9 GHz are given in Figure 4.12 (a). Furthermore, for the purpose of comparison, the realized gain patterns of an arbitrary non-optimized RA antenna with the parameters of $\epsilon_r=2.2$, $h=1.5$ mm, $n=0.90$ at the same frequencies are obtained with the same procedure and depicted in Figure 4.12(b) and the compared performance values take place in Table 4.3.



(a)



(b)

Figure 4.12 (a) Fully-optimized RA with $\epsilon_{r_{opt}}=3.1694$, $h_{opt}=1.7916\text{mm}$, $n_{opt}=0.8438$;
 (b) Non-optimized RA with $\epsilon_r=2.2$, $h=1.5\text{mm}$, $n=0.90$.

Table 4.3 Performance comparison of the fully optimized reflectarray with a non-optimized reflectarray

Antenna	Freq. (GHz)	Realized Gain (dB)	Side Lobe Level (dB)	Angular Width (3 dB) (Deg.)
Optimized RA $\epsilon_{r_{opt}}=3.1694$, $h_{opt}=1.7916$, $n_{opt}=0.8438$	10.5	22.5	-12.5	7.9
	11	25	-18.6	7.4
	11.9	22.5	-13.2	7.1
Non-Optimized RA $\epsilon_r=2.2$, $h=1.5$, $n=0.90$	10.5	19.2	-13.2	8.8
	11	24.4	-17.5	7.5
	11.9	21	-12.4	6.3

In order to examine the influence of dielectric property optimization, the gain variation with respect to the frequency are obtained with the same optimized indentation ratio $n_{opt} = 0.8438$ and thickness $h_{opt} = 1.7916\text{mm}$, but on some traditional substrates which are Taconic RF-35 with $\epsilon_r=3.5$, Taconic TRF41 with $\epsilon_r=4.1$, Rogers TMM4 with $\epsilon_r=4.5$ and depicted in Figure 4.13. The performance values corresponding to Figure 4.13 take place in Table 4.4. Figure 4.14 depicts the gain versus frequency variations of the optimized RAs designed on the dielectric $\epsilon_{r_{opt}}=3.1694$ and the traditional substrates. The performance values belonging to the Figure 4.14 are given in Table 4.5.

Table 4.4 Comparison of the fully optimized RA and the other RAs designed on the different substrates with same optimized parameters (n_{opt} , h_{opt})

Realized Gain (dB)			
	Fully Optimized RA	Rogers RT5880	Rogers TMM4
Freq. (GHz)	$\epsilon_{r_{opt}}=3.1694$	$\epsilon_r=2.2$	$\epsilon_r=4.5$
	$h_{opt}=1.7916\text{mm}$, $n_{opt}=0.8438$	$h_{opt}=1.7916\text{mm}$, $n_{opt}=0.8438$	$h_{opt}=1.7916\text{mm}$, $n_{opt}=0.8438$
10	17	13.2	17.7
10.5	22.5	18.2	22.3
11	25	23.9	23.5
11.5	24.3	24.7	18.5
12	21.2	23.5	8.5

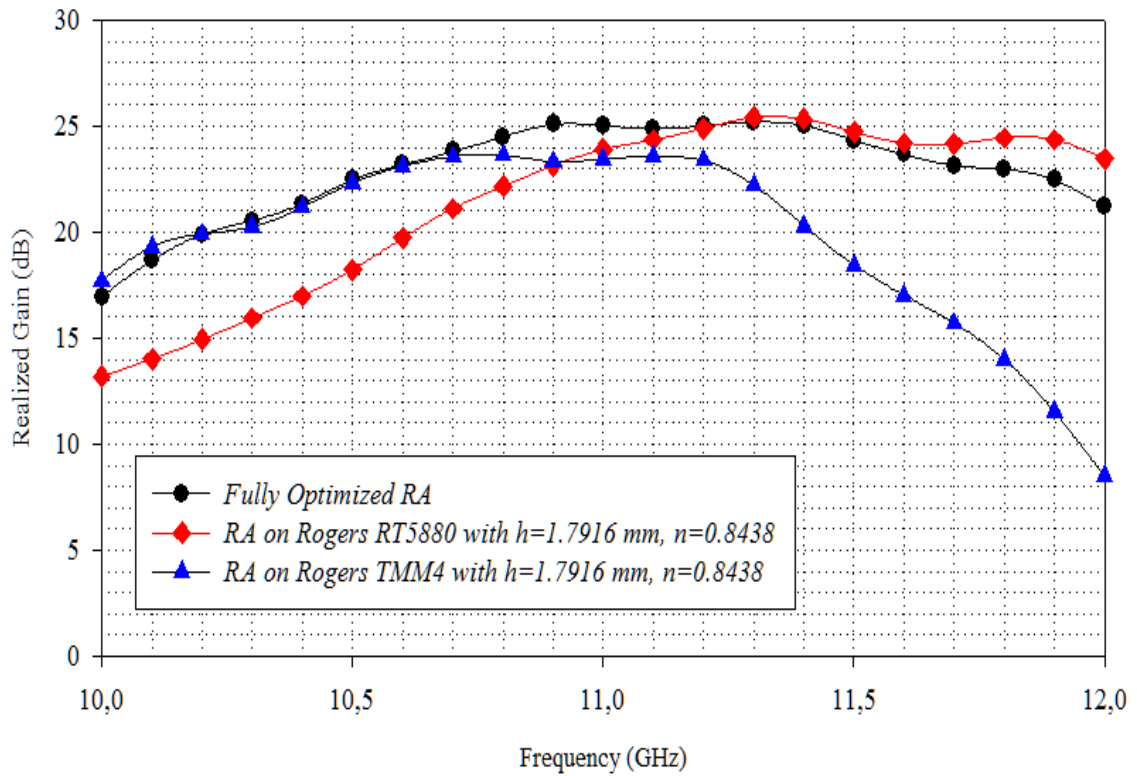


Figure 4.13 Realized gain versus frequency graphs for the fully optimized RA and the other RAs on the different substrates with the optimized parameters (n_{opt}, h_{opt})

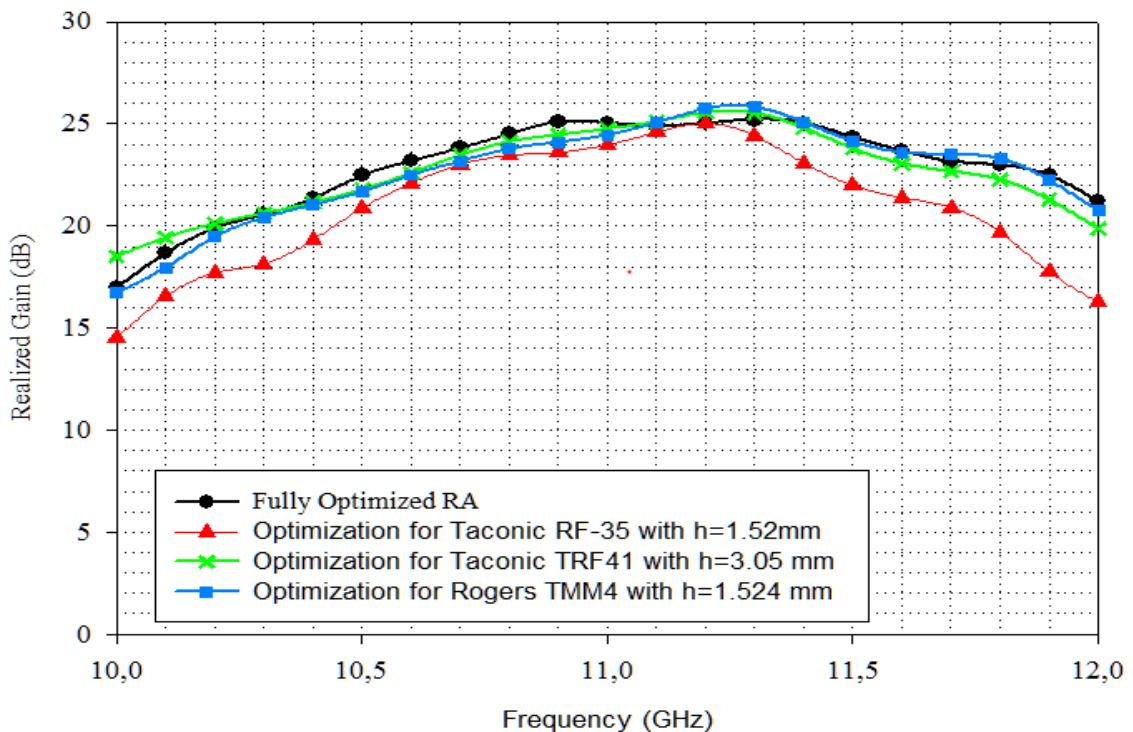


Figure 4.14 Realized gain versus frequency variations for the comparison of fully optimized RA with only patch geometry n_{opt} optimized RAs on the given dielectric permittivity ϵ_r and substrate thickness h

Table 4.5 Comparison of the Fully Optimized RA and RAs with the optimized minkowski shapes on the traditional substrates.

Freq. (GHz)	Realized Gain (dB)			
	Optimized RA $\epsilon_{ropt}=3.1694,$ $h_{opt}=1.7916,$ $n_{opt}=0.8438$	Taconic RF-35 $\epsilon_r=3.5,$ $h=1.52,$ $n_{opt}=0.7848$	Taconic TRF41 $\epsilon_r=4.1,$ $h=3.05,$ $n_{opt}=0.6212$	Rogers TMM4 $\epsilon_r=4.5,$ $h=1.524,$ $n_{opt}=0.3604$
10	17	14,5	18,5	16,7
10,5	22,5	20,9	21,8	21,7
11	25	24	24,8	24,5
11,5	24,3	22	23,8	24,1
12	21,2	16,3	19,9	20,7

4.6 Circular Polarization Characteristics of Fully-Optimized Minkowski RA

Slant polarization is known that slant polarized field components are the tangential components rotated by an angle Ψ (ψ). Thus, the E-field components are figured out as in ;

$$\begin{aligned} E_{cross} &= \cos(\psi)E_1 - \sin(\psi)E_2 \\ E_{co} &= \sin(\psi)E_1 + \cos(\psi)E_2 \end{aligned} \quad (4.8)$$

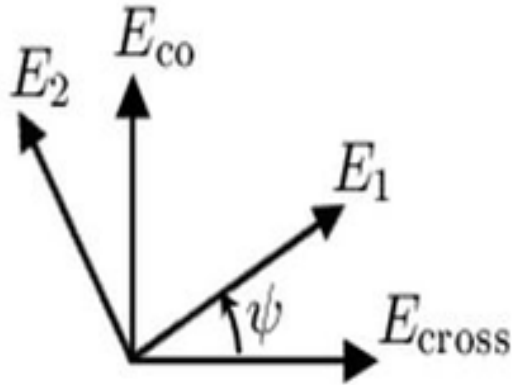


Figure 4.15 Vector illustration of circular slant polarization

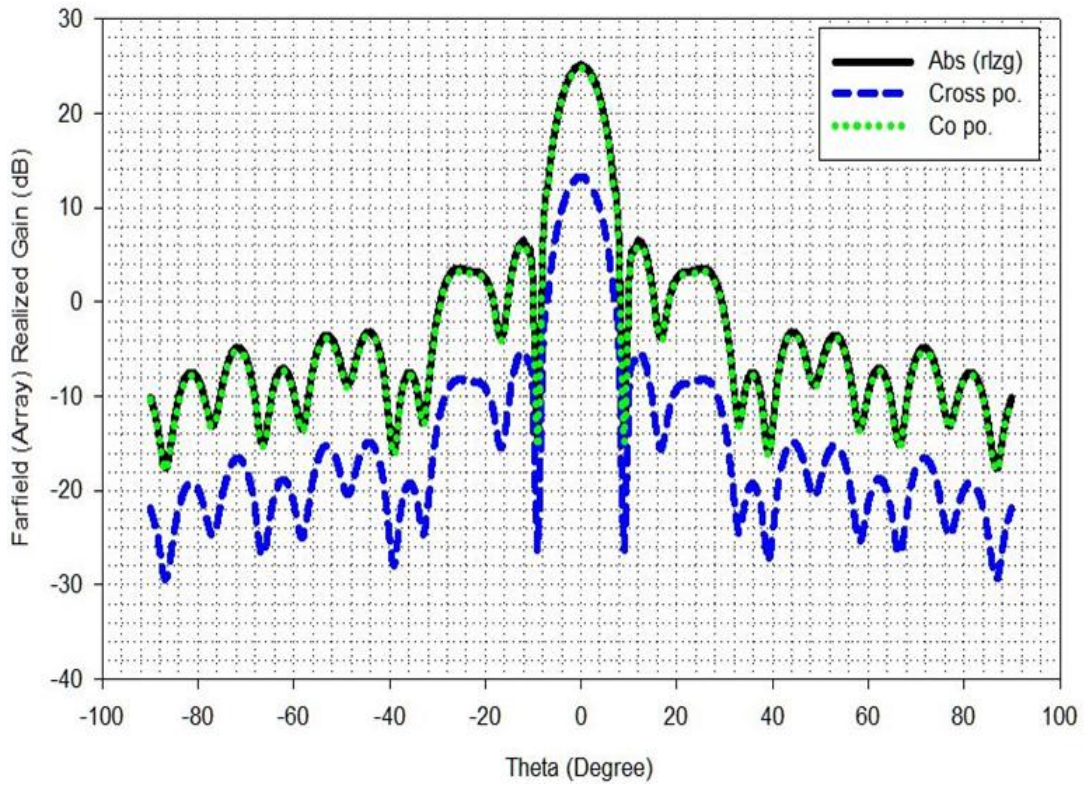


Figure 4.16 Circular polarization characteristics of optimized minkowski RA at 11 GHz for slant angle=15°

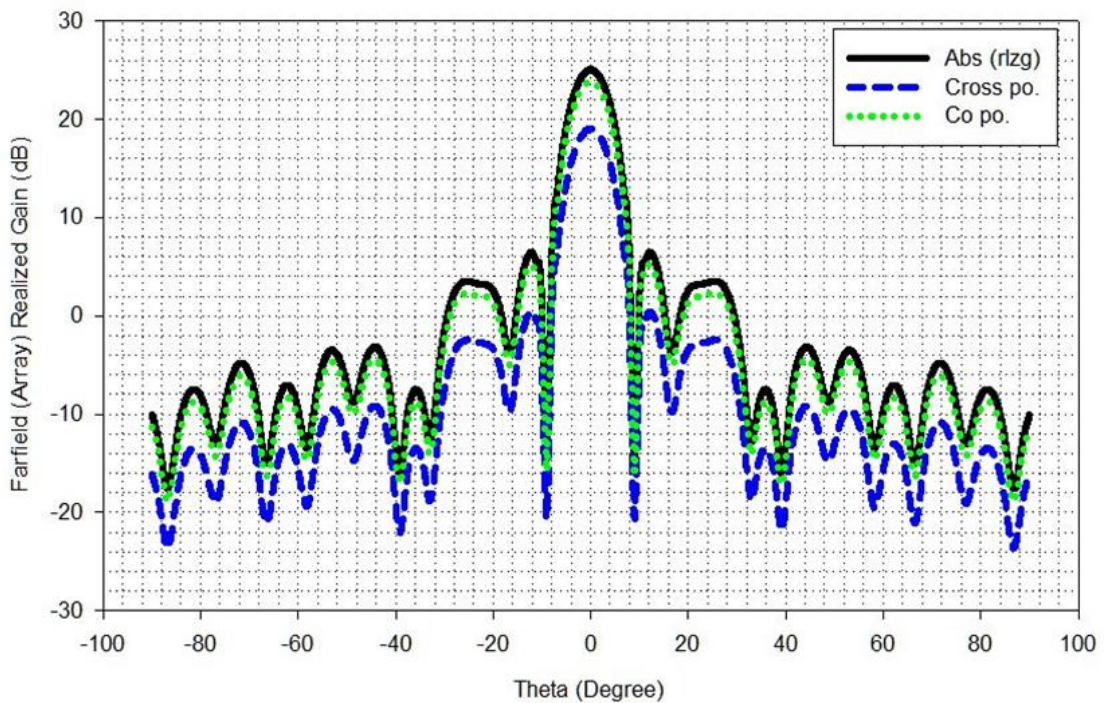


Figure 4.17 Circular polarization characteristics of fully-optimized minkowski RA at 11 GHz for slant angle=30°

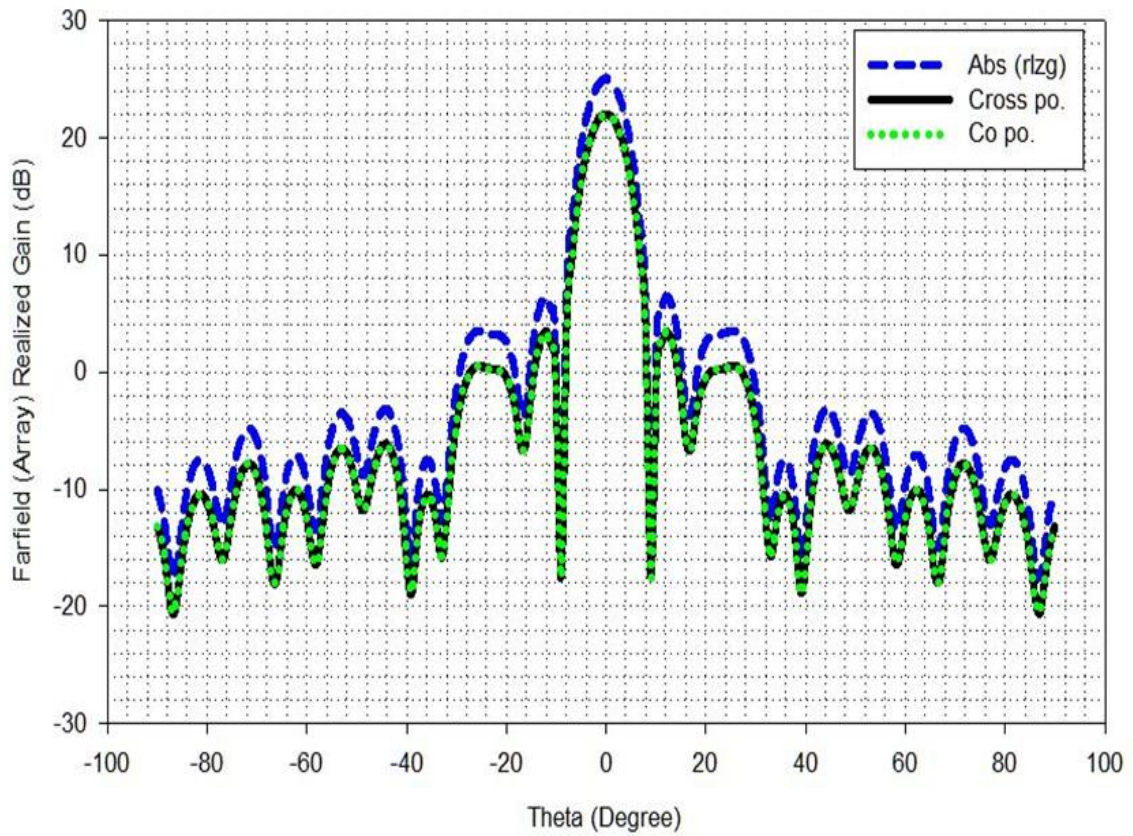


Figure 4.18 Circular polarization characteristics of fully-optimized minkowski RA at 11 GHz for slant angle=45°

Table 4.6 Circular polarization characteristics of fully-optimized minkowski RA

Type	Realized Gain (dB)	Cross Polarization (dB)	Co-Polarization (dB)
Slant Angle= 15°	25.0	13.3	24.7
Slant Angle= 30°	25.0	19.0	23.8
Slant Angle= 45°	25.0	22.0	22.0

CONCLUSION

Doubtlessly, microstrip reflectarray antennas are of prime importance in today's antenna technology, since they combine the advantages of both the printed phased arrays and parabolic reflectors to create a new generation of high gain antennas.

Contemporary antenna design is challenging and necessitates optimization of dimensional and material parameters of the antenna in order to satisfy various, often conflicting objectives concerning matching requirements as well as radiation characteristics. Since in most cases the analytical models are not available, Electromagnetic (EM) simulation and simulation driven optimization are ubiquitous in contemporary antenna design. Unfortunately, accurate simulation is CPU intensive so that employing EM solvers directly in the optimization loop may be impractical. Therefore the models as fast as the coarse models and as accurate as the fine models are desperately needed to be utilized efficiently in the design and analysis of the antenna.

In the first design application of this thesis, a single, accurate and fast MLP NN model is performed to be employed in both design and analysis of the minkowski RA based on the 3-D CST MWS. All the stages of building the MLP NN model and its utilization in design and analysis of a minkowski RA are given in details as a general systematic method that can be applied different types of antennas. The reconstructed results of MLP NN model have been also compared to the output of the minkowski RA. Besides, the effect of the feed movement along the focal length on the gain-bandwidth and the radiation pattern and is also obtained using the MLP NN model. Furthermore, the radiation characteristics of the designed minkowski RA are compared to its counterparts' radiation characteristics. Compared with the counterpart RA with square shape element and the parabolic reflector, this optimized minkowski reflectarray antenna is resulted to be capable of providing the higher realized gain and the lower side lobe level (SLL).

In the second design, a robust and systematic method has been proposed to be used in the design and analysis of a Minkowski reflectarray antenna. Hereinbefore, the most important and critical stage of a reflectarray design is the design optimization of its element. Therefore, firstly a complete, accurate and fast MLP ANN model of a Minkowski patch radiator is performed based on the 3-D CST MWS that takes into account all the main factors influencing the performance of the Minkowski RA. When the outputs of performed MLP NN model and 3-D simulations are compared, it has been verified that the MLP is very accurate and fast solution method to construct the highly nonlinear phasing characteristics within the continuous domain of the geometrical and substrate parameters of the RA element and frequency. All the stages of building the MLP ANN model and its utilization in design of a Minkowski RA are given in details as a general systematic method that can be applied to the differently shaped patch radiators. In the second stage, the overall parameters of Minkowski RA including dielectric permittivity of the substrate ϵ_r are optimized for an optimum linear phasing range of an ultra- wideband RA in the X-band by applying a standard novel evolutionary hybrid combination of global GA and local NM Algorithms. In addition to optimization process, the sensitivity and yield analyses are performed for the tolerance analysis in order to specify the tolerance limits of optimized design parameters and the commercially available substrate options which are compatible with our optimized design parameters. The optimum dielectric permittivity tolerance limits are qualified rounding up the values of the optimum substrate thickness, h_{opt} , and indentation ratio of Minkowski patch, n_{opt} , for the three characteristic values of the standard deviation. Thus, this tolerance analysis results in the limits of design parameters and the proper commercially available dielectric substrate as Rogers RO4232. In the final stage, a fully-optimized 15×15 Minkowski RA is designed as a worked example. Thus, its radiation characteristics are analyzed based on the 3-D CST MWS and graphically represented, then compared with the performances of the non-optimized and the partially-optimized Minkowski RAs.

Finally, it may be concluded that the presented robust and systematic multi-objective design procedures are conveniently applied to the MRAs constructed from the advanced patches.

REFERENCES

- [1] Huang, J., (1994). "Analysis of a microstrip reflectarray antenna for micro-spacecraft applications," TDA Progress Report, 143–173.
- [2] Balanis, C.A., (2012). *Antenna theory: analysis and design*: John Wiley & Sons.
- [3] Lo, Y.T. and Lee, S., (1993). *Antenna Handbook: Volume III Applications*: Springer.
- [4] Huang, J., (2008). *Reflectarray antenna*: Wiley Online Library.
- [5] Berry, D. Malech, R. and Kennedy, W., (1963). "The reflectarray antenna", *Antennas and Propagation, IEEE Transactions on*, 11: 645-651.
- [6] Roederer, A.G., (2009). "Reflectarray antennas": IEEE.
- [7] Kiyani, N. and Hajian, M., (2007). "Design, analysis and measurements of reflectarray using variable length microstrip patch antennas at Ka-band": IEEE.
- [8] Pozar, D.M. Targonski, S.D. and Syrigos, H., (1997). "Design of millimeter wave microstrip reflectarrays", *Antennas and Propagation, IEEE Transactions on*, 45: 287-296.
- [9] Wang, X.-T. Xue, Q.-Z. and Liu, P.-K., (2010). "Novel Broadband Reflectarray Antenna with Two-Type Elements for Millimeter-Wave Application", *Journal of Infrared, Millimeter, and Terahertz Waves*, 31: 833-839.
- [10] Pozar, D. and Metzler, T., (1993). "Analysis of a reflectarray antenna using microstrip patches of variable size", *Electronics Letters*, 29: 657-658.
- [11] Bialkowski, M. and Sayidmarie, K., (2008). "Phasing characteristics of a single layer microstrip reflectarray employing various basic element shapes": IEEE.
- [12] Bialkowski, M.E. and Sayidmarie, K.H., (2008). "Investigations into phase characteristics of a single-layer reflectarray employing patch or ring elements of variable size", *Antennas and Propagation, IEEE Transactions on*, 56: 3366-3372.
- [13] Li, Q.-Y. Jiao, Y.-C. and Zhao, G., (2009). "A novel microstrip rectangular-patch/ring-combination reflectarray element and its application", *Antennas and Wireless Propagation Letters, IEEE*, 8: 1119-1122.
- [14] Tsai, F.-C. and Bialkowski, M.E., (2003). "Designing a 161-element Ku-band microstrip reflectarray of variable size patches using an equivalent unit cell waveguide approach", *Antennas and Propagation, IEEE Transactions on*, 51: 2953-2962.

- [15] Li, H. Wang, B.-Z. and Du, P., (2007). "Novel broadband reflectarray antenna with windmill-shaped elements for millimeter-wave application", *International Journal of Infrared and Millimeter Waves*, 28: 339-344.
- [16] Pozar, D., (2003). "Bandwidth of reflectarrays", *Electronics Letters*, 39: 1490-1491.
- [17] Misran, N. Cahill, R. and Fusco, V., (2003). "Design optimization of ring elements for broadband reflectarray antennas", *IEE Proceedings-Microwaves, Antennas and Propagation*, 150: 440-444.
- [18] Hasani, H. Kamyab, M. and Mirkamali, A., (2010). "Broadband reflectarray antenna incorporating disk elements with attached phase-delay lines", *Antennas and Wireless Propagation Letters, IEEE*, 9: 156-158.
- [19] Chaharmir, M. Shaker, J. Cuhaci, M. and Ittipiboon, A., (2006). "A broadband reflectarray antenna with double square rings", *Microwave and Optical Technology Letters*, 48: 1317-1320.
- [20] Chaharmir, M. Shaker, J. and Legay, H., (2009). "Broadband design of a single layer large reflectarray using multi cross loop elements", *Antennas and Propagation, IEEE Transactions on*, 57: 3363-3366.
- [21] Yusop, S.H. Misran, N. Islam, M.T. and Ismail, M.Y., (2009). "Analysis of concentric split ring square reflectarray element for bandwidth enhancement": *IEEE*.
- [22] Rajagopalan, H. Xu, S. and Rahmat-Samii, Y., (2010). "Reflectarray phase analysis: A simple and intuitive understanding": *IEEE*.
- [23] Sayidmarie, K.H. and Bialkowski, M.E., (2008). "Phasing of a microstrip reflectarray using multi-dimensional scaling of its elements", *Progress In Electromagnetics Research B*, 2: 125-136.
- [24] Carrasco, E. Barba, M. and Encinar, J.A., (2007). "Reflectarray element based on aperture-coupled patches with slots and lines of variable length", *Antennas and Propagation, IEEE Transactions on*, 55: 820-825.
- [25] Guclu, C. Perruisseau-Carrier, J. and Civi, O.A., (2010). "Dual frequency reflectarray cell using split-ring elements with RF MEMS switches": *IEEE*.
- [26] Chen, B.-T., (2007). "Reflectarray with variable-patch-and-slot Size", *PIERS Online*, 3: 1273-1277.
- [27] Huang, J. Hodges, R. Zawadzki, M. Rengarajan, S. Han, C. and Chang, K., (2005). "Recent development of printed reflectarrays at JPL", *Proc. URSI GA*.
- [28] Legay, H. Bresciani, D. Girard, E. Chiniard, R. Labiale, E. Vendier, O. and Caille, G., (2009). "Recent developments on reflectarray antennas at Thales Alenia Space", *EuCAP*, 2515-2519.
- [29] Devireddy, B. Yu, A. Yang, F. and Elsherbeni, A.Z., (2011). "Gain and bandwidth limitations of reflectarrays", *ACES JOURNAL*, 26: 170-178.
- [30] Huang, J., (2001). "The development of inflatable array antennas", *Antennas and Propagation Magazine, IEEE*, 43: 44-50.
- [31] Zainud-Deen, S. Mitkees, A. and Kishk, A., (2009). "Design of dielectric resonator reflectarray using full-wave analysis": *IEEE*.

- [32] Mohammadirad, M. Komjani, N. Sebak, A.R. and Chaharmir, M.R., (2011). "A Broadband Reflectarray Antenna using the Triangular Array Configuration", *ACES JOURNAL*, 26.
- [33] Zuccarelli, J. Martorelli, V. D'Arcangelo, O. De Rosa, A. Pagana, E. Mandolesi, N. and Valenziano, L., (2009). "Onset & offset configuration for Ka-band reflectarray antenna": IEEE.
- [34] Tarn, I.-Y. Wang, Y.-S. and Chung, S.-J., (2008). "A dual-mode millimeter-wave folded microstrip reflectarray antenna", *Antennas and Propagation, IEEE Transactions on*, 56: 1510-1517.
- [35] Mayumi, K. Deguchi, H. and Tsuji, M., (2008). "Wideband single-layer microstrip reflectarray based on multiple-resonance behavior": IEEE.
- [36] Chaharmir, M. Shaker, J. Cuhaci, M. and Ittipiboon, A., (2009). "Wideband reflectarray research at the Communications Research Centre Canada": IEEE.
- [37] Ismail, M.Y. and Sopian, M., (2009). "Analysis of reconfigurable reflectarray antenna using frequency tuning method within X-band frequency range": IEEE.
- [38] Ebadi, S. Gatti, R.V. and Sorrentino, R., (2009). "Linear reflectarray antenna design using 1-bit digital phase shifters": IEEE.
- [39] Salti, H. Gillard, R. Loison, R. and Le Coq, L., (2009). "A Reflectarray Antenna Based on Multiscale Phase-Shifting Cell Concept", *Antennas and Wireless Propagation Letters*, 8: 363-366.
- [40] Zubir, F. and Rahim, M., (2009). "Simulated fractals shape for unit cell reflectarray": IEEE.
- [41] Zubir, F. A Rahim, M.K. Ayop, O.B. and Majid, H.A., (2010). "Design and analysis of microstrip reflectarray antenna with minkowski shape radiating element", *Progress In Electromagnetics Research B*, 24: 317-331.
- [42] Wahid, A. Rahim, M. and Zubir, F., (2010). "Analysis of dual layer unit cell with minkowski radiating shape for reflectarray antenna on different substrate properties": IEEE.
- [43] Mussetta, M. Pirinoli, P. Cong, P. Orefice, M. and Zich, R., (2010). "Characterization of microstrip reflectarray square ring elements by means of an Artificial Neural Network": IEEE.
- [44] Mussetta, M. Pirinoli, P. Zich, R.E. and Orefice, M., (2010). "ANN characterization of printed reflectarray elements".
- [45] Galushkin, A.I., (2007). *Neural networks theory*: Springer.
- [46] Haykin, S., (1994). *Neural networks: a comprehensive foundation*: Prentice Hall PTR.
- [47] M. Caputo, D. Pirisi, A. Grimaccia, F. Valbonesi, L. and Zich, R., (2009). "Neural networks and evolutionary algorithm application to complex EM structures modeling": IEEE.
- [48] Caputo, D. Pirisi, A. Mussetta, M. Freni, A. Pirinoli, P. and Zich, R.E., (2009). "Neural Network characterization of microstrip patches for reflectarray optimization".

- [49] Nazzal, J.M. El-etary, I.M. and Najim, S.A., (1818). "Multilayer Perceptron Neural Network (MLPs) For Analyzing the Properties of Jordan Oil Shale 1", World Applied Sciences Journal, 5: 546-552.
- [50] Weise, T., (2010). Global Optimization Algorithms-Theory and Application, E-book at [http://www. it-weise. de/](http://www.it-weise.de/), 11 November 2008.
- [51] Güneş, F. Türker, N. and Gürgen F., (2008) "Support vector design of the microstrip lines, International Journal of RF and Microwave Computer-Aided Engineering", 18(4): 326-336,.
- [52] Dieter, S. Fischer, C. and Menzel, W., (2010). "Design of a folded reflectarray antenna using Particle Swarm Optimization": IEEE.
- [53] Bialkowski, M.E. and Sayidmarie, K.H., (2008). "Bandwidth considerations for a microstrip reflectarray", Progress In Electromagnetics Research B, 3: 173-187.
- [54] Nelder, J.A. and Mead, R., (1965). "A simplex method for function minimization", The computer journal, 7: 308-313.
- [55] Konstantinidis, A. Yang, K. Chen, H.-H. and Zhang, Q., (2007). "Energy-aware topology control for wireless sensor networks using memetic algorithms", Computer Communications, 30: 2753-2764.
- [56] Cengiz, Y. and Kılıç, U., (2010). "Memetic optimization algorithm applied to design microwave amplifier for the specific gain value constrained by the minimum noise over the available bandwidth", International Journal of RF and Microwave Computer-Aided Engineering, 20: 546-556.
- [57] Mahmoud, K.R., (2010). "Design optimization of a bow-tie antenna for 2.45 GHz RFID readers using a hybrid BSO-NM algorithm", Progress In Electromagnetics Research, 100: 105-117.

CURRICULUM VITAE

PERSONAL INFORMATION

Name Surname : Selahattin NESİL
Date of birth and place : 27/06/1980
Foreign Languages : English - German
E-mail : snesil@gmail.com

EDUCATION

Degree	Department	University	Date of Graduation
Master	Elektrik-Elektronik Mühendisliği	Fatih Üniversitesi	31.08.2007
Undergraduate	Elektronik Mühendisliği	Fatih Üniversitesi	30.06.2004
High School	Fen Bilimleri	Gemlik Süper Lisesi	15.06.1998

WORK EXPERIENCE

Year	Corporation/Institute	Enrollment
2013 - ...	TÜBİTAK BİLGEM	
2011-2013	Fatih Üniversitesi	
2004-2008	Fatih Üniversitesi	

PUBLISHERMENTS

Papers

1. Güneş, F. Demirel, S. ve Nesil, S., (2014). "A Novel Design Approach to X-Band Minkowski Reflectarray Antennas using the Full-Wave EM Simulation-based Complete Neural Model with a Hybrid GA-NM Algorithm", *Radioengineering*, 23: 145.
2. Güneş, F. Nesil, S. and Demirel, S., (2013). "Design and analysis of minkowski reflectarray antenna using 3-D CST microwave studio-based neural network model with particle swarm optimization", *International Journal of RF and Microwave Computer-Aided Engineering*, 23: 272-284.
3. Mohais, A. Nikov, A. Sahai, A. ve Nesil, S., (2011). "Swarm-optimization-based affective product design illustrated by a pen case-study".

Conference Papers

1. Nesil, S. Güneş, F. ve Demirel, S., (2013). "Phase Characterization of X-band Minkowski Reflectarray Antennas Using 3-D CST Microwave Studio-based Neural Network Model Included Dielectric Properties": *THE ELECTROMAGNETICS ACADEMY*.
2. Güneş, F. Demirel, S. ve Nesil, S., (2013). "3-D CST microwave studio-based neural network characterization and Particle Swarm Optimization of Minkowski reflectarray in use microspacecraft applications": *IEEE*.
3. Nesil, S. Güneş, F. and Kaya, G., (2012). "Analysis and design of X-band Reflectarray antenna using 3-D EM-based Artificial Neural Network model": *IEEE*.
4. Nesil, S. Güneş, F. Demirel, S., (2012). "Yansıtıcı Dizi Antenlerde Geometri ve Taban Özelliklerinin Optimizasyonu için Yansıtma Karakteristiğinin Çok Katmanlı Algılayıcı Yapay Sinir Ağı ile Modellenmesi", *URSI-Türkiye 2012 Bilimsel Kongresi ve Ulusal Genel Kurulu, İstanbul/Türkiye, Sep. 2012, URSI*,
5. Nesil, S. Güneş, F. ve Özkaya, U., (2011). "Phase characterization of a reflectarray unit cell with Minkowski shape radiating element using multilayer perceptron neural network": *IEEE*.
6. Nesil, S. Güneş, F. Özkaya, U. and Türetken, B., (2011). "Generalized regression neural network based phase characterization of a reflectarray employing Minkowski element of variable size" *URSI 2011*.
7. Nikov A., Mohais, A., Nesil, S., (2007). "Emotive design by swarm-intelligence-modelling", *9th International Symposium, TECHNOMAT 2007, Materials, Methods and Technology, Scientific Articles, 204-214, Bulgaria*,

8. Nesil, S. Korkmaz, E., (2006), Kanser Tedavisinde Hyperthermia Uygulaması, URSI-TÜRKİYE Bilimsel Kongresi ve 4. Ulusal Genel Kurul Toplantısı, Ankara/Türkiye.

Projects

1. Katot ve Mikrodalga Tüp Araştırma Merkezi Altyapısı Projesi (Proje Yürütücüsü) TÜBİTAK
2. Katot Geliştirme Projesi (KAGEP) – Araştırmacı- TÜBİTAK
3. Yansıtıcı Dizi Anten Analiz Ve Sentezi, Üniversite Araştırma Proje Fonu, Yıldız Tek. Üniversitesi, Temmuz 2012-Temmuz 2014.
4. OFDMA Sistemlerinde Uydu-Yer Bağlantısı için Geribildirim Bitlerinin İncelenmesi, Yıldız Tek. Üniversitesi (Haziran, 2009).
5. Calculation of scattered fields from any moving object, Fatih Üniversitesi Araştırma Proje Fonu- (2007-2009).